1969

Electrical And Optical Properties Of Electroless Nickel Films

John Peter Marton

CANADA

MICROFILMED

BY

CENTRAL MICROFILM UNIT

PUBLIC ARCHIVES

OF

CANADA

OTTAWA, ONTARIO

MICROFILMÉ

PAR LE

SERVICE CENTRAL DU MICROFILM

ARCHIVES PUBLIQUES

DU

CANADA

OTTAWA, ONTARIO

DATE July 10/69 REDUCTION 15

OPERATOR / OPERATEUR L. Langlois EXPOSURE / EXPOSITION 93

ARC-178(1/66)

CANADA

NATIONAL LIBRARY OF CANADA

CANADIAN THESES ON MICROFILM

BIBLIOTHÈQUE NATIONALE DU CANADA

THÈSES CANADIENNES SUR MICROFILM

NL-101(1/66)

ELECTRICAL AND OPTICAL PROPERTIES OF ELECTROLESS NICKEL FILMS

by

John Peter Marton

Department of Physics

Submitted in partial fulfillment
of the requirements for the degree of
Doctor of Philosophy

Faculty of Graduate Studies
The University of Western Ontario
London Canada
October 1968

ABSTRACT

Electrical and optical properties of electrolessly deposited Ni-P films were studied. The film thicknesses ranged from 100Å to 1mm and the P content varied between 0 percent (pure Ni) and 16 percent by weight (w/o). The film properties were studied at room temperature. The electrical and optical properties of freshly deposited films deviated excessively from those of the corresponding bulk material. The DC resistivity was found to be orders of magnitude higher than is expected from the Fuchs-Sondheimer theory, and the optical properties of fresh films were found to be non-metallic. An examination of the nucleation, growth and structure of films provided a partial understanding for the reasons of the anomalies: The structure of fresh films was determined to be liquid-like and the film geometry was found to be discontinuous. The discontinuity is three dimensional i.e. the fresh films were determined to consist of small Ni-P aggregates in a random three dimensional arrangement. Upon heating in vacuum, fresh Ni-P films undergo a compacting process and crystallize at a characteristic temperature. Along with the structural changes the electrical and optical properties approach those of the parent bulk. For heat treated films, approximate values of the constants τ, N and m^* were established. The role of the P ions in the Ni host material is suggested to act as scatterers for electron transport, and to possibly widen the energy bands of nickel. A working model of Ni-P films is developed. It describes

the fresh and heat treated states of films and explains the anomalous behaviours of some of the films in terms of current thin film theories. A generalization of the results gained from experiments with Ni-P films leads to suggestions to refine and extend some of the current film theories. These ideas and their consequences are discussed.

ACKNOWLEDGEMENTS

The author would like to express his appreciation to Dr. M. Schlesinger for his continued interest and advice throughout this work.

The author wishes to express his gratitude to Mr. R. Wilton, President, Welwyn Canada Limited, for his permission to use the necessary equipment and materials in the Research Laboratory of Welwyn Canada Limited for the experimental part of this work. His permission to publish certain parts of the present work is also acknowledged with sincere appreciation.

Thanks are due to Dr. J. Brown, Engineering Department, U.W.O. for his valuable assistance in the electron diffraction experiments, and to Mr. J. Kiss for his help in creating the numerous computer programmes used in the present work.

The continuous help and encouragement of Drs. Fraser, Hay and Whippey throughout this work is gratefully acknowledged.

This work has been supported partly by The Defence Research Board of Canada, partly by Welwyn Canada Limited and partly by the Department of Physics, U.W.O. These supports are acknowledged with appreciation.

TABLE OF CONTENTS

LIST OF TABLES

LIST OF FIGURES

CHAPTER 1

INTRODUCTION

The electrical and optical properties of solid metals are independent of their size, provided that all three dimensions are greater than a certain length, characteristic of the specific metal. If one of the three dimensions is comparable with the characteristic length, the metal is said to be in thin film form, and if all three dimensions are of this order we speak of microparticles. The characteristic length for metals is related to the mean free path of conduction electrons, and is of the order of a few hundred angstroms at room temperature.

Thin films and microparticles of metals exhibit physical properties that may be very different from those of the corresponding metal in bulk form. Typical examples are the high DC resistivity and the brilliant colors of some metal films. Ideally, current theories of metal films are capable of predicting the deviations of film properties from those of the corresponding bulk metal. Films which do not exhibit properties predicted by these theories are referred to as "anomalous".

Thin film theories of interest in the present work are: The film thickness dependent DC conductivity of continuous plane parallel

films (1), (2); the DC conductivity of discontinuous (island type) films (3), (4); and the structure dependent optical constants of discontinuous films (5), (6). In the development of these theories it is assumed that the film or the microparticles (islands) forming the film are identical in all respects to the corresponding bulk metal i.e. as if films were thin slices of the bulk.

In experimental situations, films are assembled atom by atom on a suitable substrate and are thus grown to the desired thickness. The resulting film seldom resembles a thin slice of the bulk metal; therefore films grown by various means under different deposition conditions are usually anomalous. A survey of the literature (7) shows that the concern of most workers is the study of film anomalies for the sake of a better understanding of thin films.

One of the few exceptions to this approach is the work of Mayer and co-workers (8), (9). Their study is concerned with the electronic structure of simple bulk metals, and they use thin films of those metals as a convenient experimental medium. Their method of deposition (ultrapure metals evaporated in ultrahigh vacuum) yields films that are similar to a thin slice of the parent bulk. From measurements on such films, and from film theories, they were able to determine some electronic constants of a number of alkali metals, e.g. mean free path (8) and effective mass (9) of conduction electrons.

In the present work, structural, electrical and optical properties of electrolessly deposited Ni-P films were examined. Electroless deposition was chosen for its simplicity, and for some

drastic anomalies of the resulting films (10). The deposition of electroless nickel on catalytic substrates (11 - 14) and on dielectric surfaces (15), (16) is well documented. Deposits from a number of different solutions have been determined (14) to consist of Ni and P with $2\% \leq P \leq 15\%$ by weight (w/o). Fresh bulk deposits were stated to have amorphous (17) or fine crystalline (18) structures. Published work on electroless Ni-P films deposited on dielectric substrates is practically non-existent. The few exceptions include work on the nucleation, growth and structure of thin Ni-P films (19), the effect of P content on the magnetization of Ni-P films (20), and a study of the structure dependent DC resistivity of films (21), (22). Publications (19), (21) and (22) resulted from the present work.

The main concern of the present work was the study of film anomalies. This resulted in a working model for Ni-P films. In certain cases it was possible to interpret experimental results by theories, yielding numerical estimates of some electronic constants of the films.

The presentation of the material is in six parts. Chapter two is technical in content, and describes the experimental considerations, methods and apparatus that were applied and used in the work. The actual experiments and the experimental data are discussed and tabulated in Chapter three. Part 3.1 is an exception. In this section the nucleation growth and structure of Ni-P films is discussed completely, as this knowledge was necessary in the following section. In the first part of Chapter four, current thin film theories are

reviewed, the mathematics of the theories being relegated to the appendices. In the second part of Chapter four the experimental results are recalled from previous sections and are interpreted. In the first part of Chapter five a model for Ni-P films is developed and presented. In the second part the consequences of the model are discussed and some comments made on the present theoretical situation. Finally, in Chapter six a summary is presented and future work is proposed.

CHAPTER 2

EXPERIMENTAL PROCEDURE

The techniques, methods and apparata used in the present experimental work are discussed below. In what follows, we distinguish between bulk and film specimens, and in both cases between Ni-P and Ni specimens. Unless otherwise specified, bulk Ni (or Ni-P) will be understood to be a solid slab with dimensions not less than 1mm. Films on the other hand are defined to have one dimension (thickness) that may range from a few tens of angstroms to a few microns. Deposits referred to as Ni-P will be understood to be those deposited from electroless solutions, and those referred to as Ni will be understood to be deposits grown by vapor condensation in a vacuum chamber. Ni-P deposits are nickel with $9\ \text{w/o} \leq P \leq 16\ \text{w/o}$, and Ni deposits are 99.98% pure. w/o denotes percent by weight.

2.1 Preparation of Film Specimens. Both electroless Ni-P films and vacuum evaporated Ni films were deposited on a number of different substrates. The choice of substrates was usually dictated by the experiment for which the film was to be used. Films used in electrical experiments were grown on either glass, Mica or quartz substrates; those in optical experiments were grown on nickel, quartz or glass

substrates, and those used for electron microscopy were grown on nickel, glass, Mica or Formvar substrates.

2.11 Substrate Cleaning. Nickel substrates were mechanically polished and etched in nitric acid, followed by repeated water rinses and a vapor cleaning with acetone as the source. A schematic representation of the vapor cleaning appartus is shown in Figure 1.

Glass and quartz substrates were first cleaned in chromic acid-sulfuric acid solution with composition of 200 gr chromic acid, 75 ml sulfuric acid and 400 ml distilled water at a temperature of 80°C for a few hours, followed by repeated water rinses. The wet substrates were loaded into the vapor cleaning unit for a cleaning using isopropyl alcohol, followed by a cleaning using acetone.

Mica substrates required no cleaning as they were freshly cleaved prior to film deposition. Formvar was freshly deposited on microscope slides from solution, therefore it required no cleaning.

As the surface of substrates are required to be free from foreign matter for a successful film deposition, the freshly cleaned substrates were tested for cleanness by the black breath method (23). If they showed no breath figure, they were used immediately for film deposition, and if they were not acceptable, they were recleaned. Clean substrates were never stored for later use.

2.12 Substrate Activation. Electroless deposition of nickel is only possible on substrates whose surface is suitably catalytic (14). As Ni is a catalyst for electroless deposition, Ni substrates need

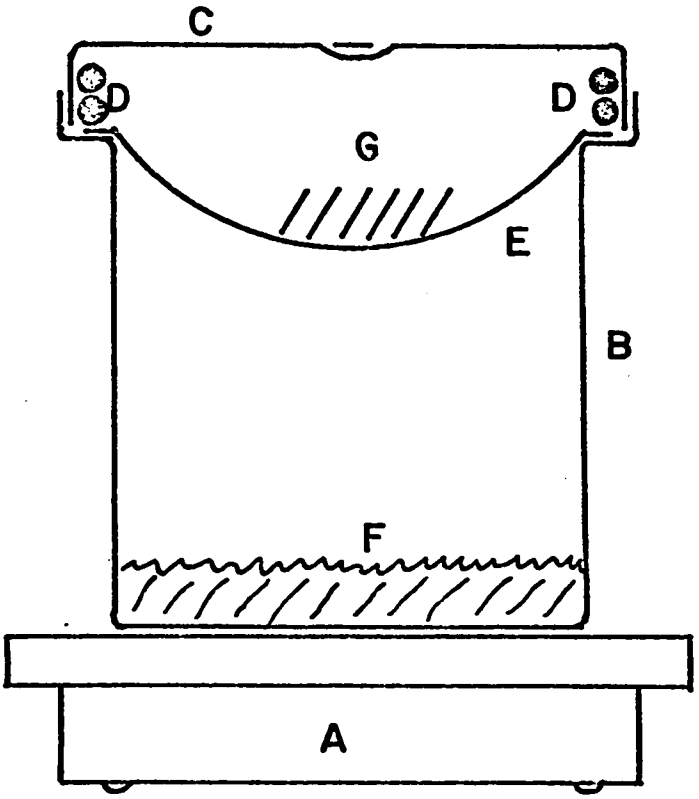

FIGURE 1: Schematic representation of vapor cleaning for substrates. The cleaning of substrates G is by the condensing of vapor of liquid F on the cool substrates. Cleaning is completed and condensation stops when substrates reach vapor temperature. A is hotplate; B is stainless steel vessel; C is stainless steel lid; D is cooling coil; E is nylon sieve; F is source liquid (alcohol or acetone); G is substrates.

not be catalized. Non-catalytic substrates need to be "activated" for film deposition. This is achieved by treating the surface of the substrates with catalytic agents.

Mica, glass, Formvar and quartz substrates were activated for electroless nickel deposition by a process similar to that proposed by Bergstrom (16). The clean substrates were immersed in a solution of stannous chloride at room temperature, and rinsed well with distilled water. They were then immersed in a solution of palladium chloride solution, also at room temperature, and again rinsed well in distilled water. The composition of solutions for the activation process is listed in Table I. The treatment catalizes the substrates sufficiently for Ni-P deposition to begin. Once deposition starts in the electroless solution, and nickel forms on the substrate, it will continue, due to the catalytic nature of the film.

TABLE I

Composition of Solutions
Used for Substrate Activation

$SnCl_2$ Solution:	$SnCl_2$		0.1 gr/ℓ
	HCl		0.1 cc/ℓ
Rinse:	H_2O	at	pH = 7
$PdCl_2$ Solution:	$PdCl_2$		0.1 gr/ℓ
	HCl		0.1 cc/ℓ
Rinse:	H_2O	at	pH = 7

2.13 Electroless Nickel Deposition. Freshly activated substrates were immersed in electroless nickel solutions at a controlled temperature and pH value, and the time of deposition was used to adjust the film thickness. The deposition apparatus is shown in Figure 2. The composition of typical solutions used are listed in Table II.

TABLE II

Composition of Electroless Nickel Solutions, Range of Deposition Temperature and Phosphorus Content of Deposits

Composition	pH = 5.3	pH = 4.3	pH = 3.3
Nickel Sulphate, gr/ℓ	29	29	29
Sodium Hypophosphite, gr/ℓ	17	17	17
Sodium Succinate, gr/ℓ	15	8.6	1.6
Succinic Acid, gr/ℓ	1.3	4.0	6.8
Solution Temperature, °C	25 to 65	35 to 65	45 to 65
P Content* in deposits, w/o	9.5	13.0	16.0

Macroscopic rates of deposition for various solutions at typical temperatures are shown in Figures 3 and 4. In the following, Ni-P samples will be identified by solution pH or P content, and deposition temperature as deposition parameters.

* The phosphorus content in deposits was established by the Atomic Energy of Canada Ltd., using neutron activation analysis.

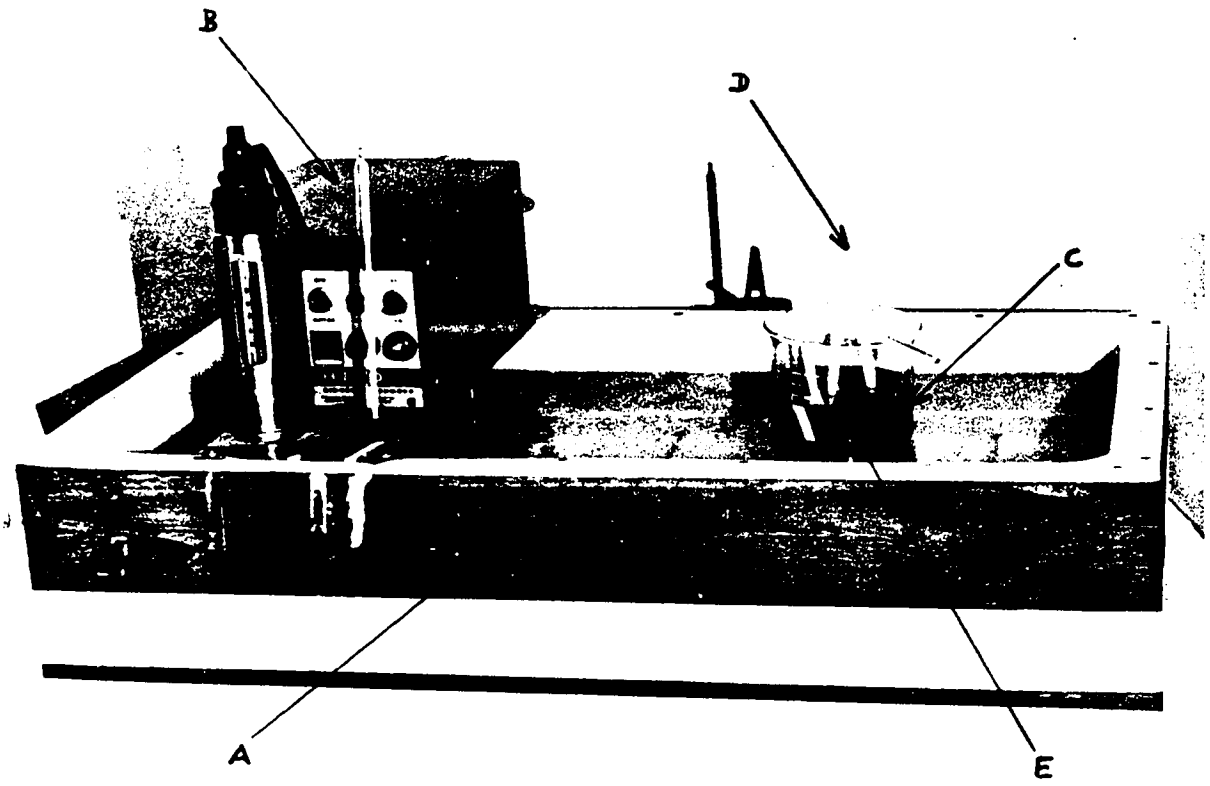

FIGURE 2: Controlled temperature bath and electroless solution for electroless Ni-P film deposition. A is water bath; B is heater, stirrer and temperature control unit; C is electroless solution in beaker; D is substrate holder; E is substrate.

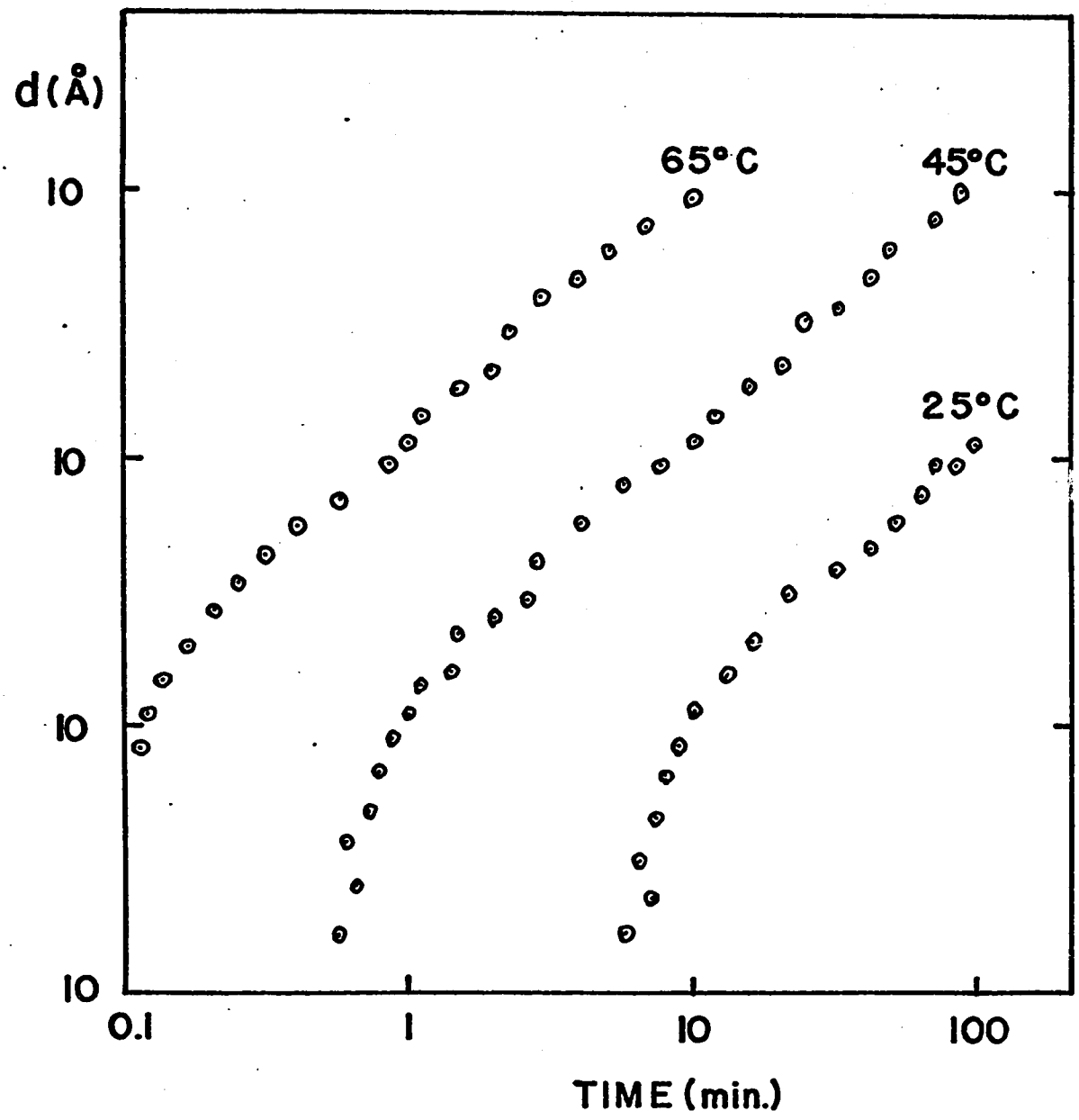

FIGURE 3: Rates of deposition of electroless Ni-P films in pH = 5.3 solution at temperatures of 25°C, 45°C and 65°C. d is mass-thickness of films (mass/unit surface area) in angstroms.

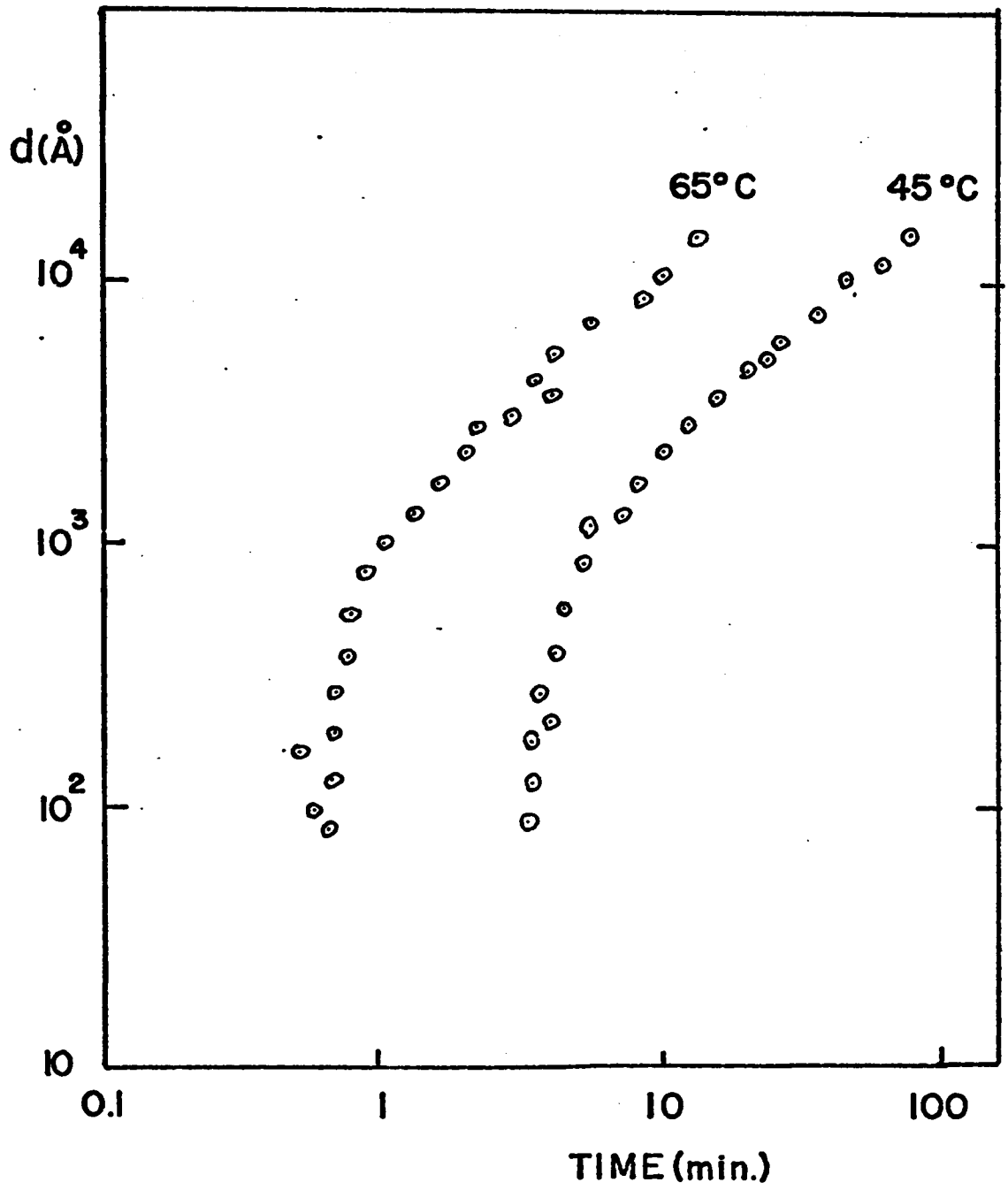

FIGURE 4: Rates of deposition of electroless Ni-P films in pH = 4.3 solution at temperatures of 45°C and 65°C. d is mass-thickness of films (mass/unit surface area) in angstroms.

Upon completion of film deposition, samples were rinsed in distilled water and were allowed to dry in air at room temperature. In the following, films in this condition will be referred to as "fresh films".

The chemical reactions in the electroless solution during film deposition are not accurately understood. Brenner and Riddell (11) proposed the reaction to proceed as

$$NiCl_2 + NaH_2PO_2 + H_2O \xrightarrow{\text{catalyst}} Ni + NaH_2PO_3 + 2\,HCl$$

$$NaH_2PO_2 + H_2O \xrightarrow{\text{catalyst}} NaH_2PO_3 + H_2$$

and Goldenstein et al. (17) describe the reaction as

$$n(H_2PO_2)^- \xrightarrow[\text{catalyst}]{-\,2\,nH} n(PO_2)^-$$

$$2H^+ \rightarrow H_2$$

$$(PO_2)^- + H_2O \rightarrow H(HPO_3)^-$$

$$Ni^{++} + 2H \xrightarrow{\text{catalyst}} Ni^\circ + 2H^+$$

$$(H_2PO_2)^- + 3\,Ni^{++} + 7H \xrightarrow{\text{catalyst}} Ni_3P + 5H^+ + 2\,H_2O$$

The latter set of reactions is the more accurate of the two. It accounts for the phosphorus found (14) in all deposits.

Whatever the accurate description of the reaction is, the main product of the reaction is found to be metallic nickel deposited on the catalytic substrate, along with some phosphorus in the deposit. The P is claimed to form either Ni_2P (24) or Ni_3P (17) compounds with

the nickel. Generally, lower pH values give higher P concentration. The by-product is hydrogen gas that is allowed to escape. As the deposition proceeds, the solution is depleted of nickel and its acidity increases. If this process were permitted, the pH of the solution and consequently the P content of deposits would change during deposition. To prevent film inhomogenities due to this cause, a buffer was added to the solution and excessive amounts of solutions were used in the experiments to grow each film specimen.

2.14 Vacuum Deposition of Nickel. Vacuum deposition of metals from their vapors on solid substrates is well documented (25). Nickel is known (26) to form polycrystalline films on substrates held at room temperature, if the rate of deposition is not too high (preferably a few angstroms per second). These films (as most others) nucleate in small three-dimensional islands of a few angstroms in size, widely separated from each other. As deposition proceeds the islands grow in size and eventually merge to form a continuous film. The critical thickness at which continuity is reached depends on the substrate material, substrate cleanness, rate of deposition, substrate temperature, the type of residual gasses in the chamber and their pressure.

During the present experiments, pure* nickel was thermally evaporated by an electron gun device and the vapor was condensed on freshly cleaned glass and quartz substrates. The vacuum chamber and its components are shown in Figure 5. The substrates were held at room temperature during deposition and the rate of deposition was

---

* Johnson-Mathey and Malloroy 99.98% pure.

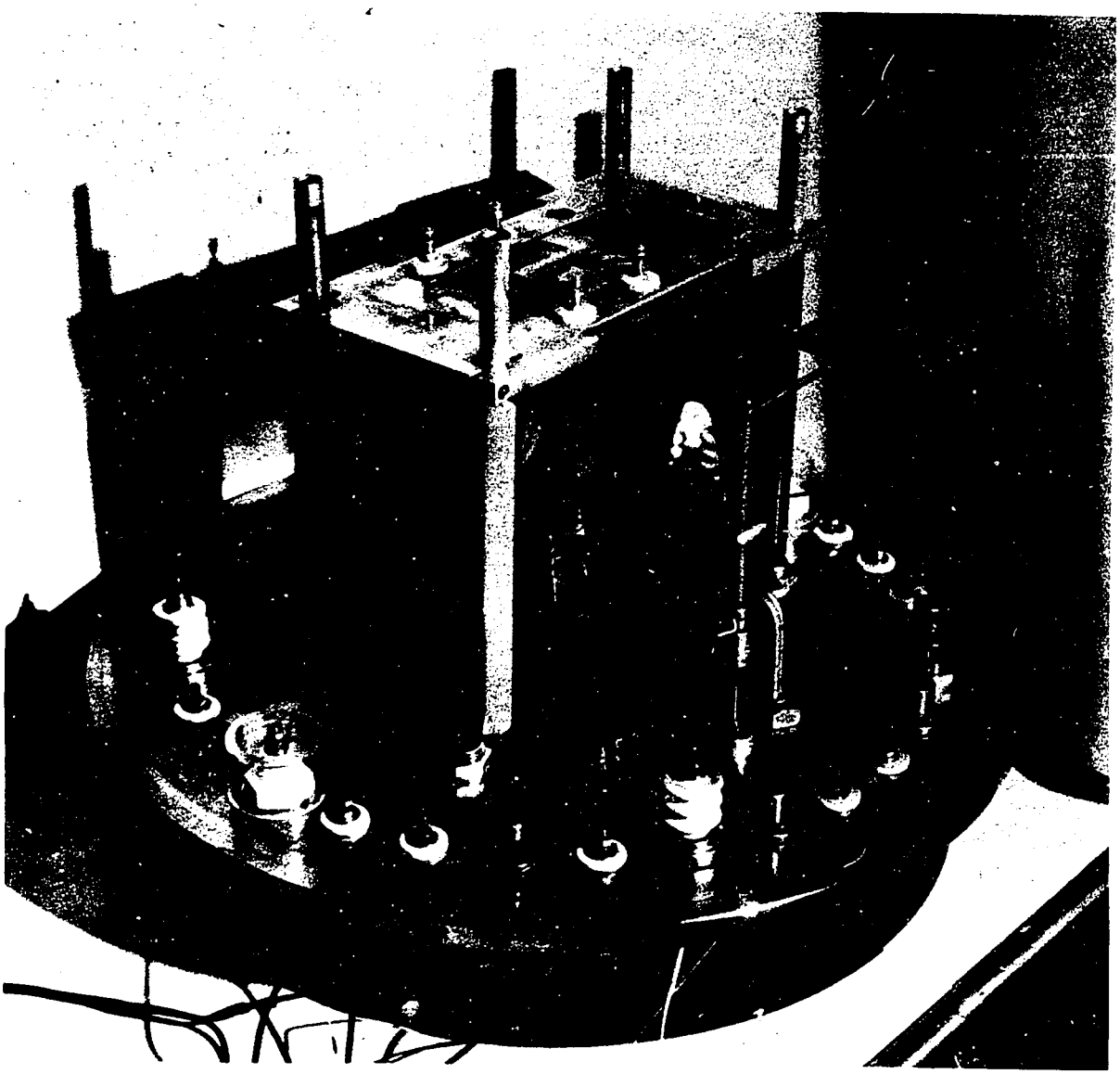

FIGURE 5: Base plate of the vacuum chamber complete with the evaporation source (A) and substrate holder (B).

controlled at 5Å/sec. The pressure during deposition runs was kept below 10^{-6} torr. All nickel films were grown thick enough to be continuous, at which thickness they were determined to be relatively plane parallel. In the following, "fresh" films will be understood to be those just deposited and taken out of the vacuum chamber.

An attempt was made to evaporate Ni-P material, which was initially grown in an electroless solution, but the attempt failed due to the separation of components of the alloy on vaporization. Phosphorus evaporated first, leaving a nickel rich residue behind, thus producing a P gradient in the film. No further attempts were made to vapor deposit electroless nickel.

2.15 Vacuum Heat Treatment of Films. Films that required heat treatment were placed on a heated ceramic plate in the vacuum chamber and were kept at the desired temperature at 10^{-6} torr pressure. The ceramic plate was heated by resistance wire, and the heating current was controlled to maintain the desired temperature. The temperature was measured by a thermocouple in the range 25°C to 600°C. The time rate of heating and cooling was controlled manually by the adjustment of the heating current. The vacuum was always maintained when sample temperature was over 50°C, to prevent oxidation.

2.2 Film Thickness and Density Measurements. In thin film work, two of the most ambiguous quantities are film thickness and film density. When films are discontinuous or non plane parallel, a macroscopic film thickness cannot be defined. Equally, in such cases

the volume of the material on the substrate cannot be measured, therefore the density cannot be calculated. For films of unknown geometry, the best substitute for film thickness is the mass of film material per unit substrate surface area. A thickness may be calculated from this if the film density is known. The thickness is referred to as the mass-thickness (d_m) of the film in the case when the density is taken to be that of the bulk parent material. On the other hand, the thickness referred to as the geometrical thickness (d_{opt}) is the physical measure of the thickness, independent of mass or density.

2.21 Film Thickness Measurements. The thickness of Ni films, both electroless and vacuum deposited were measured in three ways. (i) The mass-thickness was calculated from the measured film mass m, and film area A as $d_m = m/\rho A$ where ρ was taken to be the density of the corresponding parent (bulk) material. The mass was measured with a microbalance with an accuracy of 5×10^{-6} gr. (ii) The geometrical thickness (d_{opt}) was measured directly by multiple beam interference method due to Tolansky (27). The schematic arrangement of the sample film and measuring apparatus is shown in Figure 6, along with a typical interference image. The instrument was a Leitz microscope fitted with a sodium vapor lamp. The spacing of the fringes in the image is $\lambda/2$, which for sodium D lines is 2946Å. The film thickness is given by the height of the steps in the fringe pattern in units of 2946Å. The accuracy of the instrument is about 50Å. This method was used for films whose thickness was greater than 200Å. (iii) The geometrical thickness was also measured indirectly using the reflectance

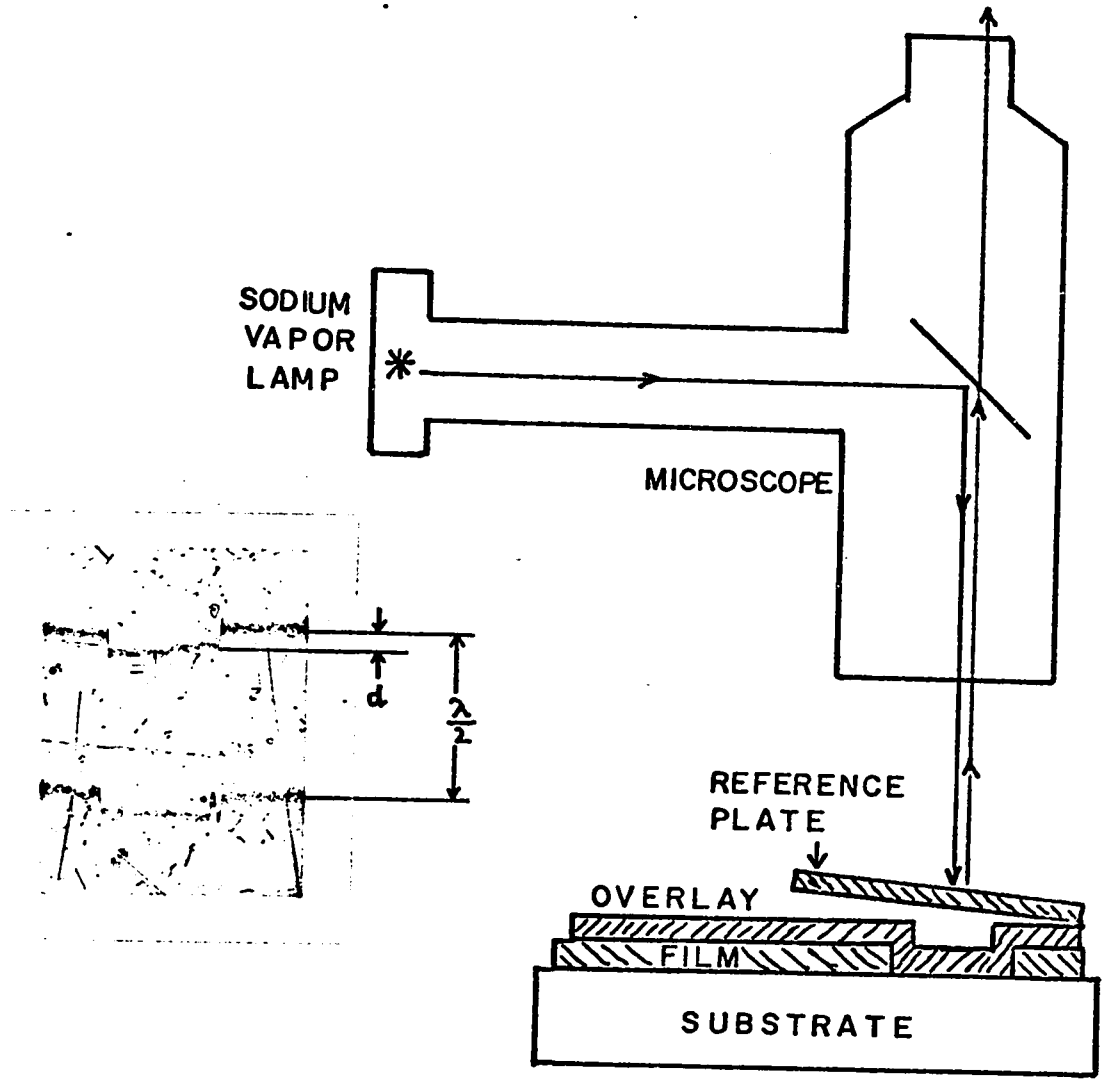

FIGURE 6: Schematic representation of film thickness measurement using a multiple beam interferrometer. The photograph shows the interference fringes of a film. d is the film thickness in units of λ/2.

and transmittance of films. The method will be discussed in 2.5. This method gave very accurate film thickness values for films thinner than 200Å.

2.22 Density Measurements. Film density was defined through

$$\rho_F = \frac{m}{Ad_{opt}} = \frac{d_m}{d_{opt}} \rho_{bulk}$$

and was calculated from the measured quantities m, A and d_{opt}. The definition was restricted to continuous and relatively plane parallel films, as it has no meaning for films of other geometry (e.g. island type discontinuous films). To determine the density of one sample, many film thickness measurements (d_{opt}) were made, to insure uniformity of film thickness, or to calculate a $(d_{opt})_{avg}$ in case of slight thickness variations from place to place on the surface.

The density of self-supporting (bulk) Ni-P samples were measured by an immersion method. The apparatus is shown in Figure 7. The instrument was first calibrated with a 1 gr. platinum plate at room temperature. This was done to establish the amount of force exerted by the surface tension on the suspension wire as a correction factor in the weighing. The calibrated instrument (microbalance, suspension wire and alcohol) was then used for Ni-P deposits. The typical accuracy of this method was found to be 0.1%.

2.3 Electron Microscopy of Films. In the experiments a Philips EM75C and an AEI EM6G electron microscope was used. Both instruments were operated at 75 KV in the transmission mode.

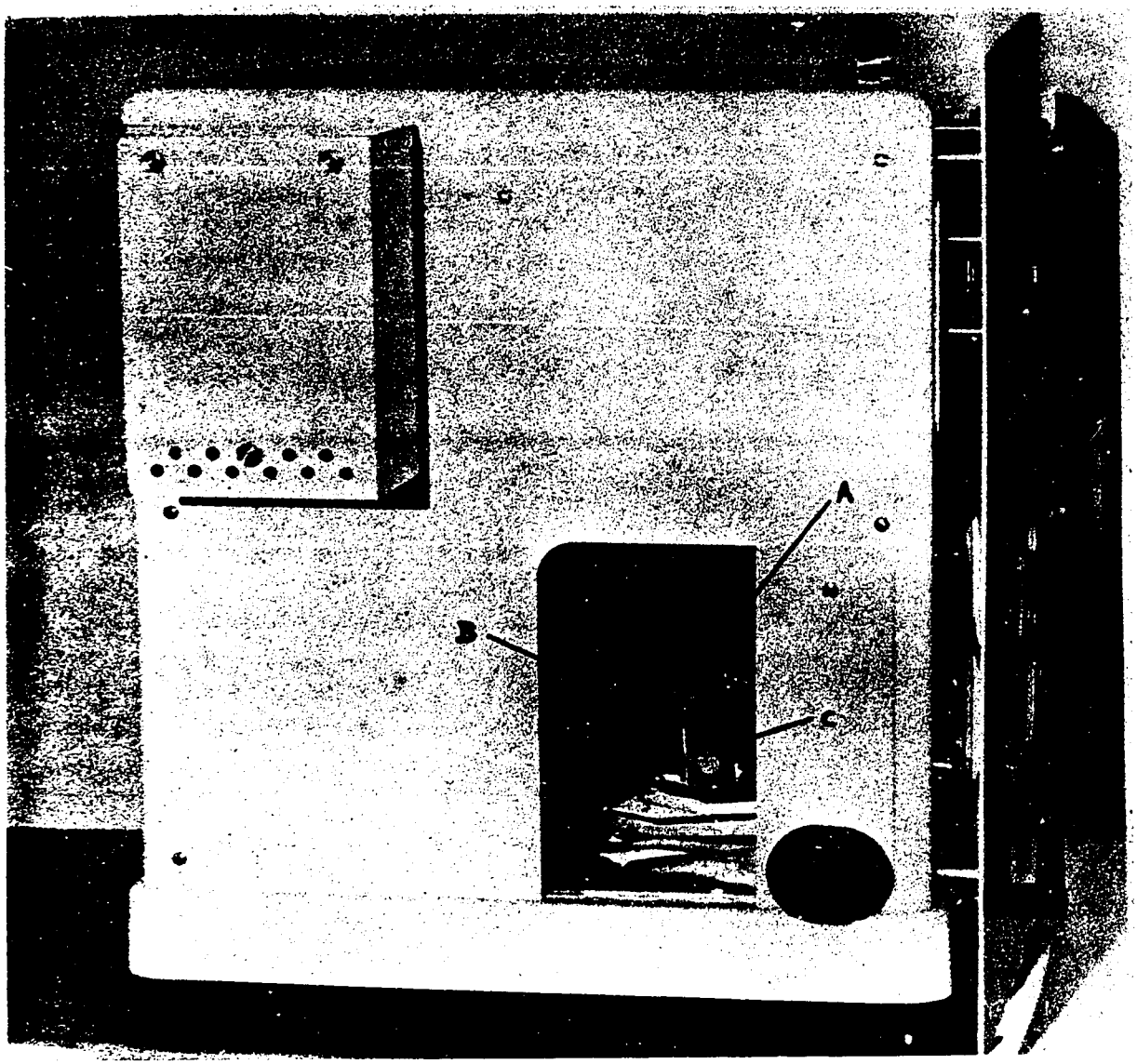

FIGURE 7: Microbalance set up for density measurement. A is fine copper wire; B is alcohol in beaker; C is sample.

The geometry of the films was examined in the electron microscope in three ways. (i) Films that were self-supporting and translucent to the electron beam were examined directly; (ii) Films too thin or discontinuous films were backed by a transparent support and examined in this form; (iii) Films that were too thick to be translucent were examined via surface replicas. The crystal structure of films was examined by transmission electron diffraction in the microscopes directly.

2.31 Direct Transmission Microscopy. Both electroless Ni-P and vacuum deposited Ni films were grown on a number of different substrates for microscope examination. Attempts were made to peel these films off their substrates. When this was successful, the flakes of the film were placed on specimen grids and inserted in the microscope for examination. The images of acceptable samples were also photographed, either on a 35mm film or on 2.5" x 3" plates. Photographic enlargements of the negatives produced the required positive images of the specimens.

Films that could not be peeled off the substrates were grown to the required thickness on substrates coated with substances (e.g. Formvar) soluble in water or some other solvent. On completion of film growth, this layer was dissolved, the film was placed on specimen grids and was examined in the microscope as before.

Very thin continuous films or discontinuous films that were not self-supporting were backed by a transparent structureless support. The support was usually Formvar. These films were grown on the

required substrates and were overcoated by a very thin film ($\sim$ 100Å) of Formvar. The Formvar film was then floated off the substrate together with the nickel film (or islands), placed on specimen grids and examined in the microscope as before.

2.32 Microscopy Using Replicas. Ni and Ni-P films that were too thick to be transparent (> 1000Å) to the 75 KV electron beam, could not be examined in the microscope directly. Instead, transparent surface replicas of these films were made and these were examined in the microscope.

The surface replica of a nickel film utilized Formvar to overcoat the nickel. This Formvar surface replica of nickel film was floated off the nickel and its "nickel side" was shadowed by evaporating a thin film (few tens of angstroms) of platinum on that side at non-normal vapor incidence. The shadowed Formvar replica was then placed on a specimen grid, inserted in the microscope, examined and photographed. The sequence of replica preparation is shown in Figure 8.

2.33 Transmission Electron Diffraction. Thin self-supporting Ni-P films were the only form of films examined by diffraction experiments, as supports of any kind would have altered the diffracted beams and would have distorted the image.

Samples were placed on specimen grids that were part of a special heated specimen holder in the AEI microscope. When heating of the sample was required, DC current was passed through the grid in the holder while the image of the sample or its diffraction pattern was projected on the viewing screen. The power supply to the heating grid

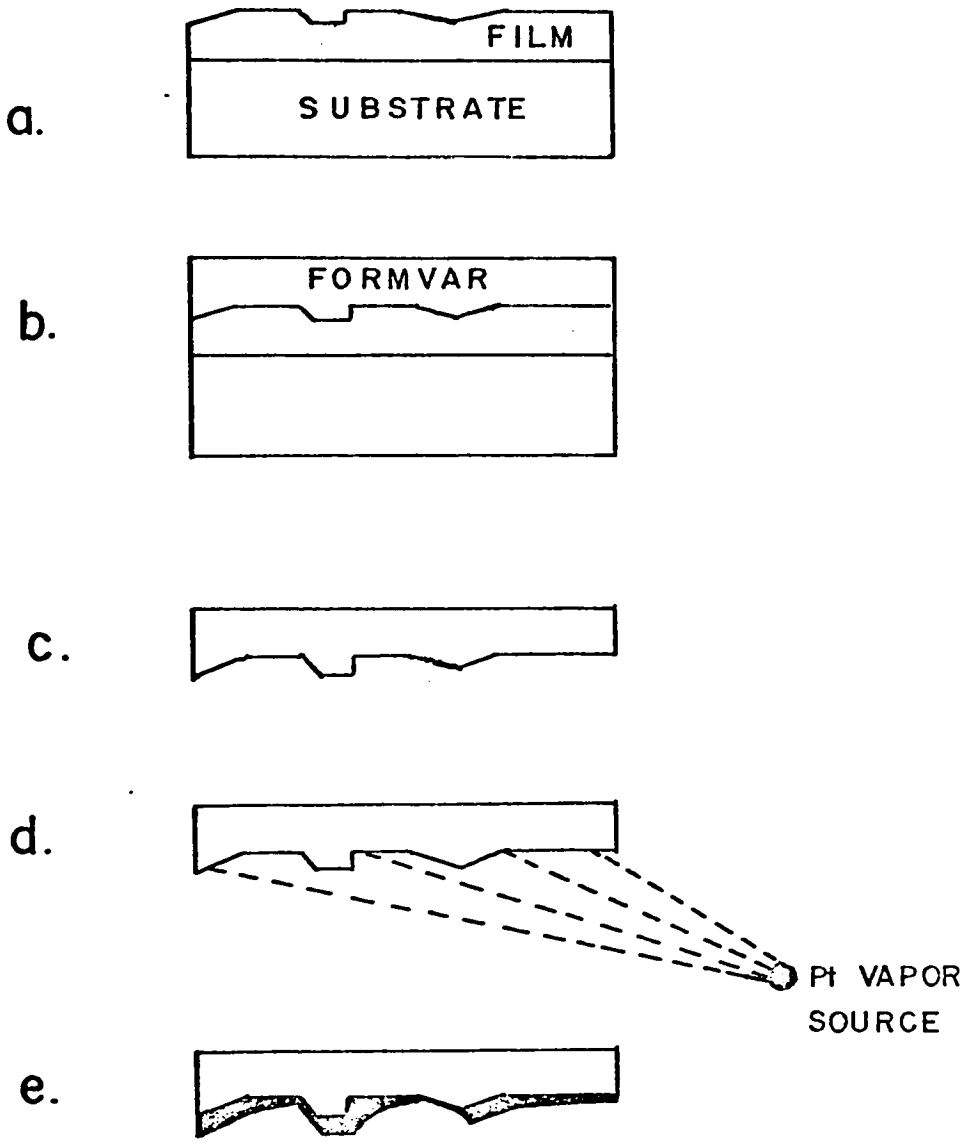

FIGURE 8: Replica preparation of film surfaces for electron microscopy. (a) substrate with film whose surface is to be examined. (b) surface coated with Formvar. (c) Formvar is floated off surface. (d) surface side of Formvar is coated with Pt at an angle to create Pt shadows. (e) shadowed surface replica to be examined in microscope.

was calibrated so that an approximate temperature of the specimen could be inferred from the intensity of heating current. At certain temperatures the image was photographed. The heated specimen holder was utilized in the study of crystalline changes of fresh Ni-P films.

2.4 Electrical Measurements. DC resistivity, deviation from Ohm's law, temperature coefficient of resistivity and Hall voltage of Ni-P films and bulk Ni-P were measured. In these experiments the following definitions were used.

The (scalar) bulk resistivity ρ_B for isotropic and homogeneous metals is defined as $\rho_B = E/J$ where E and J are the electric field strength and the current density respectively. If ρ_B is independent of E, the conductor is said to be ohmic.

The (scalar) film (or surface) resistivity ρ_F for isotropic and homogeneous films is defined as

$$\rho_F = \frac{\rho_B}{d} \qquad [1]$$

where d is the film thickness. The temperature coefficient of resistivity α at T_o is defined as

$$\alpha(T_o) = \frac{1}{\rho_B(T_o)} \left(\frac{\partial \rho_B(T)}{\partial T} \right)_{T=T_o} . \qquad [2]$$

2.41 D.C. Resistivity Measurements. The bulk resistivity ρ_B of film and bulk deposits were determined using two methods. For relatively high resistance film deposits, the film was terminated at the opposite ends of the substrate by thick deposits of platinum, and the resistance

was measured directly by means of a Wheatstone bridge. The surface resistivity ρ_F was calculated from the measured resistance and the rectangular geometry of the film, and ρ_B was calculated from ρ_F and the measured thickness d, using relation [1].

The bulk resistivity ρ_B of thick (bulk) deposits that had relatively low resistance were measured by a method due to Van der Pauw (28) as follows. The resistivity ρ_B of a homogeneous isotropic sample with constant thickness d but otherwise of arbitrary shape is given by

$$\exp\left(-\frac{\pi d}{\rho_B} R_{AB,CD}\right) + \exp\left(-\frac{\pi d}{\rho_B} R_{BC,DA}\right) = 1 , \qquad [3]$$

where

$$R_{AB,CD} = \frac{V_D - V_C}{I_{AB}} \qquad \text{and} \qquad R_{BC,DA} = \frac{V_A - V_D}{I_{BC}} .$$

$V_D - V_C$ is the measuring potential between terminals D and C etc. and I_{AB} is the current measured between terminals A and B etc. The arrangement for both methods is shown in Figure 9.

Deviation from Ohm's law was measured by changing the measuring voltage imposed on the sample (and thus the field strength in the sample) and recording the resulting resistance changes. Care was taken not to heat thin samples by excessive measuring currents.

The temperature coefficient of film and bulk deposits were determined by resistance measurements at various temperatures between liquid nitrogen temperature and a few hundred degrees celsius. From the measured $\rho(T)$ curves α was calculated using relation [2]. Care was taken in the measurements to prevent causing irreversible resistivity changes by heating.

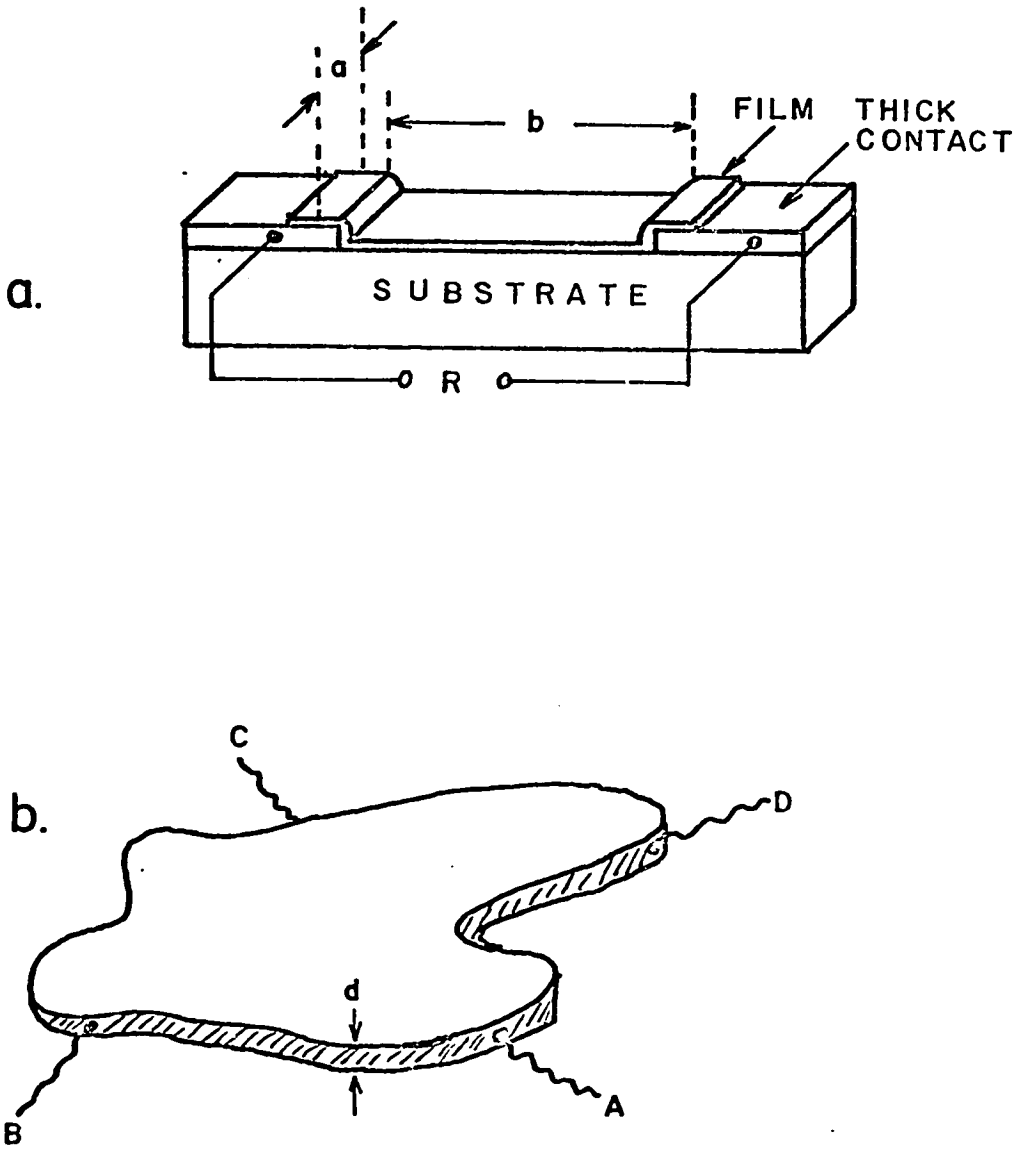

FIGURE 9: Schematic representation of arrangements to measure the DC resistivity of deposits. (a) surface resistivity measurement of a film. (b) bulk resistivity measurement of a plane parallel slab.

2.42 Hall Voltage Measurements. The object of measuring the Hall voltage of Ni-P deposits was to establish the sign of current carriers and to measure the number of carriers per unit volume (N). The arrangement of the magnet and film for measurements of Hall E.M.F. is shown in Figure 10. The magnetic induction over the region of the film was constant at the value of 0.3 Weber/m^2. The Hall EMF was measured with a high impedance ($10^{15}\Omega$) electrometer. The number of carriers was calculated from

$$N = \frac{I\ B}{d\ e\ V_H} \qquad [4]$$

where I is the current in amperes

B is the magnetic induction in Weber/m^2

d is the sample thickness in m

e is the electronic charge in Coulombs, and

V_H is the Hall E.M.F. in volts.

The resulting N has the dimension m^{-3}. The sign of N was determined by the polarity of V_H, the direction of current flow and B, according to the Lorentz force formula.

The measurements were found to be difficult, partly due to the low magnetic field available and partly to the Joule heating in the samples. Meaningful figures for N could not be obtained for thick deposits (bulk samples). However, the accuracy and repeatability was acceptable for films thinner than 5000Å and thus all Hall data pertains to films below this thickness.

2.5 Optical Measurements. Experimentally, the aim of optical measurements on metals is to determine the complex index of refraction

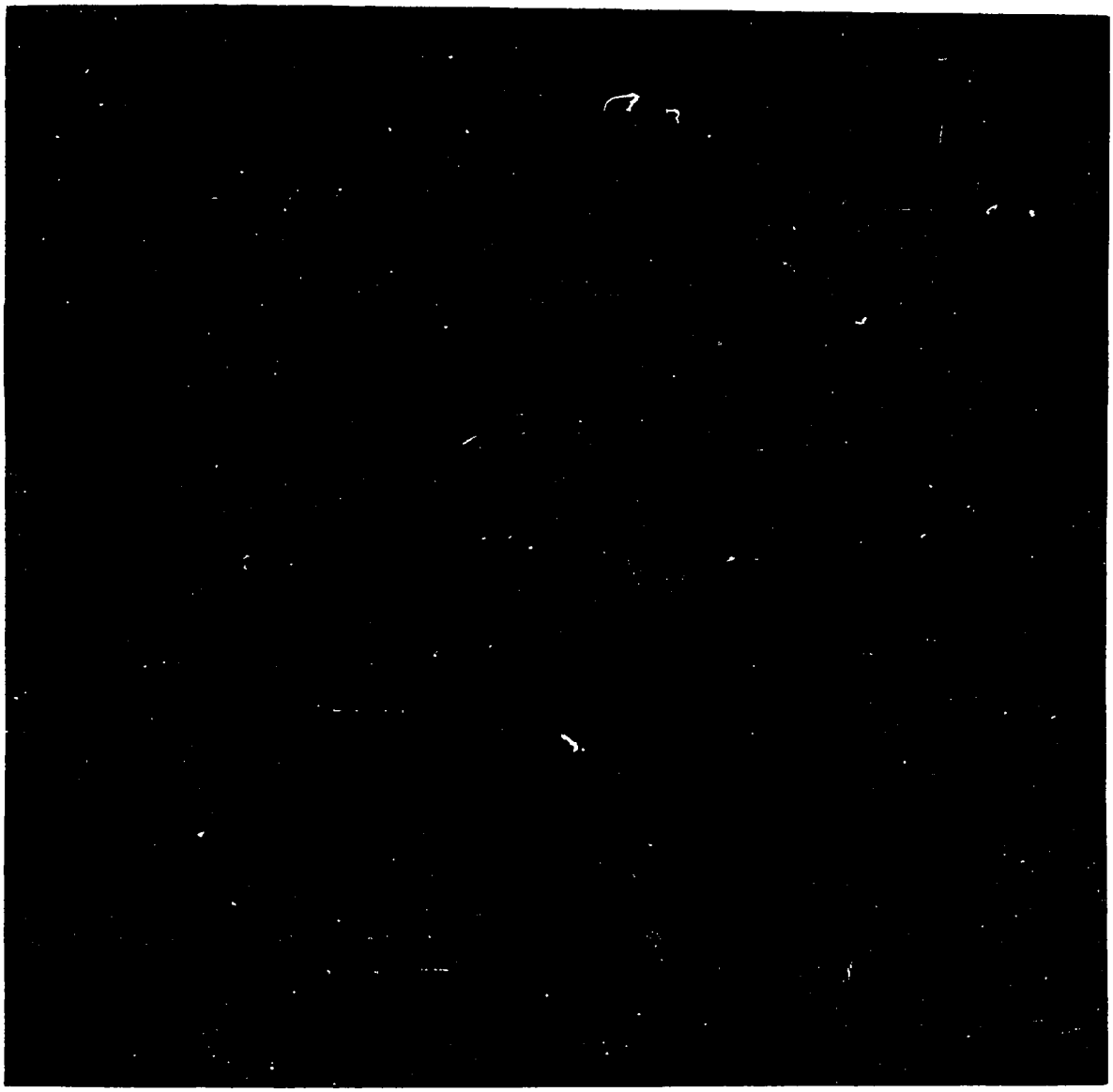

FIGURE 10: Arrangement for Hall effect measurements of nickel films. The magnetic induction in the gap of the permanent magnet was uniform within the extent of the films and measured 0.3 Weber/m^2.

$\tilde{n} = n + ik$, for as wide a wavelength range as possible. The complex index is not a directly observable quantity of materials. The optical quantities that can be directly measured are the intensities of radiation reflected by the surface, or transmitted by the bulk of the solid, and the changes of phase of radiation on reflection and transmission. For bulk metals the transmitted component of radiation cannot be measured, as it is absorbed within the surface. For thin films of metals, usually both the reflected component and the transmitted component can be measured.

Of the large number of possible methods of optical measurements (29), two methods were chosen in this work for the determination of $\tilde{n}$. The one method for $\tilde{n}$ determination known as the Kramers-Kronig analysis (30) was used for bulk (non-transparent) samples and the other, known as the R, R', T method (31) was used for film (transparent) samples. The algebra of the two methods is outlined in Appendices A and B respectively. Both methods involved intensity measurements. The measurements were performed by a modified Beckman DK2A double beam spectrophotometer, generally in the photon energy range of 0.5 - 5 eV (wavelength range of 2500Å - 2.5μ). All optical measurements were performed at room temperature.

In the experiments the following definitions were used. Complex index of refraction $\tilde{n} = n + ik$, where n is called the index of refraction and k is called the extinction coefficient. Note that in an absorbing medium (i.e. $k \neq 0$), n does not have the physical meaning of c/v (c = velocity of light in vacuum, v = velocity in the medium) except in the case of normal incidence. The reflectance R and trans-

mittance T are the reflected intensity and transmitted intensity for unit incident intensity of radiation respectively.

Subscripted R and T, e.g. R_S, R_P etc., denote the polarization of incident radiation. P refers to the linearly polarized radiation whose electric vector is parallel with the plane of incidence, and S refers to the linearly polarized wave normal to the P component.

2.51 Optical Measurements on Bulk Samples. Bulk samples (d > 1mm) of vacuum deposited Ni and electroless Ni-P were grown on polished solid nickel substrates and were used to perform optical measurements in their fresh state, as well as after heat treatment in vacuum at 500°C. The optical measurements were carried out in the integrating sphere of the Beckman spectrophotometer in three steps. First, the homogeneity and isotropy of samples were checked at 45° angle of incidence, then ratios of R_P/R_S were measured at angles of incidence of 45° and 80° and finally $R(\lambda)$ was measured at near normal incidence for $2.5\mu \geq \lambda \geq 0.2\mu$. A schematic representation of the measuring apparatus with the sample arrangement is given in Figure 11.

From the measured data $n(\lambda)$ and $k(\lambda)$ were calculated by computer (for details see Appendix A). The optical constants $n(\lambda)$ and $k(\lambda)$ of a bulk specimen were considered the end result of the experiment i.e. the initial data.

2.52 Optical Measurements on Film Samples. Films of vacuum deposited Ni and electroless Ni-P were grown on quartz and glass substrates, their thickness d_{opt} was measured by the Tolansky (27) method (also c f. 2.2) and were used to perform optical measurements. The films

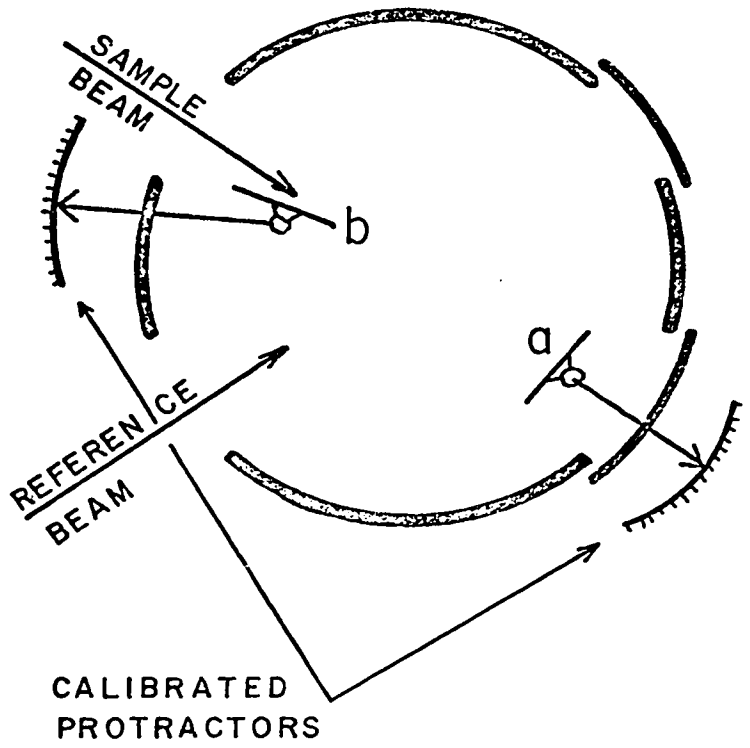

FIGURE 11: Schematic top view of the modified integrating sphere of the DK2A spectrophotometer, complete with sample holders. For small angles of incidence, sample holder (a) is used and for oblique incidence, sample holder (b) is used.

were then heat treated in vacuum at various temperatures up to 500°C, their thicknesses were remeasured and they were again subjected to optical measurements. There were three measurements performed on each film: $R_M(\lambda)$, $R'_M(\lambda)$ and $T_M(\lambda)$. R'_M denotes the reflectance on the substrate side. All three measurements were carried out at near-normal incidence. The sample arrangements in these measurements are shown in Figure 12.

From the three independently measured quantities R_M, R'_M and T_M it is possible to derive $n(\lambda)$, $k(\lambda)$ and d_{opt} uniquely, at least in principle (for details see Appendix B). It was indeed possible to get meaningful and accurate values of n, k and d_{opt} for good homogeneous and isotropic, continuous and plane-parallel films. This is the method for film thickness determination that was referred to in Section 2.21.

Computer calculations of $n(\lambda)$ and $k(\lambda)$ from the measured quantities $R_M(\lambda)$, $R'_M(\lambda)$ and $T_M(\lambda)$ completed the optical experiments of films. The optical constants of a film specimen along with its thickness were considered to be initial data.

In a few instances when the knowledge of only the product of the optical constants n and k was necessary, an approximation (39) was used. The product nk was calculated directly from the measured values of R, T, d and λ as

$$nk = \frac{\lambda}{4\pi d} \frac{1 - R - T}{T} n_D \qquad [5]$$

where n_D is the index of the substrate and d was measured independently by the Tolansky (27) method.

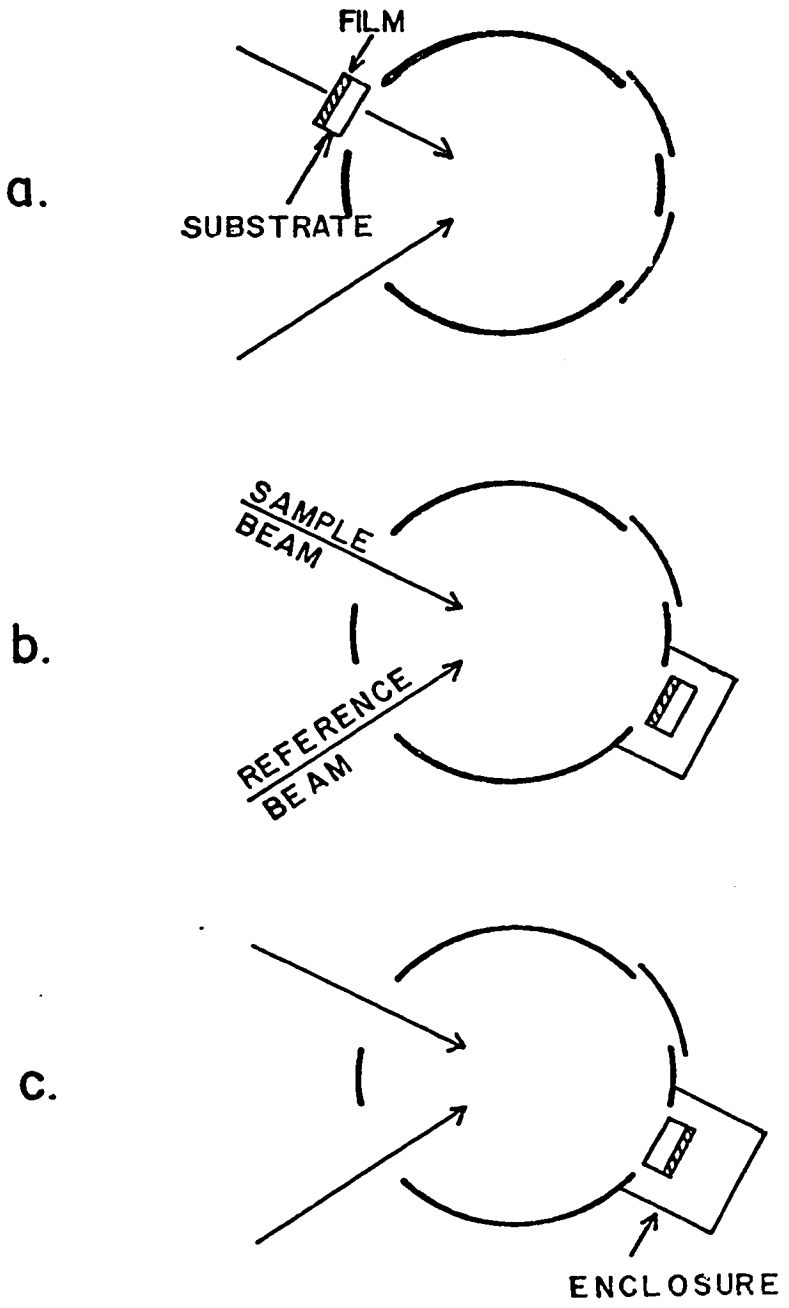

FIGURE 12: Schematic top view of the integrating sphere of the DK2A spectrophotometer with samples in place for the measurements of (a) transmittance T_M, (b) reflectance from the film side R_M and (c) reflectance from the substrate side R'_M.

CHAPTER 3

EXPERIMENTAL RESULTS

Numerical results of the present experiments are tabulated below with little or no interpretation. These results will serve as data in Chapter 4 and will be interpreted there. An exception to this is the nucleation, growth and structure of Ni-P films: Experimental results concerned with this topic are fully discussed and interpreted in this part because an understanding of film growth and structure is necessary for the discussion in the sections that follow.

3.1 Nucleation, Growth and Structure of Films. The nucleation, growth and structure of electroless Ni-P films have not been studied, consequently very little information was available from the literature. As an understanding of film geometry and structure is essential in the study of electrical and optical properties of films, the growth and structure of Ni-P films were examined as part of this research.

In the literature, fresh bulk electroless Ni-P deposits are stated to be either amorphous (17) or polycrystalline (18). Electroless films of Co-P and Ni-Fe-P deposited on activated substrates were shown (33 - 35) to have an island-type growth and agglomerated structure. Judge et al. (33) found a "hemispherical clumpy growth" of

Co-P, and the surface of electroless Ni-Fe-P was reported by Schmeckenbecher (34) to consist of an "agglomeration of balls". Frieze and Weil (35) reported that nucleation of electroless Co-P films occurred on isolated Pd particles on the activated substrate, followed by lateral growth tc produce a continuous film. Our findings show a similar nucleation and growth for Ni-P films. The structure of fresh Ni-P films was found to be liquid-like. On heating the films the structure changed to crystalline.

3.11 Nucleation and Growth of Films. The deposition of Ni-P from solutions listed in Table II on substrates activated according to the method in Table I was found by electron microscopy to be selective. Deposition appeared to start at certain points on the substrate and continue at these points only. As deposition progressed, islands formed on these nucleation points. If deposition was allowed to proceed, the islands grew in size and eventually merged to form a continuous film. Figure 13 is an electron microscope transmission image of a typical deposit. Parts of the deposit are islands, other parts are already continuous. In contrast with the island-type growth, Ni-P deposits that were formed on bulk nickel substrates and on nickel and palladium coated microscope slides (Ni and Pd were deposited in the vacuum) were homogeneous and showed no island structure. The electron microscope image of a shadowed surface replica of such a deposit is reproduced in Figure 14.

These findings show that the surface of a $SnCl_2$ - $PdCl_2$ treated dielectric substrate is not completely activated. The activation is visualized to produce small catalytic sites dispersed on the surface,

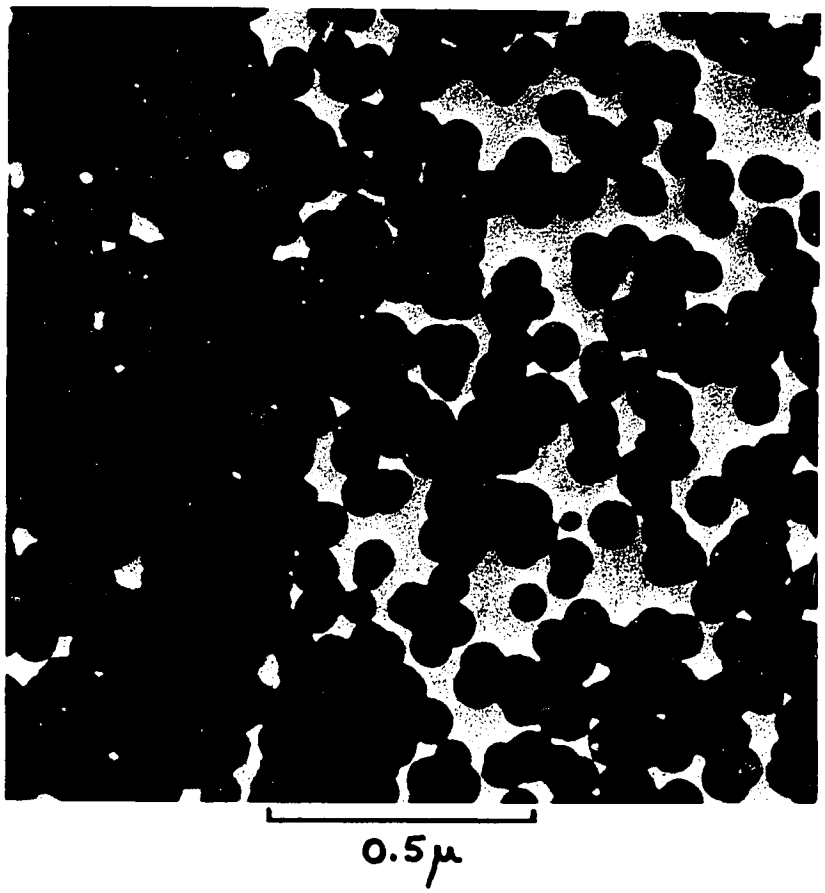

FIGURE 13: Electron microscope transmission image of a typical Ni-P deposit on $SnCl_2$-$PdCl_2$ activated substrate. Parts of the deposit are islands, other parts are continuous.

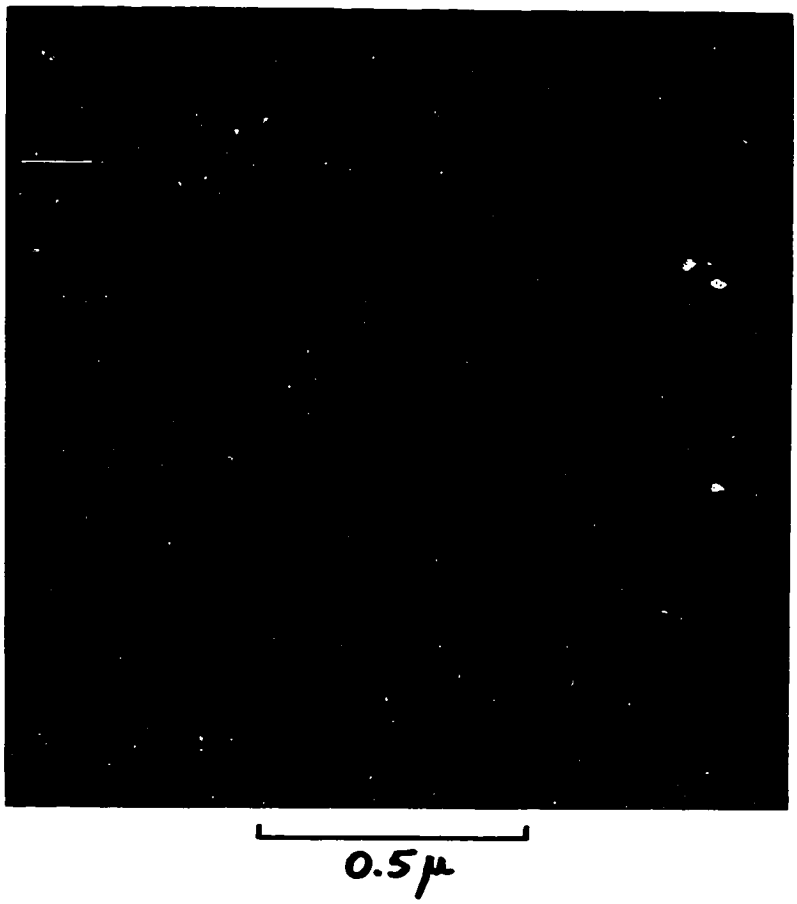

FIGURE 14: Shadowed surface replica of a Ni-P deposit on a solid nickel substrate. Note the absence of islands.

serving as the nuclei for Ni-P deposition. The sites were estimated to be less than 30Å in diameter, as they could not be detected in the electron microscope having a point resolution of 30Å. A closer estimate of size of the catalytic sites was made indirectly; the diameter (2r) of the growing Ni-P islands was measured and was plotted against deposition time. This is shown in Figure 15. The diameter of catalytic sites was estimated by extrapolation (dotted line), to be less than 10Å.

Again from Figure 15, the microscopic time rate of Ni-P growth c(= dr/dt) is seen to be constant. Also, the geometry of growing islands was observed to be circular in all deposits. These findings imply isotropic growth, and one expects the islands to be half spheres situated base down on the substrate. The circular geometry is shown in Figure 16 for islands ranging in size from 200 to 2000Å.

The number of activation sites per unit surface area σ was found to be different for different substrates. The value of σ ranged from $10/\mu^2$ to $10^4/\mu^2$. The value of σ was large on substrates with hydrophilic surfaces (i.e. glass), and small on those with hydrophobic surfaces (i.e. Formvar). This is shown in Figure 17. Figure 17a is the transmission image of sites on glass, and Figure 17b is the image of sites on Formvar. The respective average values of σ are $10^4/\mu^2$ and $10^2/\mu^2$. It was found possible to decrease the difference in σ between hydrophilic and hydrophobic surfaces by adding isopropyl alcohol (10 cc/ℓ) to the activating solutions (cf. Table 1), and to eliminate the difference by adding Kodak "Photo-flow" (5 cc/ℓ) to the activating solutions. In both cases the small σ increased and the large σ remained constant. Attempts to increase the value of σ beyond $10^4/\mu^2$ failed.

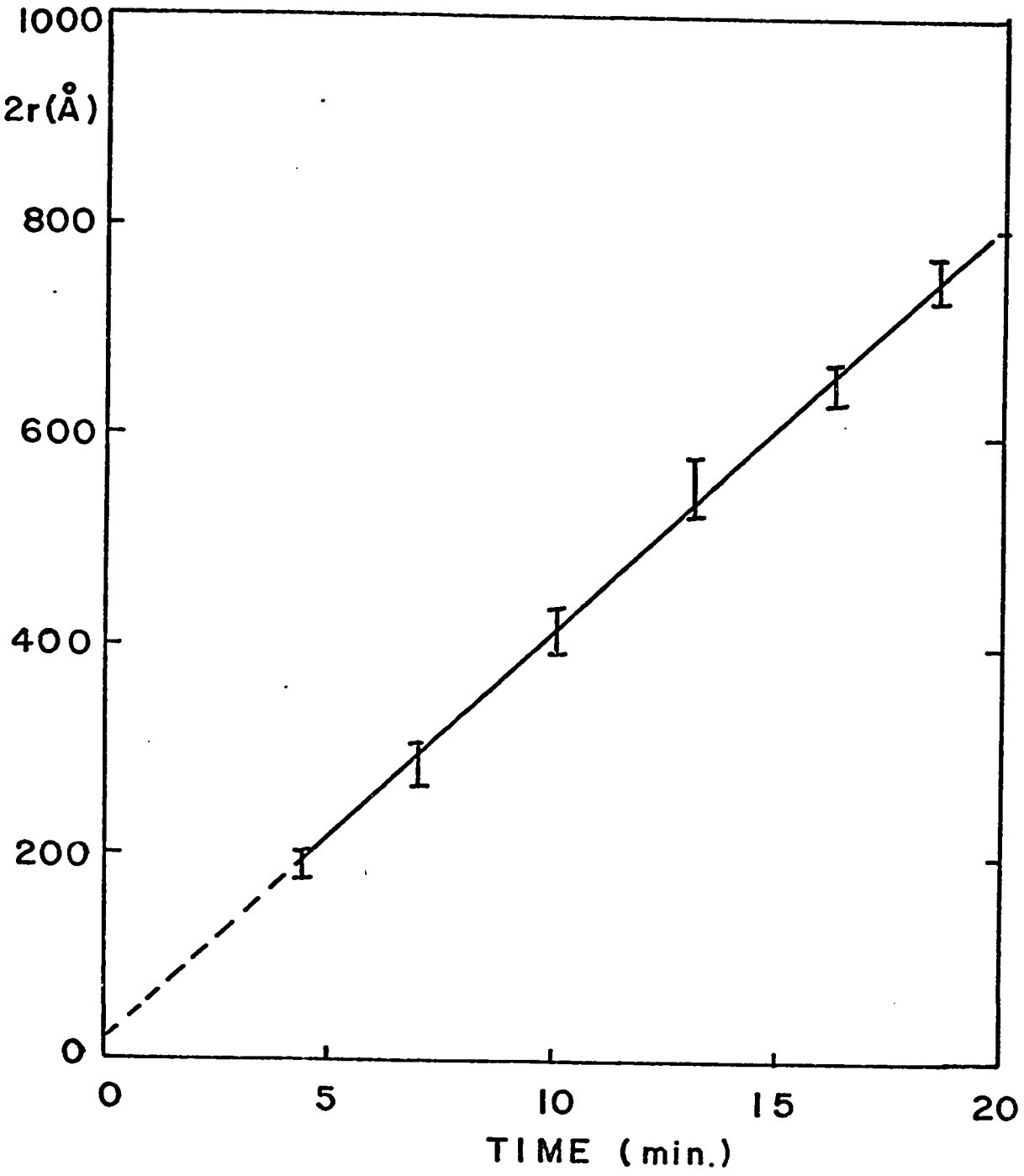

FIGURE 15: Plot of diameter (2r) of the growing Ni-P islands against time of deposition. Rate of growth c = dr/dt is constant. Extrapolation (dashed line) at t = 0 gives average size of active sites to be less than 10Å.

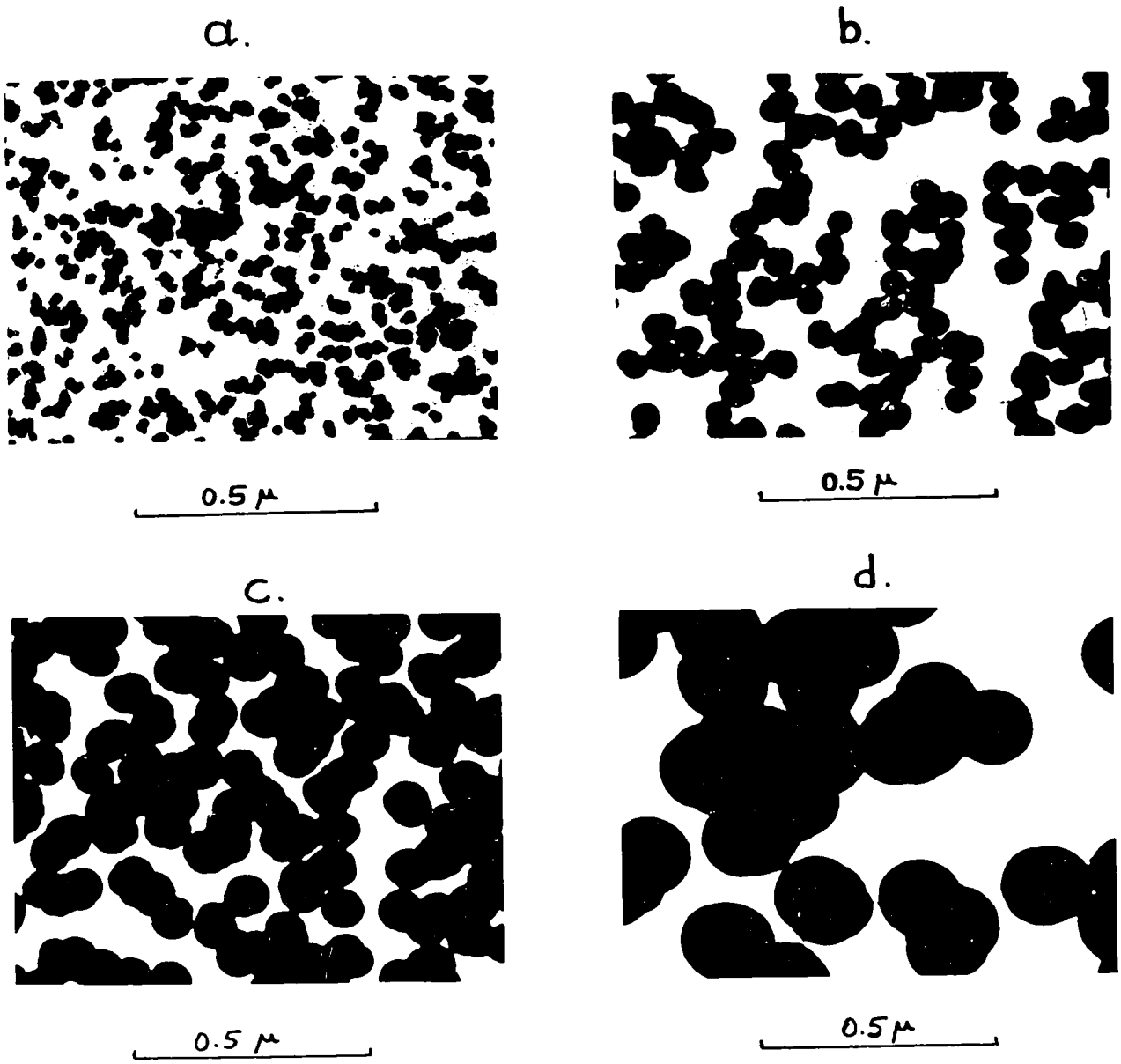

FIGURE 16: Circular transmission images of islands ranging in size from 200Å to 2000Å in four different deposits (a, b, c, d). The islands are visualized to be half spheres situated "base down" on the substrate for all deposits. (a) island size 200Å, (b) island size 600Å, (c) island size 1000Å, (d) island size 2000Å.

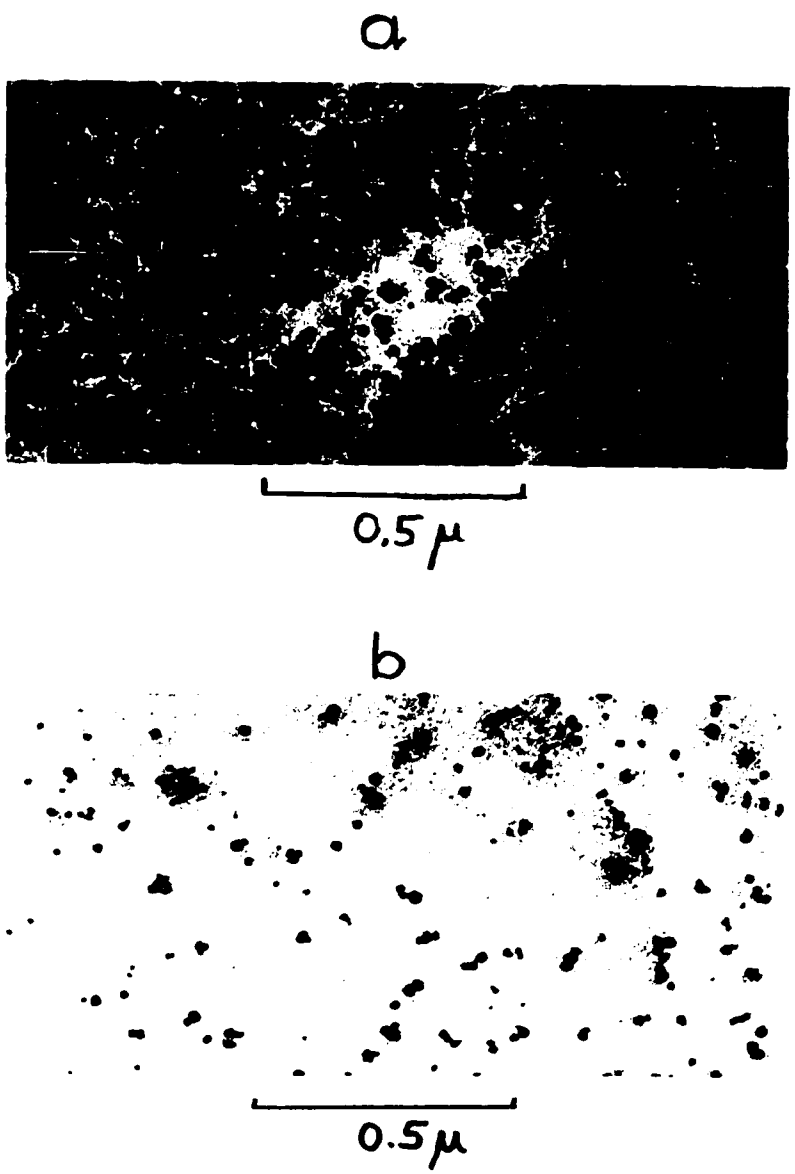

FIGURE 17: Transmission images of active sites on (a) glass, and (b) Formvar substrates made visible by a slight deposit of Ni-P on them. The surface density of sites is $10^4/\mu^2$ for glass and $10^2/\mu^2$ for Formvar.

3.12 Film Geometry. The natural consequence of the variation of σ is a variation in Ni-P film geometry. This is shown in Figure 18 by the transmission image of three different deposits. The films were deposited on substrates with average σ values of $10^4/\mu^2$ (Figure 18a); $10^3/\mu^2$ (Figure 18b) and $10^2/\mu^2$ (Figure 18c). The quantitative dependence of film growth and geometry on σ may be expressed (see Appendix C) as

$$d = 2\pi\sigma ct\left(r_o^2 + r_o ct + \frac{1}{3}c^2t^2\right); \quad 0 \le t \le (c\sqrt{\sigma\pi})^{-1} \qquad [6]$$

and

$$d = 2r_o(1 + r_o\sqrt{\sigma\pi}) - \frac{1}{3\sqrt{\sigma\pi}} + ct; \quad t \ge (c\sqrt{\sigma\pi})^{-1} \qquad [7]$$

where d is the mass-thickness of deposit; c is the microscopic rate of deposition (increase of local thickness per unit time and/or dr/dt); σ is the activation surface density (number of active sites per unit surface area); $2r_o$ is the diameter of active sites; and t is the time of deposition. Expression [6] describes the growth of discontinuous (island-type) films and the description of growth after continuity is attained is given by expression [7]. Transition from the former to the latter configuration occurs at $t = (c\sqrt{\sigma\pi})^{-1}$.

Figure 19a is the plot of expressions [6] and [7] at $r_o = 5\text{Å}$. The dashed line represents the transition between discontinuous films (below dashed line) and continuous films (above dashed line) and the solid straight line represents a linear (d = ct) film growth. In Figure 19b a comparison is made between the mass-thickness of growing deposits and the theoretical curves. Both solid Ni and $SnCl_2$ - $PdCl_2$ activated substrates were used. With $c = 20\text{Å/min}$, σ was found to

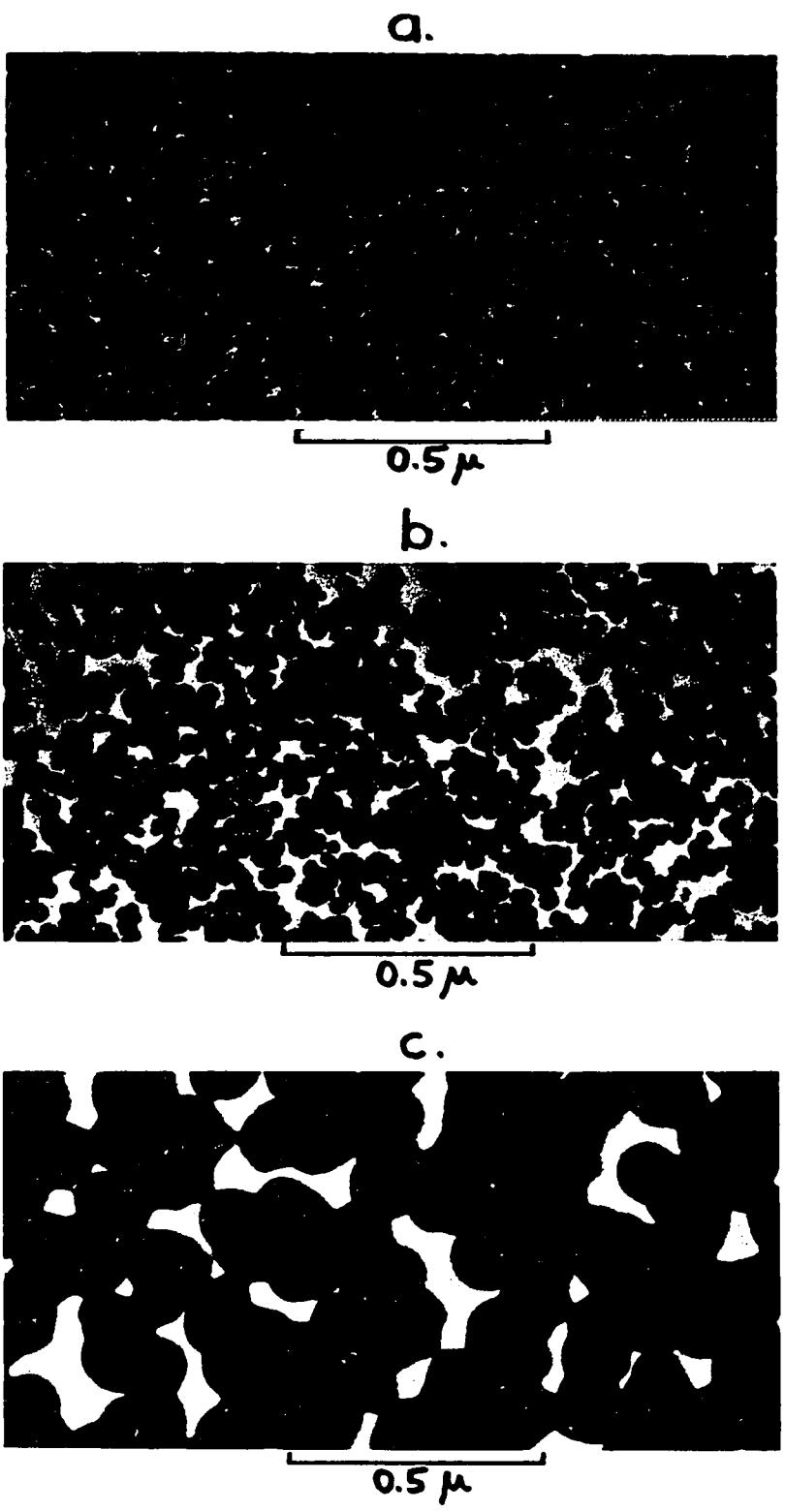

FIGURE 18: Transmission images of Ni-P films on substrates with different activation densities. (a) $10^4/\mu^2$, (b) $10^3/\mu^2$, (c) $10^2/\mu^2$. Note the dependence of film geometry on activation density.

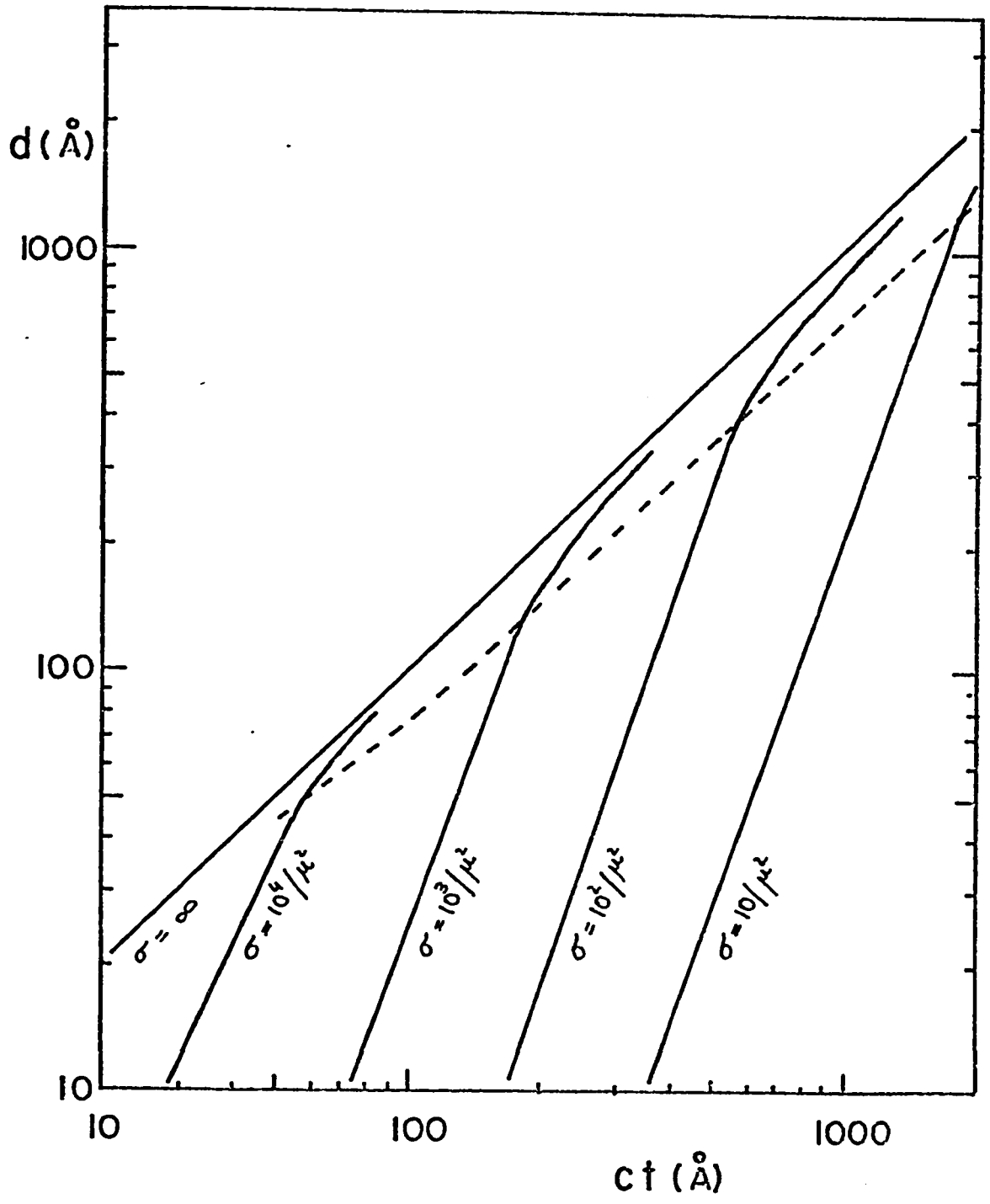

FIGURE 19a: Mass thickness d of Ni-P deposits. Theoretical curves of d as a function of ct calculated from relations [6] and [7] for different activation densities σ . The dashed line represents transition between islands and continuous film.

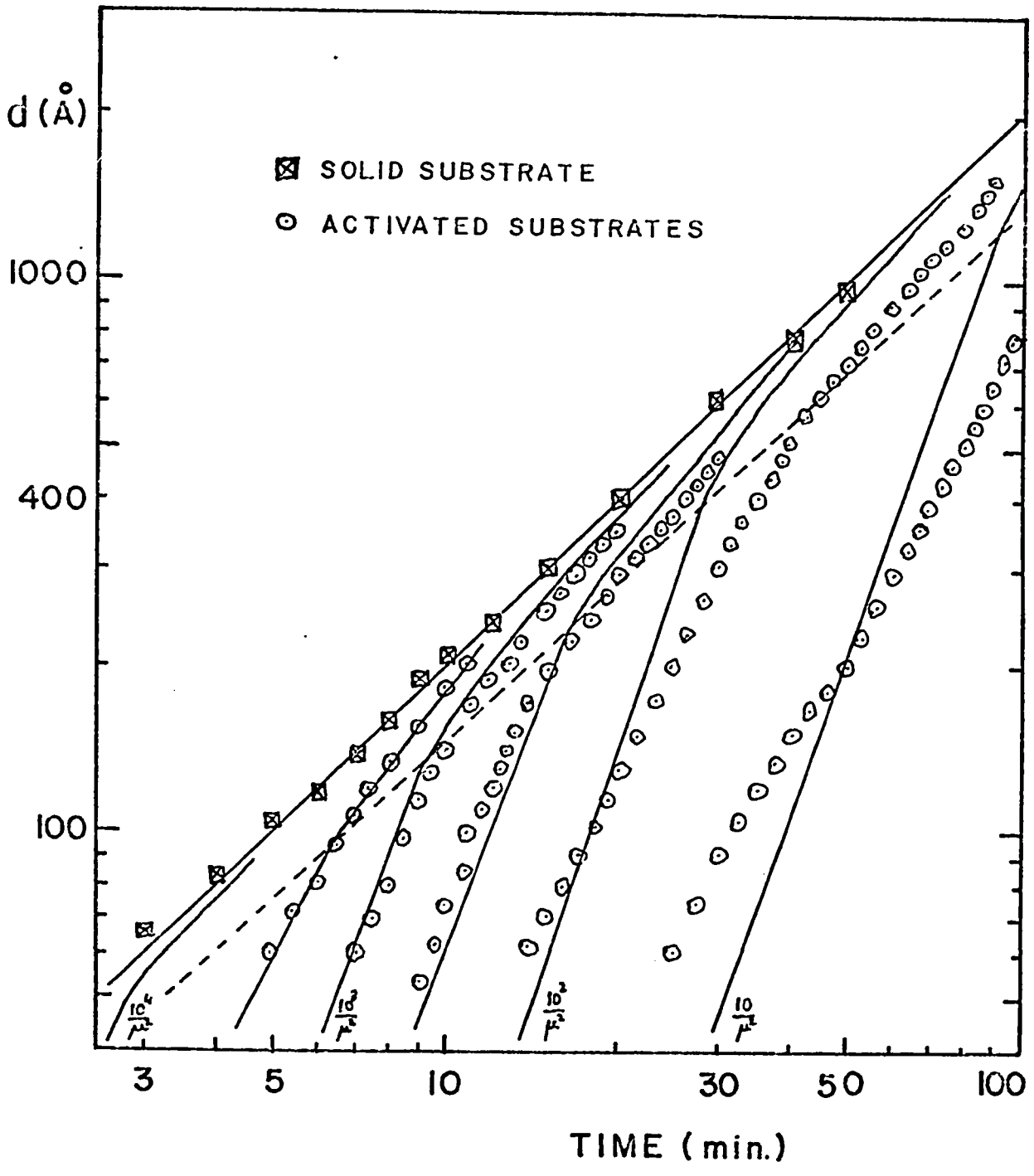

FIGURE 19b: Mass thickness d of Ni-P deposits. Comparison of theoretical curves 19a and experimental values for c = 20Å/min. ⊙ activated substrates, ⊠ solid Ni substrate. Activation density is seen to range between $10^4/\mu^2$ and $10/\mu^2$.

range between $10^4/\mu^2$ and $10/\mu^2$ for the activated substrates, in agreement with our previous results.

The constant rate of microscopic growth and the island type geometry of films thus accounts for the non-linear macroscopic growth pattern of films that were found previously (cf. Figures 3 and 4).

Subsequent to these findings, for all electrical and optical experiments, care was taken to provide a maximum nucleation density for Ni-P films deposited on dielectric substrates. Consequently films grown under such conditions were continuous for thicknesses greater than 100Å, and had a maximum island size of 150Å.

3.13 Structure of Fresh Films. The crystal structure of fresh Ni-P bulk deposits has been investigated in the past with somewhat conflicting results. Goldenstein et al. (17) found an amorphous liquid-like structure for bulk deposits by x-ray diffraction; while Graham and co-workers (18) found fresh bulk deposits to be polycrystalline using electron diffraction.

Fresh Ni-P film deposits grown in the present experiments were found to be liquid-like, regardless of growth conditions, film geometry or P content. The electron diffraction patterns showed a liquid-like halo and one or two very broad concentric rings. Typical electron diffraction patterns of two films along with their transmission images are reproduced in Figures 20. The film in Figure 20a consists of small islands and in Figure 20b consists of large islands.

The patterns allow the existence of very small crystallites as the diffraction resolution of the electron microscope is a few tens of angstroms. The similarity of the diffraction patterns 20a and 20b shows

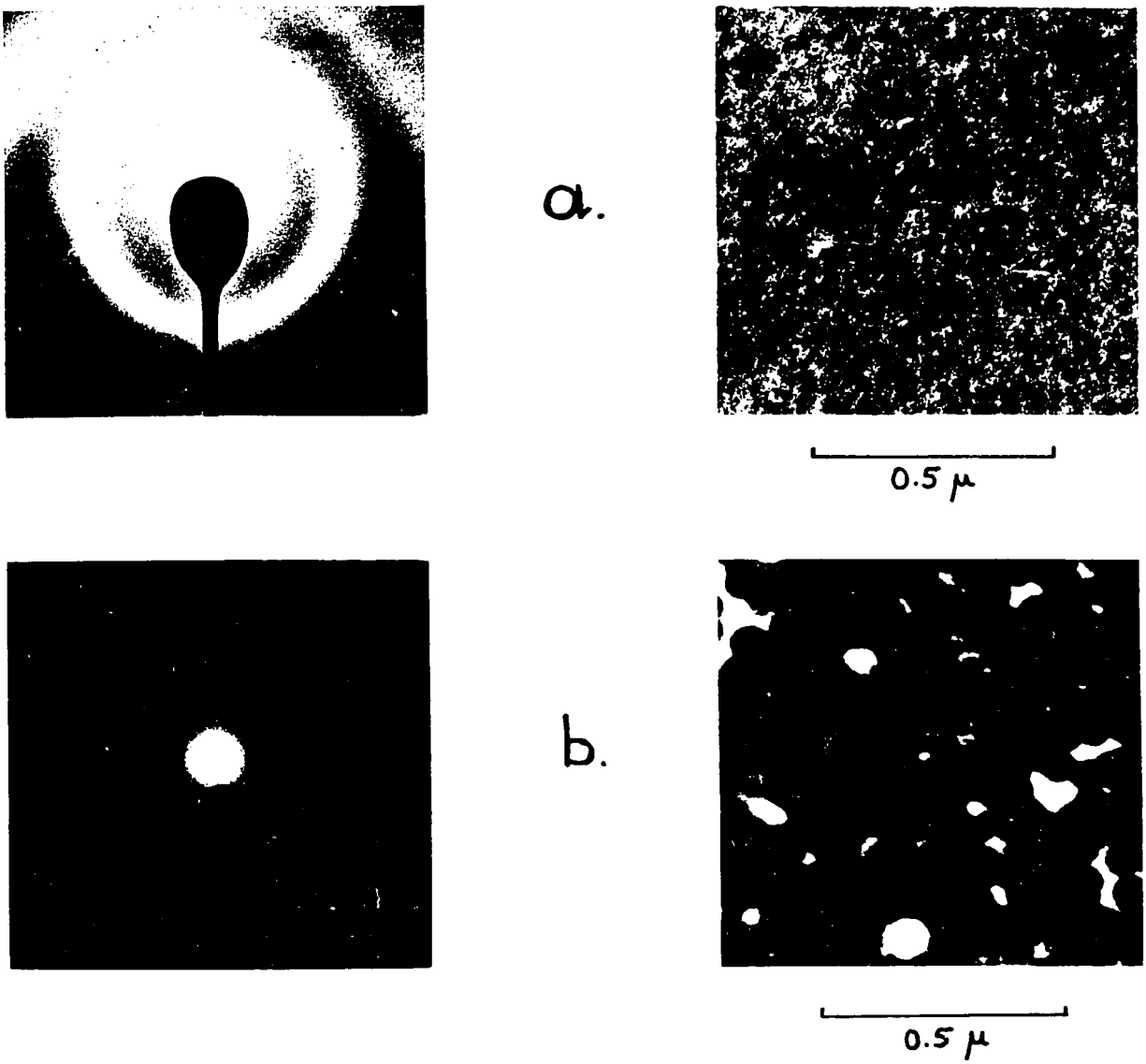

FIGURE 20: Diffraction patterns and transmission images of two Ni-P films in the as-deposited (fresh) condition. (a) film consisting of small islands, (b) film consisting of large islands.

however that the individual islands are not single crystals. The structure of individual islands in discontinuous films, or of the islands in continuous films, may thus be either amorphous or extremely fine polycrystalline.

The present findings of a liquid-like structure is in apparent contradiction with the crystalline interpretation of Graham et al. (18). However the difference may be explained by the difference in sample preparation. In their experiments, thick deposits were prepared at 90°C for many hours and they may have crystallized during growth, whereas our thin samples were grown at 25°C for only a few minutes and remained liquid-like.

3.14 Structure of Heat Treated Films. Fresh Ni-P films, either continuous or discontinuous, were found to undergo a drastic structural change upon heating in the vacuum. Fresh films placed on the heated specimen holder of the AEI microscope showed a liquid-like structure while the temperature was slowly increased from room temperature to a temperature between 300°C and 500°C. At this temperature the patterns changed seemingly instantaneously to a definite crystalline one. Subsequent increases of temperature up to 750°C did not change the patterns. Figures 21 illustrate this change. 21a is the diffraction pattern of the film heated in the microscope whose fresh (liquid-like) pattern is shown in Figure 20a. Similarly 21b corresponds to 20b.

Heated continuous films appeared from the patterns to be polycrystalline with crystallite sizes of the order of a few thousand angstroms. Patterns of heated discontinuous films indicate that the

a.

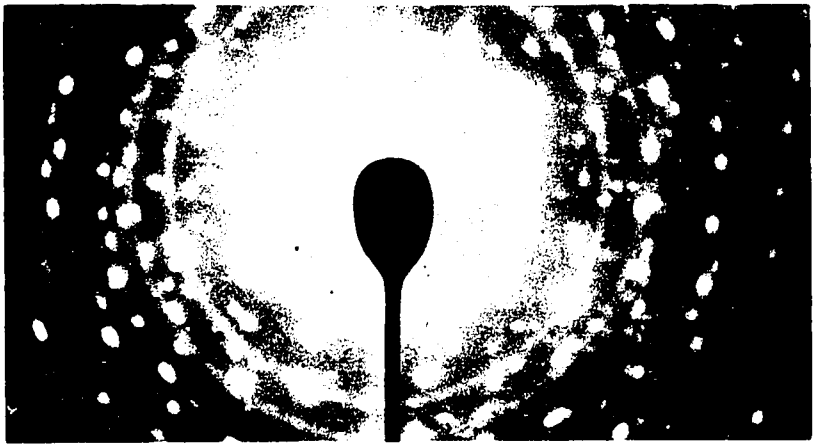

b.

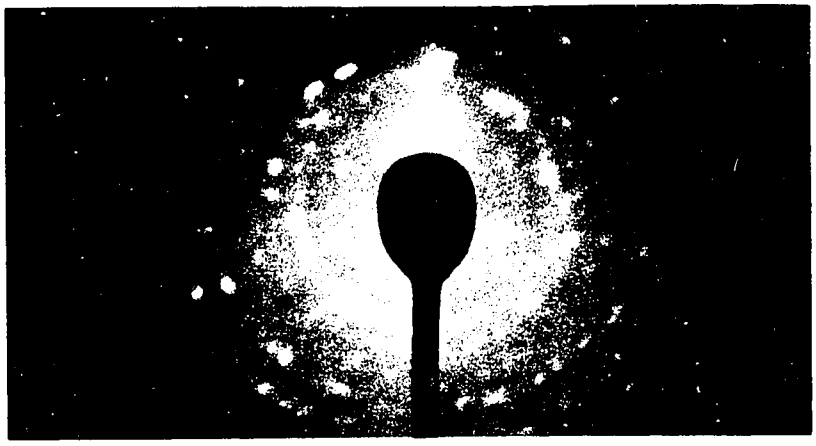

FIGURE 21: Diffraction patterns of the Ni-P films in Figures 20a and 20b after heating in the vacuum. The changes occurred at a temperature between 300°C and 500°C. Figures a and b correspond to those in Figure 20 respectively.

individual islands in the film become single crystals. The orientation of crystallites appeared to be random.

3.2 Density of Deposits. The bulk density of pure Ni at room temperature was taken to be 8.90 gr cm^{-3} (36). The densities of vacuum deposited Ni films and electroless Ni-P films were measured, as no data was available from the literature.

3.21 Density of Bulk Ni-P Deposits. The density of bulk Ni-P deposits was reported (14) to range from 8.90 to 7.65 gr cm^{-3} at P concentrations ranging from 0 w/o to 16 w/o respectively. The density of bulk deposits grown in this work, using pH = 5.3, 4.3 and 3.3 solutions and vacuum heat treated at 500°C for one hour, was determined. The P content of these samples was determined by neutron activation analysis* independently. The density values agree well with predicted values (14) based on the assumption that Ni-P deposits consist of Ni_3P + Ni (17). The calculated curve, together with the measured values, are shown in Figure 22.

3.22 Density of Ni and Ni-P Films. Measurements of densities of vacuum deposited films (25),(26),(32) generally indicate density values less than those for the bulk parent material. In some cases the low density is due to (two-dimensional) film discontinuity (26), in others, due to a (three-dimensional) "spongy" structure (25) of films.

The results of density measurements on vacuum deposited Ni and electrolessly deposited Ni-P films (pH of solution = 5.3) in their

---

* Neutron activation analysis was done by the Atomic Energy of Canada Ltd.

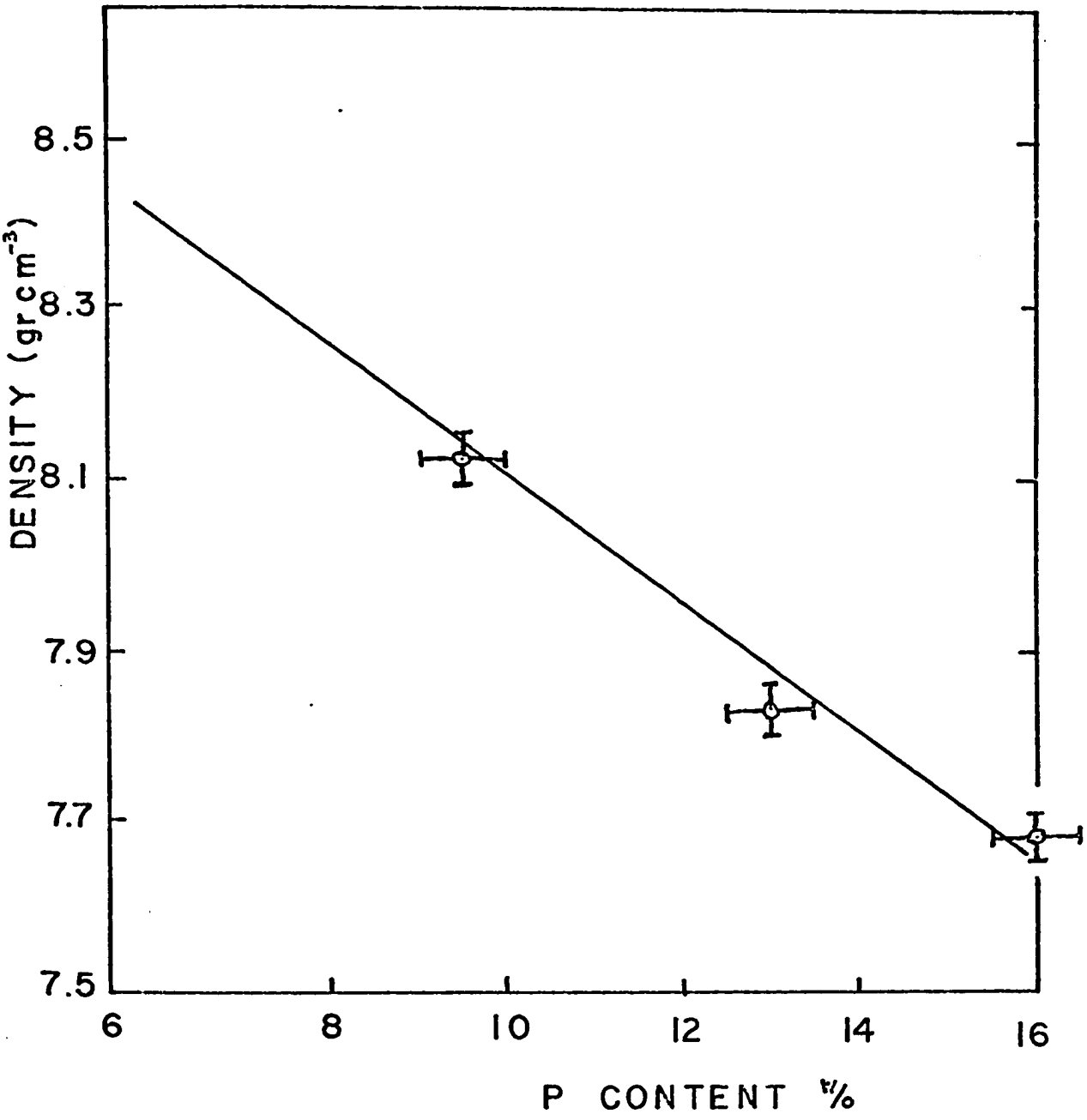

FIGURE 22: The phosphorus-dependent density of bulk Ni-P deposits. The solid line is the calculated density for Ni_3P + Ni from reference (14). The experimental values ⊣⊙⊢ are the densities of vacuum heat treated bulk Ni-P deposits whose P content was measured independently.

fresh and vacuum heat treated state are shown in Figures 23a and 23b respectively. Ni films were heat treated at 200°C and 500°C, and Ni-P films at 500°C, both for one hour. During heat treatment the Ni-P films suffered a loss of mass of up to 3%.

Note from Figures 23 the changes of density due to vacuum heating. Thin Ni films decrease their density while most Ni-P films increase their density.

3.3 Electrical Constants of Deposits. The room temperature DC resistivity of pure nickel was taken for reference to be $6.844 \cdot 10^{-6} \Omega$ cm, and its temperature coefficient α to be $6.81 \cdot 10^{-3}\ °C^{-1}$ (36).

3.31 Bulk Deposits. The room temperature resistivities ρ_B of bulk Ni-P deposits grown from the three solutions listed in Table II, and heat treated at 500°C in vacuum, ranged from $35 \cdot 10^{-6} \Omega$ cm to $60 \cdot 10^{-6} \Omega$ cm. This is in agreement with the results of Brenner et al. (37). The resistivity values for different P concentration along with the results of Brenner et al. (37) are plotted in Figure 24.

The resistivities $\rho_B(T)$ were also measured at temperatures between liquid nitrogen temperature and 200°C. For all samples the slope was positive and constant, indicating metallic conduction (see e.g. Kittel (40)). Typical $\rho_B(T)/\rho_B(25)$ curves for Ni-P bulk deposits are shown in Figure 25, where $\rho_B(25)$ denotes the room temperature resistivity.

Measurements of Hall voltage on bulk Ni-P deposits could not be made due to limitations of the measuring apparatus. Thus the carrier density (N) and its variation with the P content of samples could not

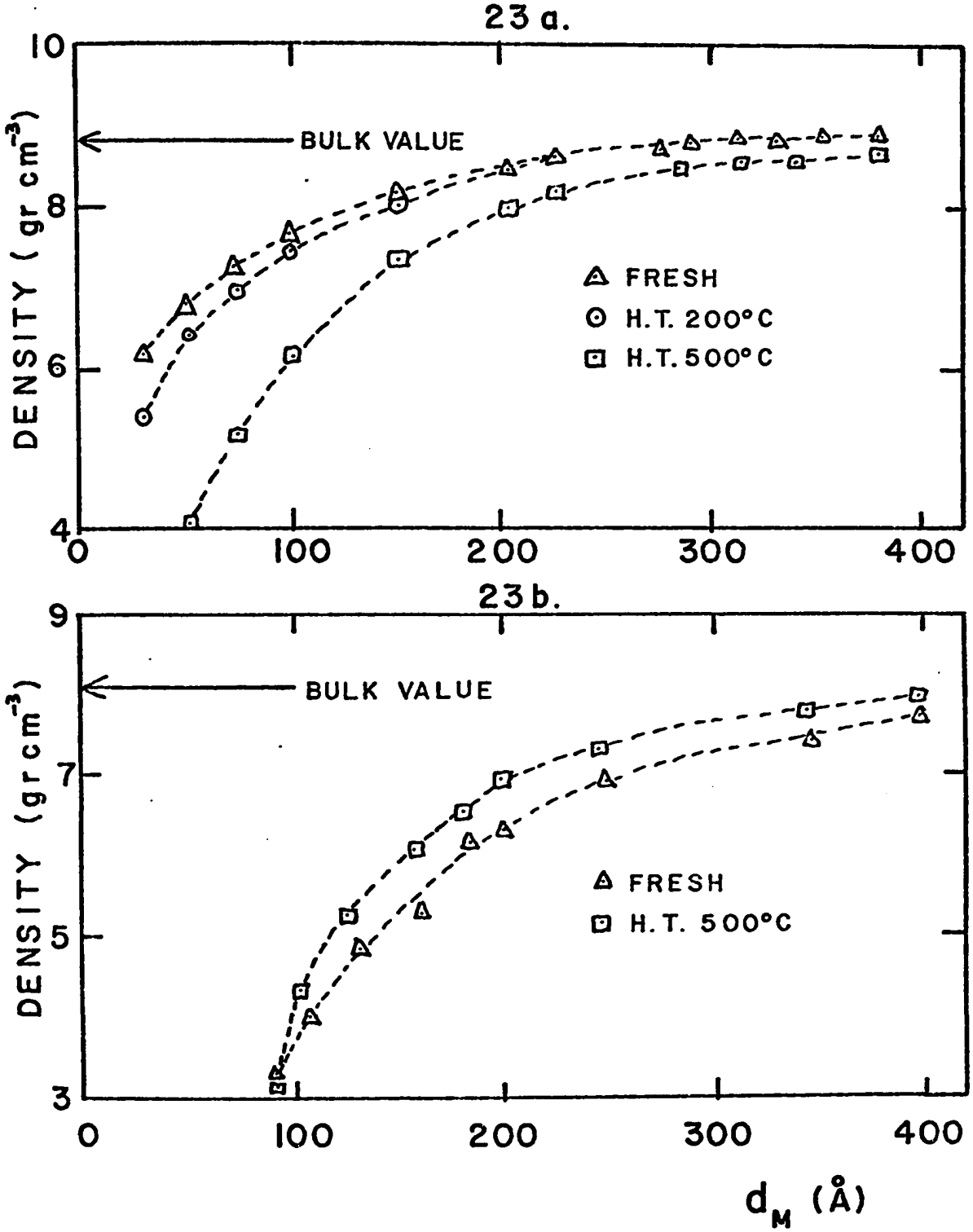

FIGURE 23: The density of Ni (23a) and Ni-P (23b) films against the mass thickness d_M of films in fresh and vacuum heat treated conditions. Ni-P films were deposited from pH = 5.3 solution. The temperatures of heat treatment are as indicated at the curves. Note the direction of changes of density of heat treatment.

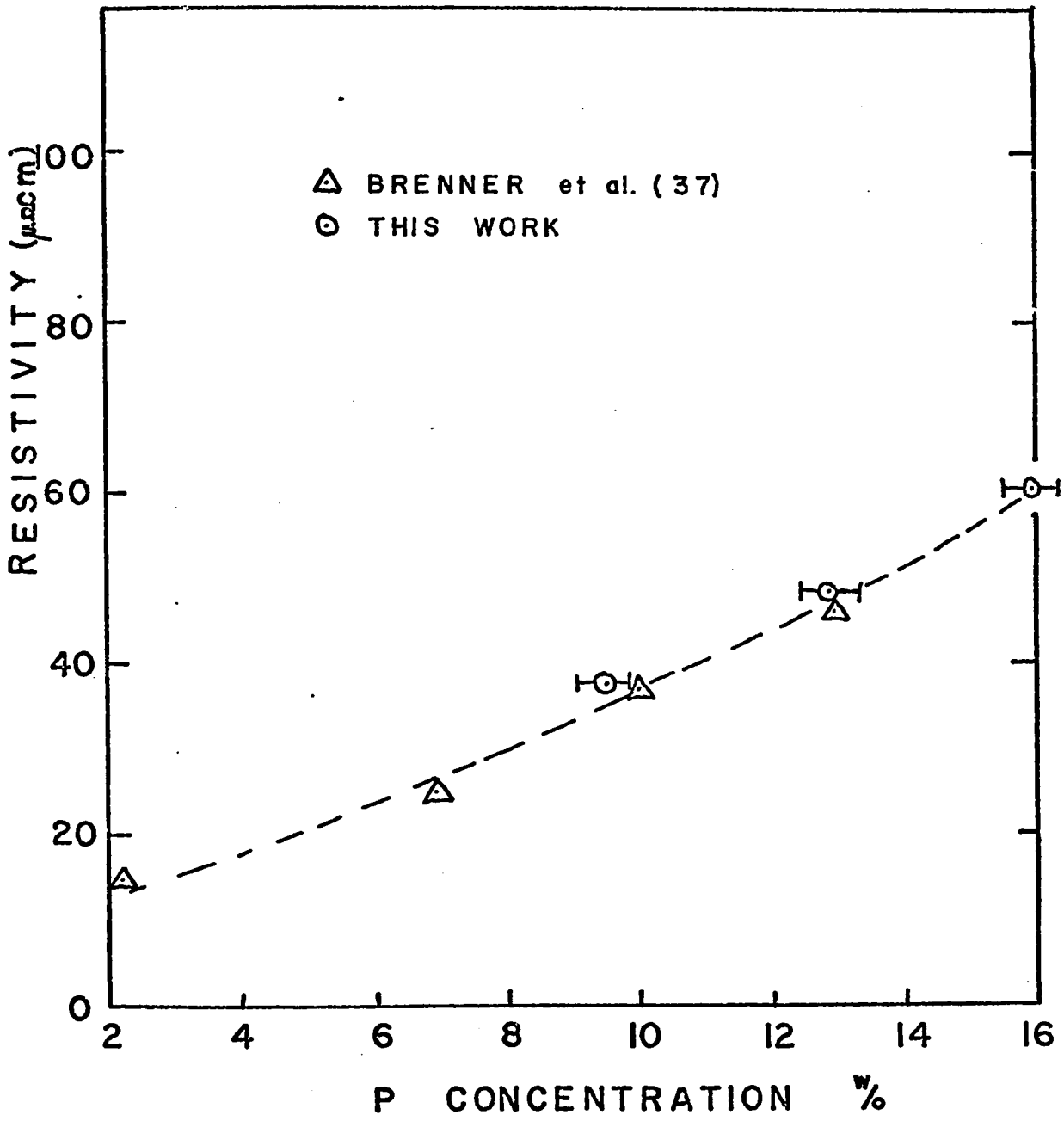

FIGURE 24: Room temperature resistivity of bulk Ni-P deposits as a function of P concentration. The samples were vacuum heat treated at 500°C. At P w/o = 0 (pure Ni) resistivity was taken to be 6.8 μΩ cm.

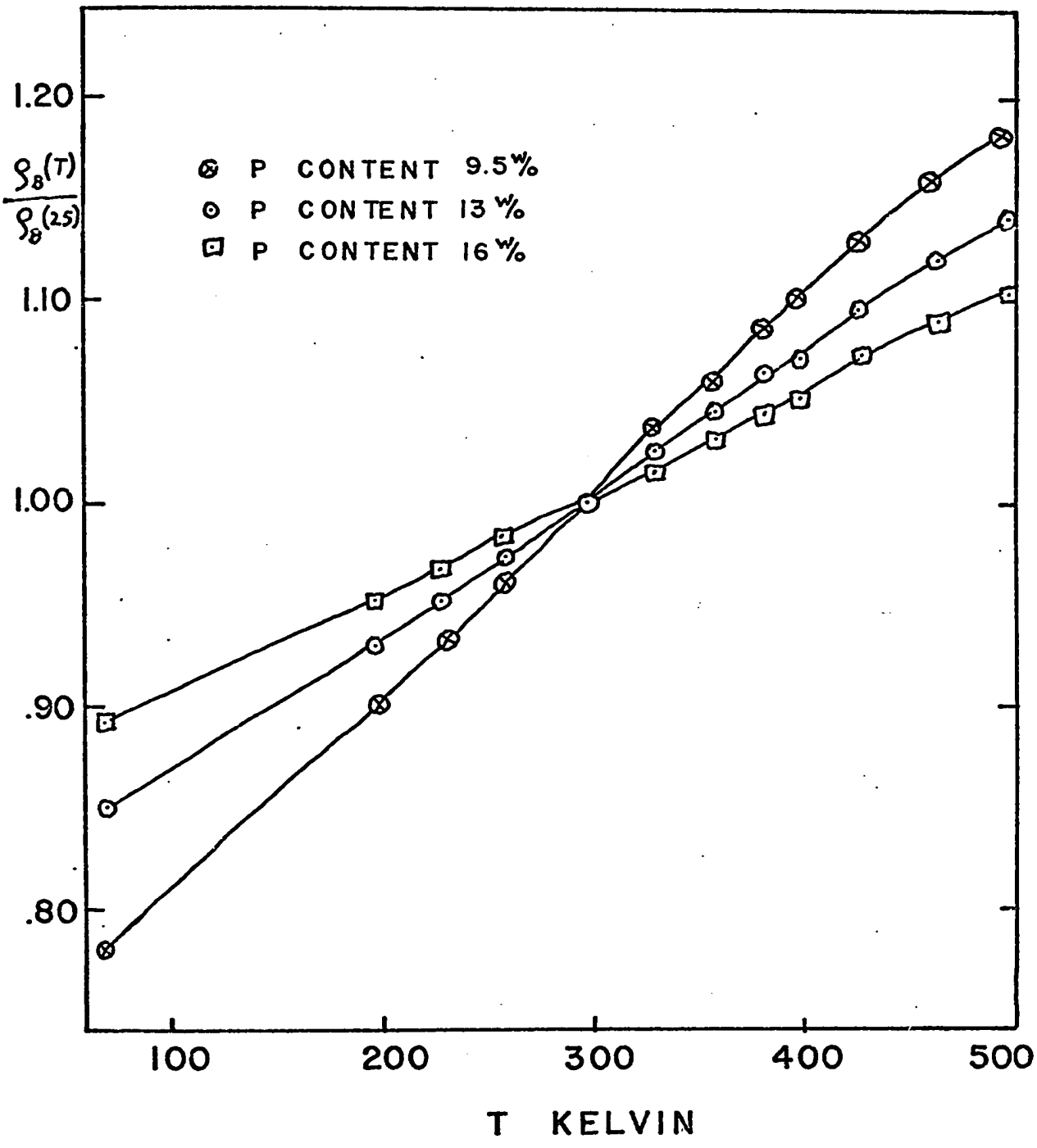

FIGURE 25: Variation of the normalized resistivity $\rho_B(T)/\rho_B(25)$ with temperature T of bulk Ni-P deposits for different P concentrations. $\rho_B(25)$ is the room temperature resistivity. The samples were heat treated in vacuum at 500°C.

be determined. It was however possible to determine the sign of the (very small) Hall voltage, which showed the majority carriers to be electrons.

3.32 Film Deposits. The room temperature resistivities of fresh Ni-P films deposited from any of the solutions of Table II and at any solution temperature were orders of magnitude higher than that of bulk Ni-P deposits. Also the resistivity of films varied with film thickness in a manner not predicted by the theory*. A typical resistivity variation of fresh films deposited at pH = 5.3 with film thickness is shown in Figure 26. The P content was found not to influence the resistivity variation of films with film thickness appreciably.

In contrast, vacuum deposited Ni films showed resistivity values close to that of bulk Ni and exhibited resistivity-film thickness variation to be in closer agreement with the theory*. This is also shown in Figure 26.

It was not possible to obtain quantitative results from measurements of temperature coefficient and Hall voltage of fresh Ni-P films as their resistivity changed in time. Qualitatively, Hall effect measurements showed the carriers to be electrons, and the temperature coefficient was found to be positive, implying metallic conductivity. The resistivity of fresh films exposed to the normal air environment at room temperature changed irreversibly. In vacuum the irreversible change was more pronounced.

The resistivity of fresh Ni-P films deposited in a pH = 5.3

---

* For resistivity variation with film thickness see the Fuchs-Sondheimer theory in 4.1.

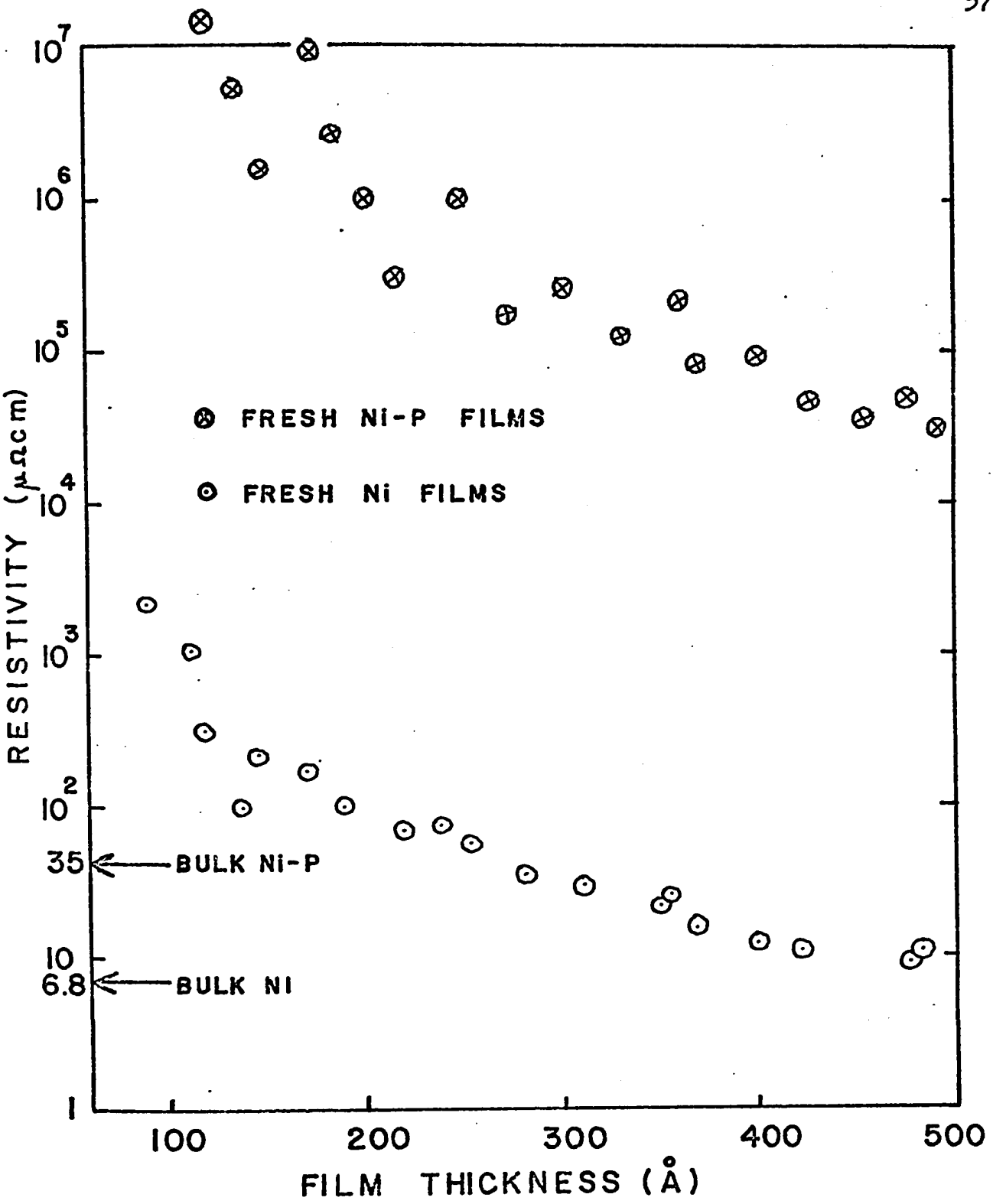

FIGURE 26: Variation of room temperature resistivity with film thickness of fresh Ni-P films and Ni films. The Ni-P films were deposited at room temperature and with 9.5 w/o P content. Note the large deviation of the resistivity of Ni-P films from that of bulk Ni-P.

solution was found to decrease on heating in the vacuum by as much as three orders of magnitude. The change of resistivity was largest for thin films and high temperatures. A typical set of "aging" curves of Ni-P films are shown in Figure 27.

In contrast, vacuum deposited Ni films showed large increases of resistivity above 300°C under the same aging conditions. This data is also included in Figure 27. The sharp increase in the Ni curves corresponds to the apparent decrease of film density (cf. 3.22). This is known (25) to be an indication of film agglomeration. Note from the figure that there is no tendency of agglomeration for Ni-P films.

The resistivity of heat treated Ni-P films did not change in time and thus it was possible to measure the temperature coefficient α and Hall voltage of these films. Resistivities of heat treated films deposited in a pH = 5.3 solution were measured between liquid nitrogen temperature and 200°C. For all samples the sign of α was positive indicating metallic conduction (see e.g. Kittel (40)). A typical set of resistivity-temperature curves is shown in Figure 28.

Hall voltage measured using the same set of films showed no pronounced film thickness variation. The measurements were difficult to carry out and were not accurate. Carriers were determined to be electrons and the carrier density was calculated (using Equation 4) to range from 10^{22} cm^{-3} to 3×10^{22} cm^{-3}.

The conduction in films was determined to be ohmic from current measurements at voltages ranging over three decades of values. The deviation from Ohm's law was less than the measuring accuracy (i.e. 0.01%).

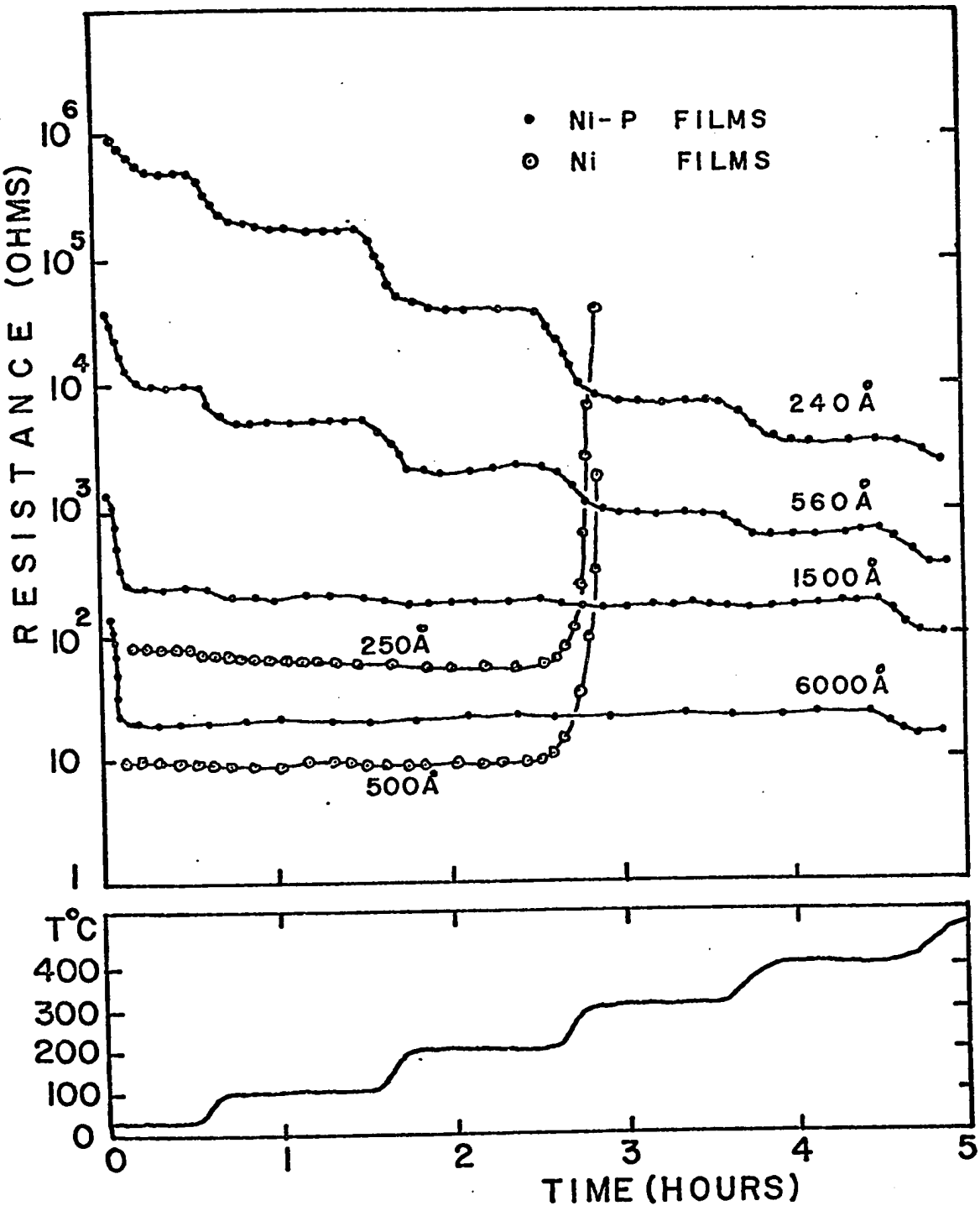

FIGURE 27: Changes of resistances on heating in vacuum of Ni-P and Ni films. The Ni-P films were deposited at room temperature with 9.5 w/o P content. The heat treating temperature as a function of time is also shown. Note the large increase of the resistance of Ni films at 300°C. During the first 30 min. the samples were kept at room temperature and were evacuated from 760mm pressure to 10^{-6} torr.

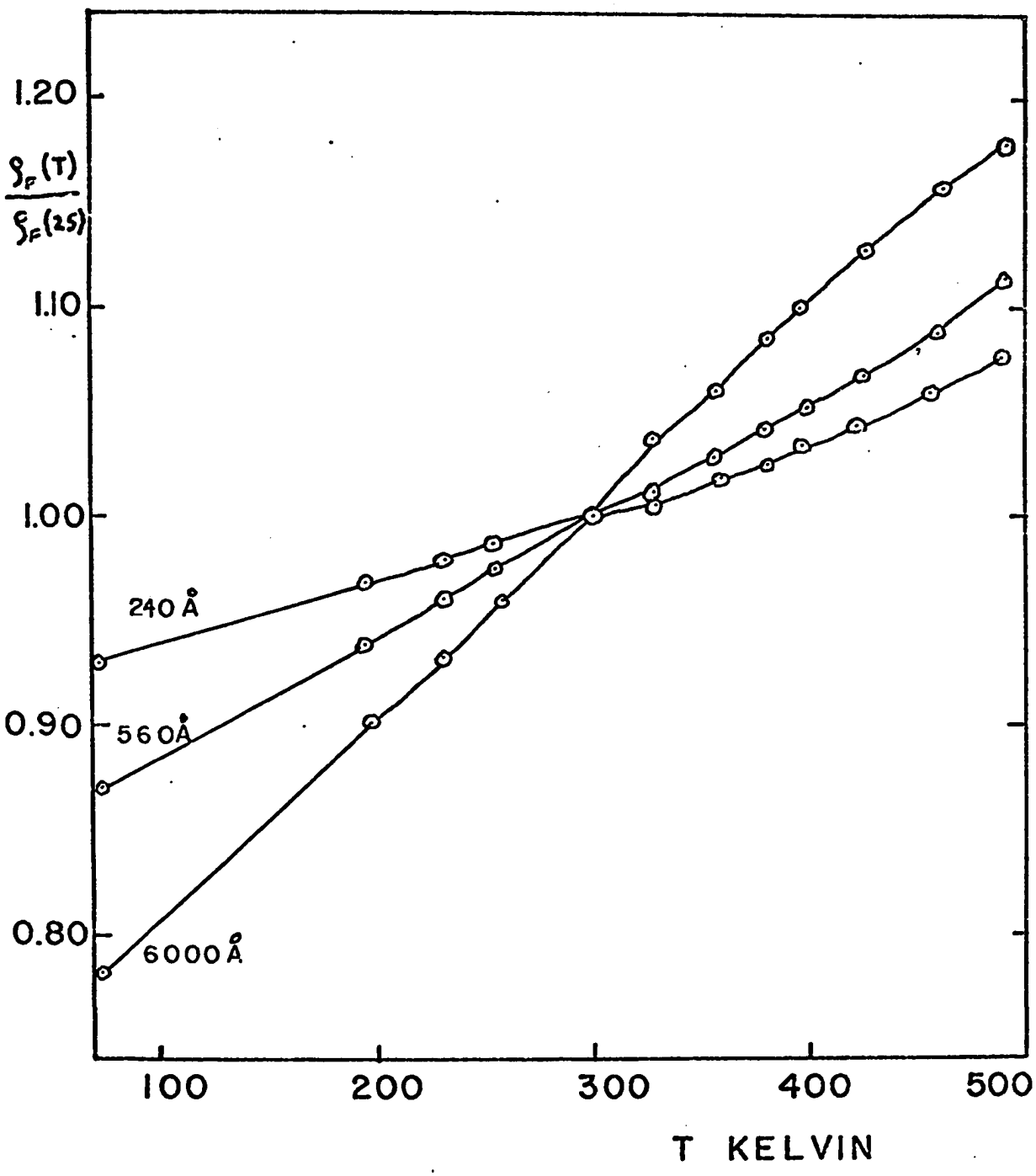

FIGURE 28: Variation of the normalized resistivity $\rho_F(T)/\rho_F(25)$ with temperature T of vacuum heat treated Ni-P films of various thicknesses. P content of films was 9.5 w/o. $\rho_F(25)$ is the room temperature resistivity.

3.4 Optical Constants of Deposits. The optical constants $n(\lambda)$ and $k(\lambda)$ of bulk and film deposits were determined from measurements that were carried out at room temperature. n and k of bulk specimens were derived from reflectivity measurements (cf. Appendix A), and those of film deposits were calculated from reflectivity and transmission measurements (cf. Appendix B). The accuracy of measurements was better than ± 0.5%.

3.41 Bulk Deposits. The spectral reflectance curves of bulk Ni and Ni-P deposits, grown on solid nickel substrates and vacuum heat treated at 500°C, are shown in Figure 29. The measurements of Ehrenreich et al. (38) using pure bulk Ni are also included in Figure 29 for reference. The optical constants n and k calculated from the reflectance curves are shown in Figures 30a and 30b.

3.42 Film Deposits. Spectral reflectance R_M and transmittance T_M curves of fresh Ni-P films deposited using a solution with pH = 5.3 on glass substrates are shown in Figure 31. R_M and T_M curves of vacuum heat treated Ni-P films are shown in Figure 32. The samples were also grown on glass substrates using a solution with pH = 5.3 and were heated for one hour at 400°C. The optical constants n and k calculated from curves 31 (fresh) and 32 (heated) are plotted in Figures 33a and 33b.

R_M and T_M of a number of Ni-P films were also measured as a function of heat treatment temperature. R_M and T_M of fresh Ni-P films deposited on glass substrates using a solution with pH = 5.3 were first measured. Films were then placed in vacuum and heated for one hour at

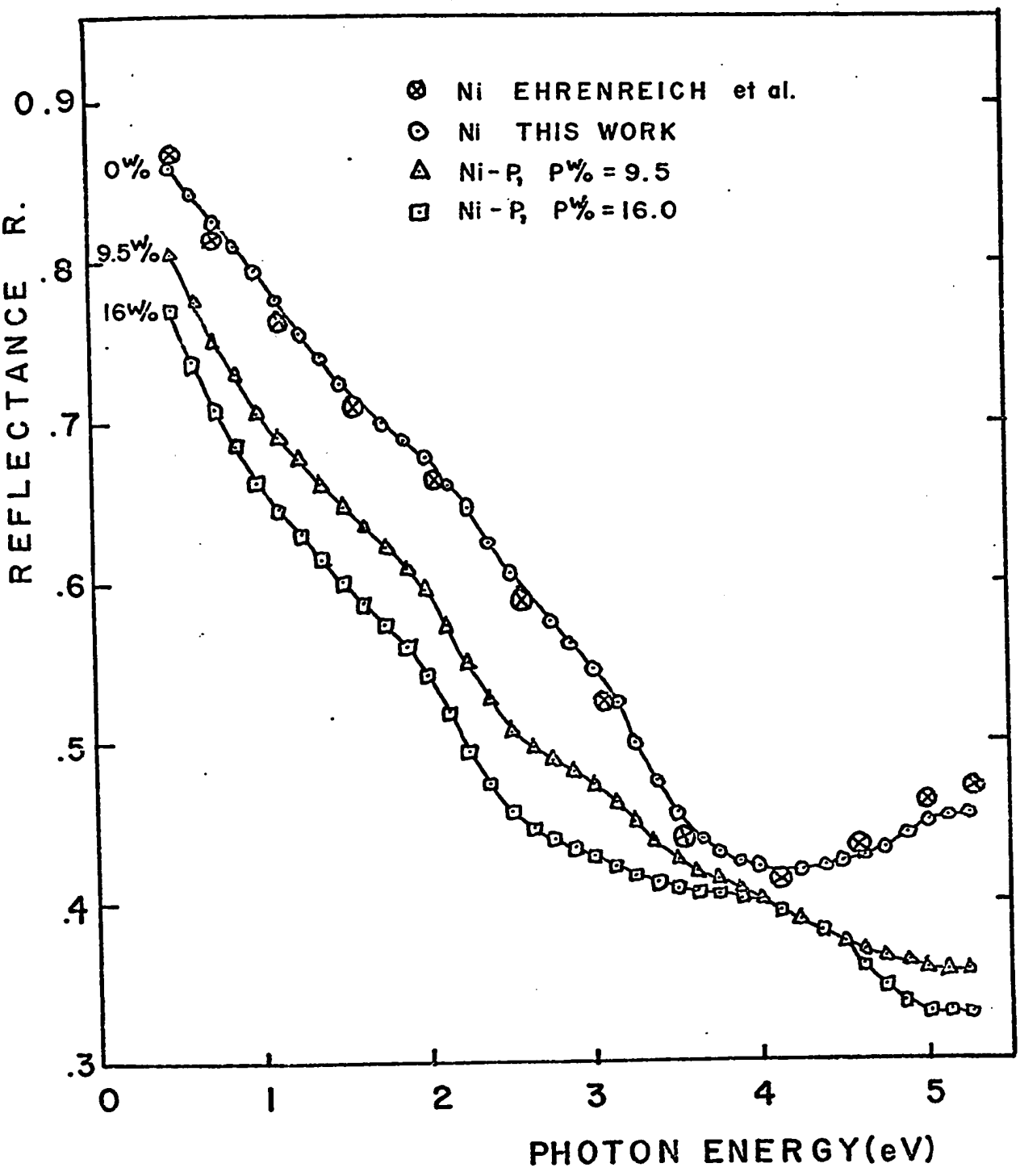

FIGURE 29: Spectral reflectance R of bulk specimens of Ni and Ni-P. Samples were vacuum heat treated at 500°C. The P content of Ni-P samples is indicated opposite the curves. The measurements of Ehrenreich et al. (38) on bulk nickel are included for reference.

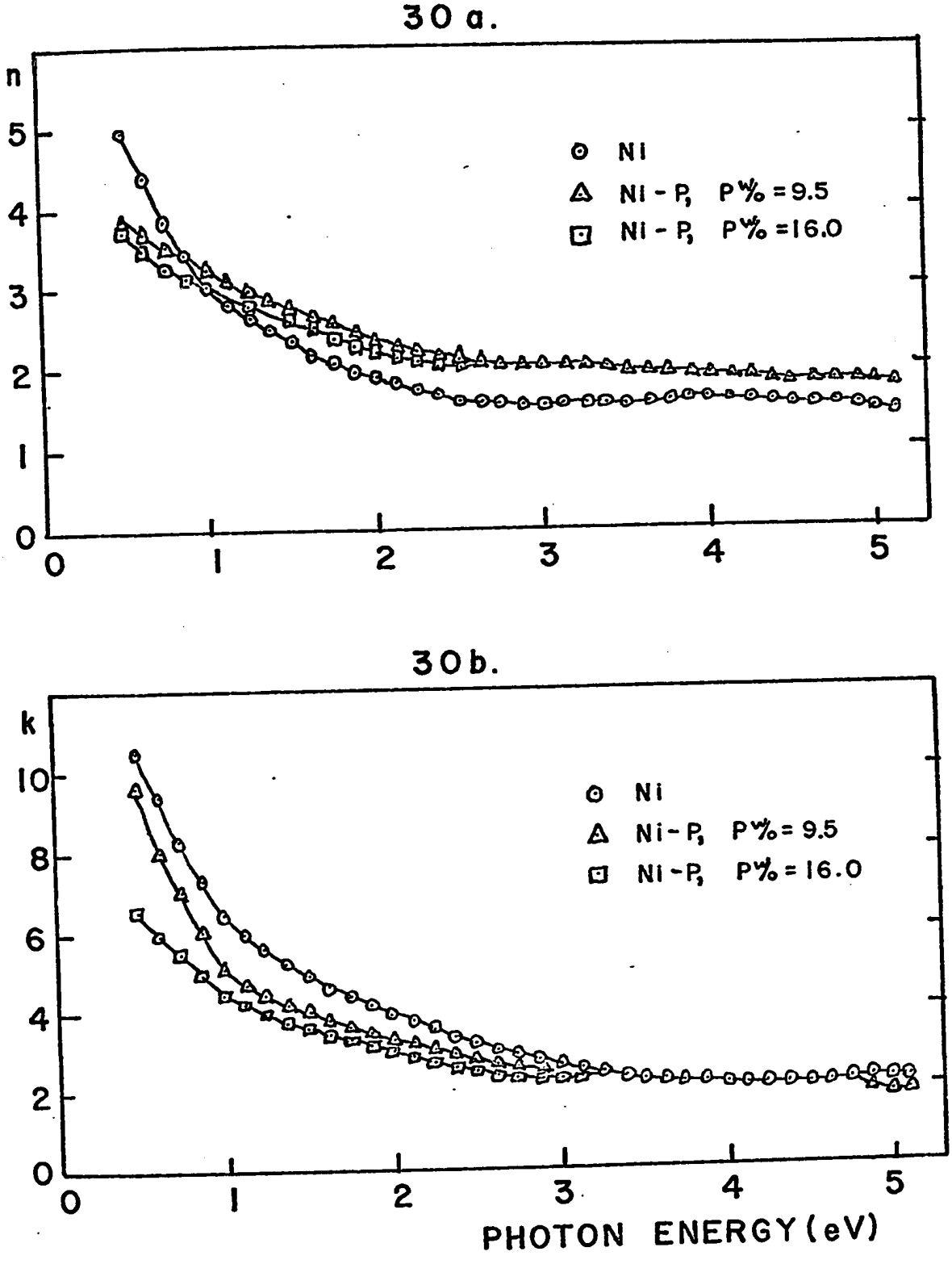

FIGURE 30: Spectral dependence of the optical constants n (Figure 30a) and k (Figure 30b) of Ni and Ni-P bulk specimens. The constants were calculated from curves in Figure 29.

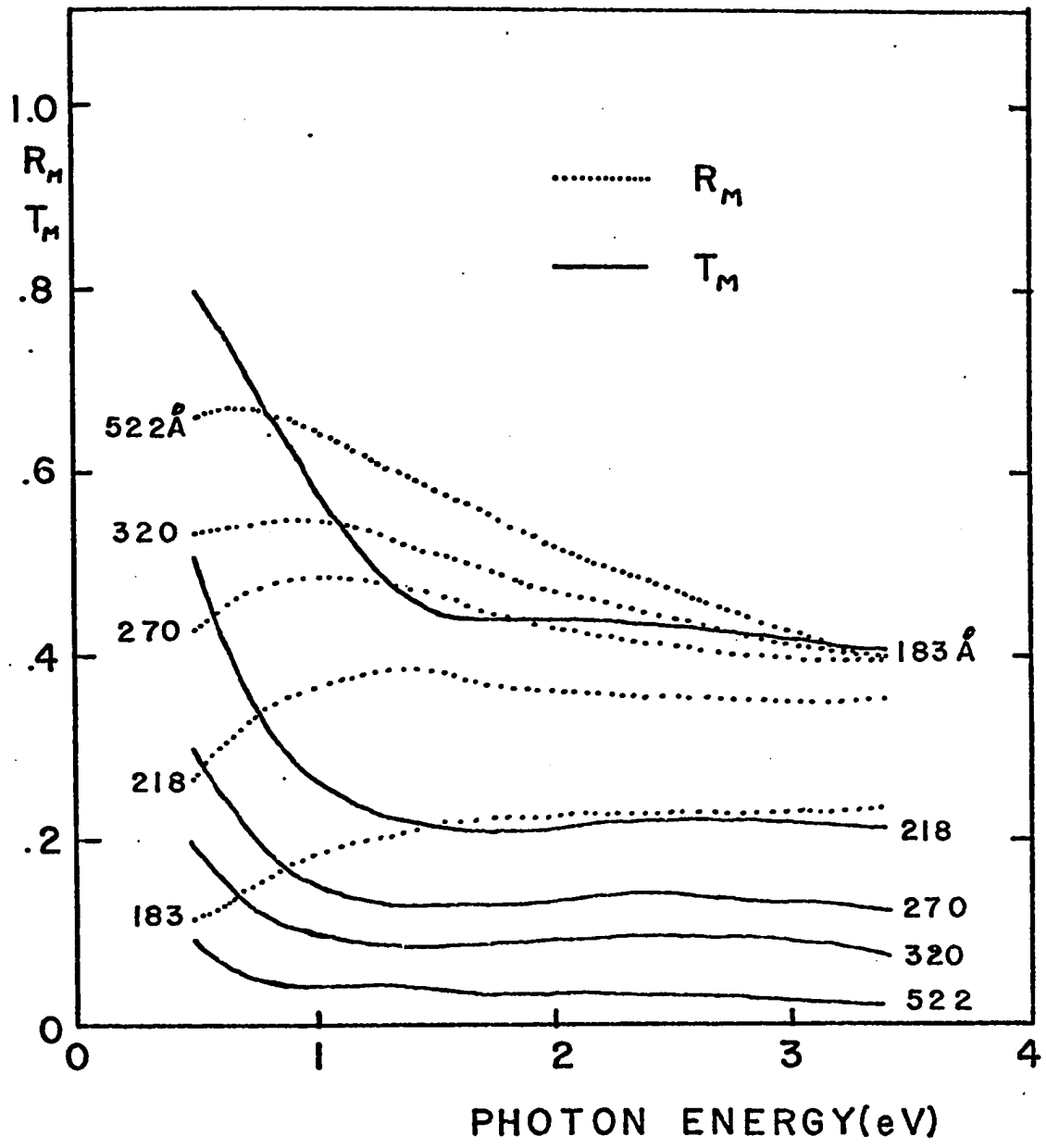

FIGURE 31: Spectral reflectance R_m and transmittance T_m of fresh Ni-P films deposited from pH = 5.3 solution. The substrate is glass with index $n_s = 1.5$. The geometrical film thickness d_{opt} is indicated opposite each curve.

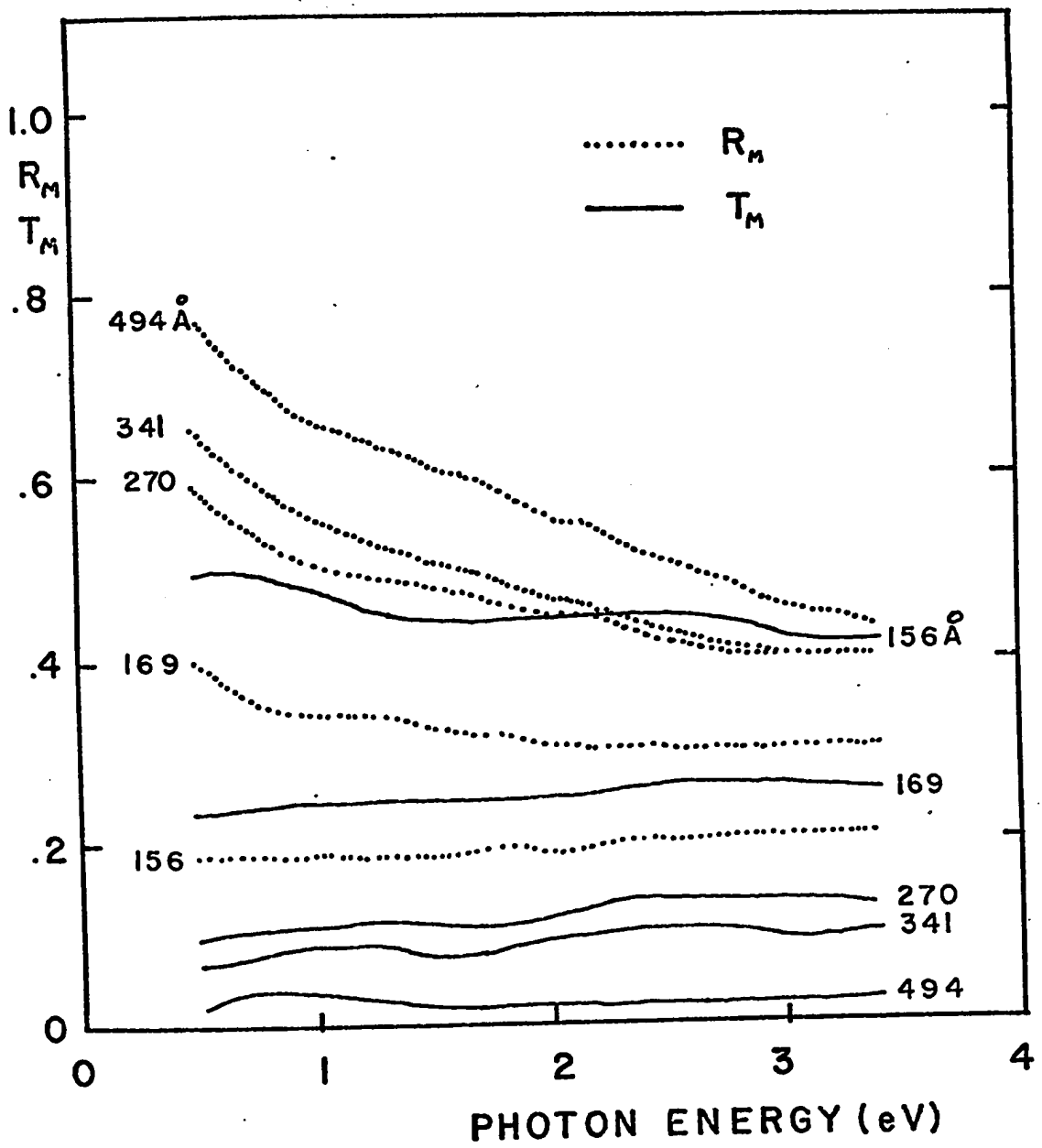

FIGURE 32: Spectral reflectance R_m and transmittance T_m of heat treated Ni-P films deposited from pH = 5.3 solution. The substrate is glass with index $n_s = 1.5$. The samples were heated in the vacuum at 400°C. The geometrical film thickness d_{opt} is indicated opposite each curve.

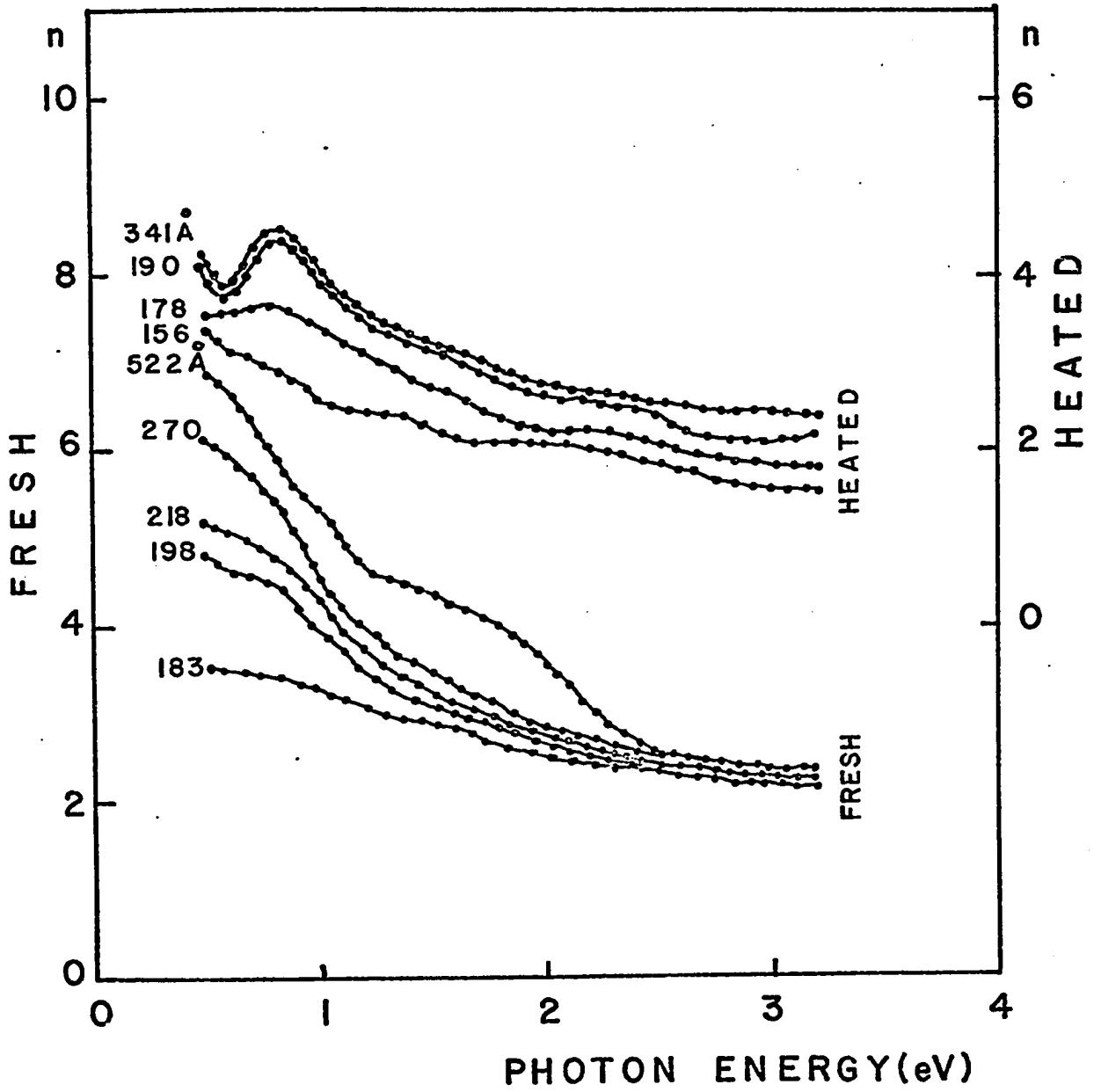

FIGURE 33a: Spectral dependence of the optical constant n of fresh and vacuum heat treated Ni-P films (deposition solution pH = 5.3, P content 9.5 w/o). The constants were calculated from experimental values of R_m and T_m such as those plotted in Figures 31 and 32. The geometrical film thickness d_{opt} is indicated opposite each curve.

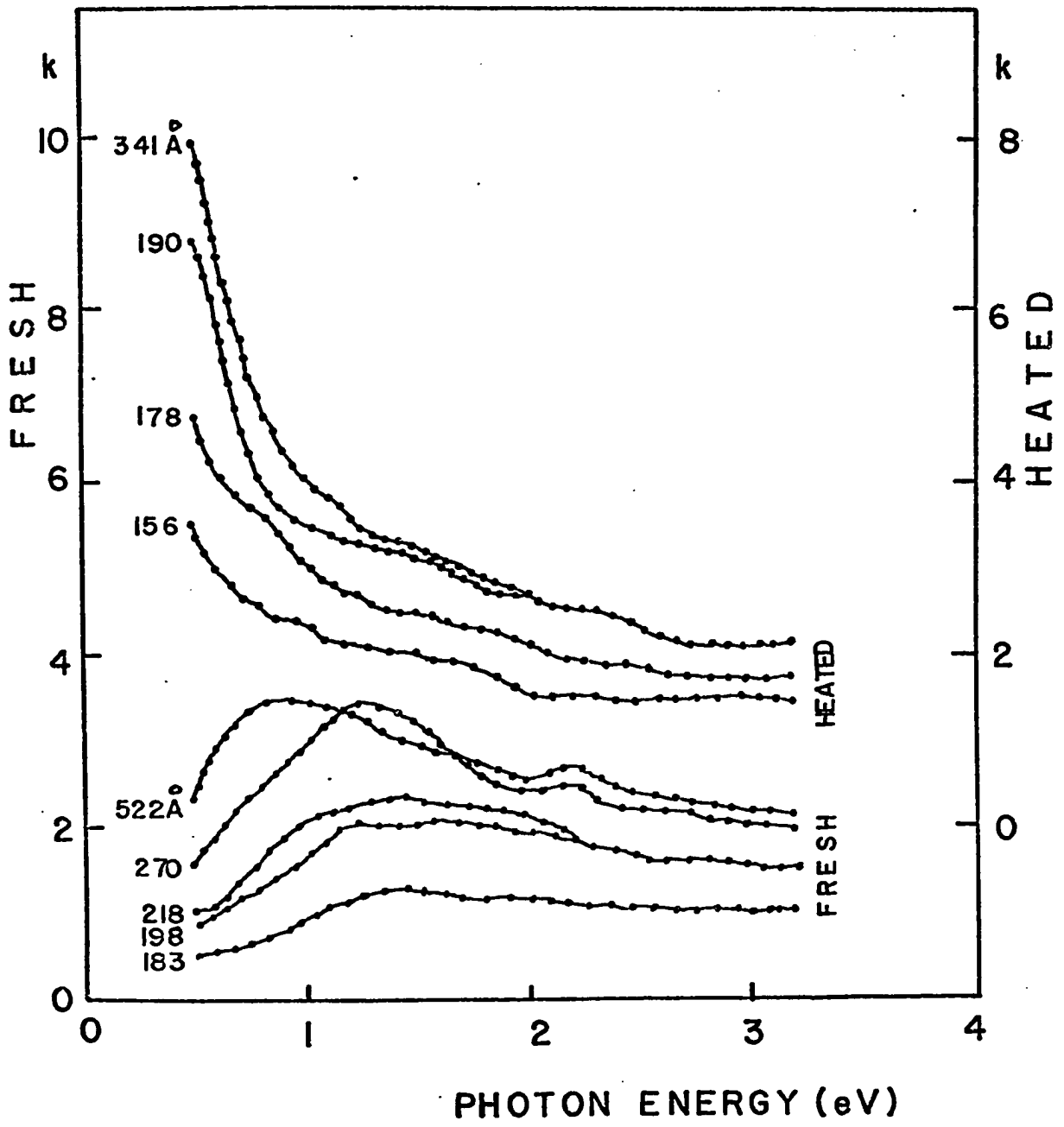

FIGURE 33b: Spectral dependence of the optical constant k of fresh and vacuum heat treated Ni-P films (deposition solution pH = 5.3, P content 9.5 w/o). The constants were calculated from experimental values of R_m and T_m such as those plotted in Figures 31 and 32. The geometrical film thickness d_{opt} is indicated opposite each curve.

a certain temperature. R_M and T_M measurements followed, and the heating was repeated at a higher temperature, etc. The spectral curves of one such Ni-P film are shown in Figure 34. The temperatures of heat treatment are shown opposite the curves. Note that T_M decreases with increasing heat treatment temperature at the long wavelength limit (small energies) in a similar fashion to the resistivity decrease of Ni-P films with increasing heat treatment temperature (cf. Figure 27).

In contrast, vacuum deposited Ni films did not show large optical changes on vacuum heat treatment, provided the temperature was below 200°C. The spectral distribution of optical constants n and k of some Ni films heat treated at 200°C in the vacuum are shown in Figures 35a and 35b for reference. For heat treatment temperatures above 250°C, Ni films became aggregated and discontinuous (cf. Figure 27). Upon complete aggregation the film disappeared, i.e. the constants n and k of the individual islands assumed such values in the visible range of wavelengths as to cause the values of reflectivity and absorptance to be close to zero.

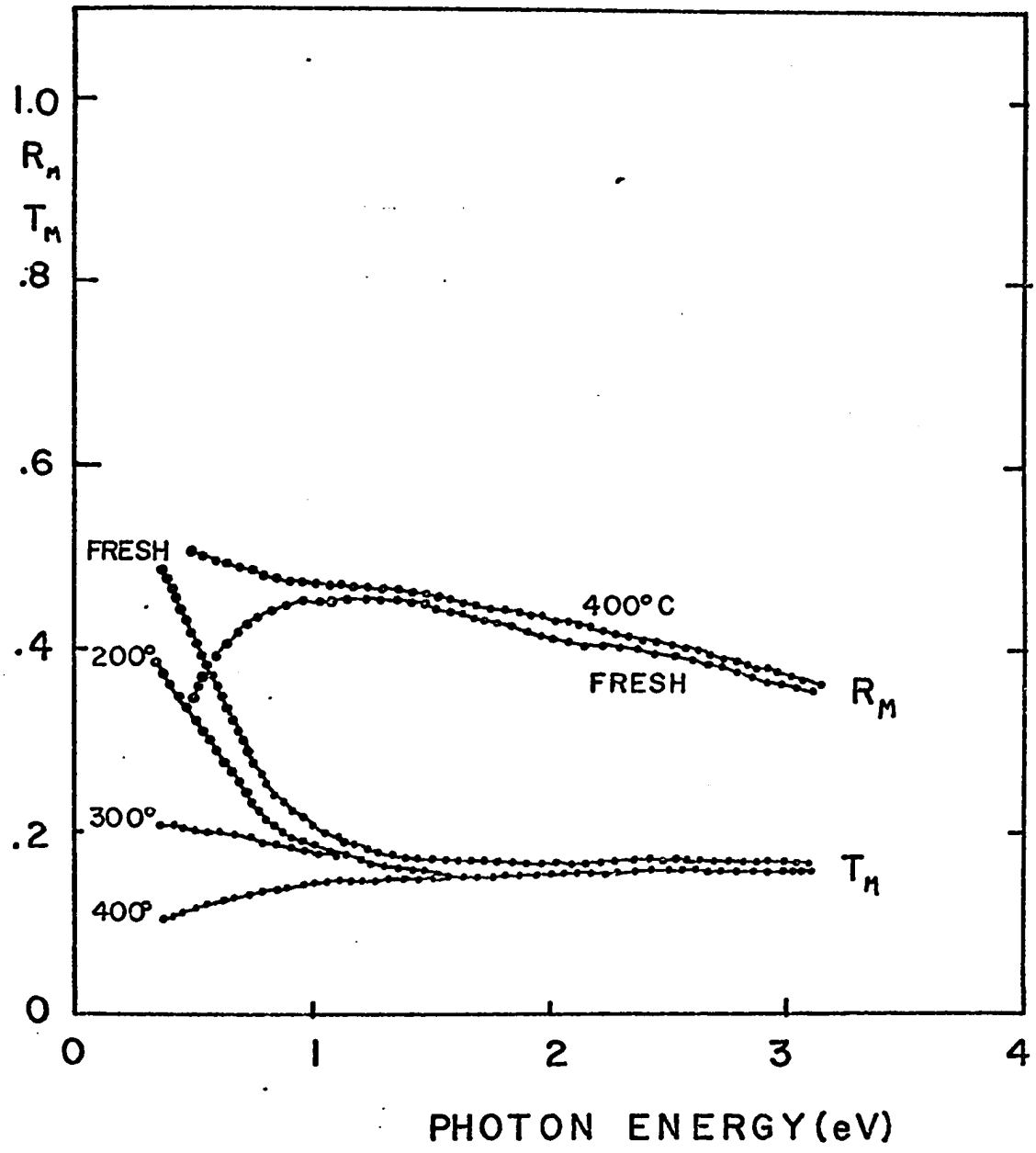

FIGURE 34: The changes of R_m and T_m with temperature of heat treatment of a Ni-P film. The film was deposited in pH = 5.3 solution at room temperature. The spectral curves were measured after heating the sample in vacuum for one hour at the temperature indicated opposite the curves.

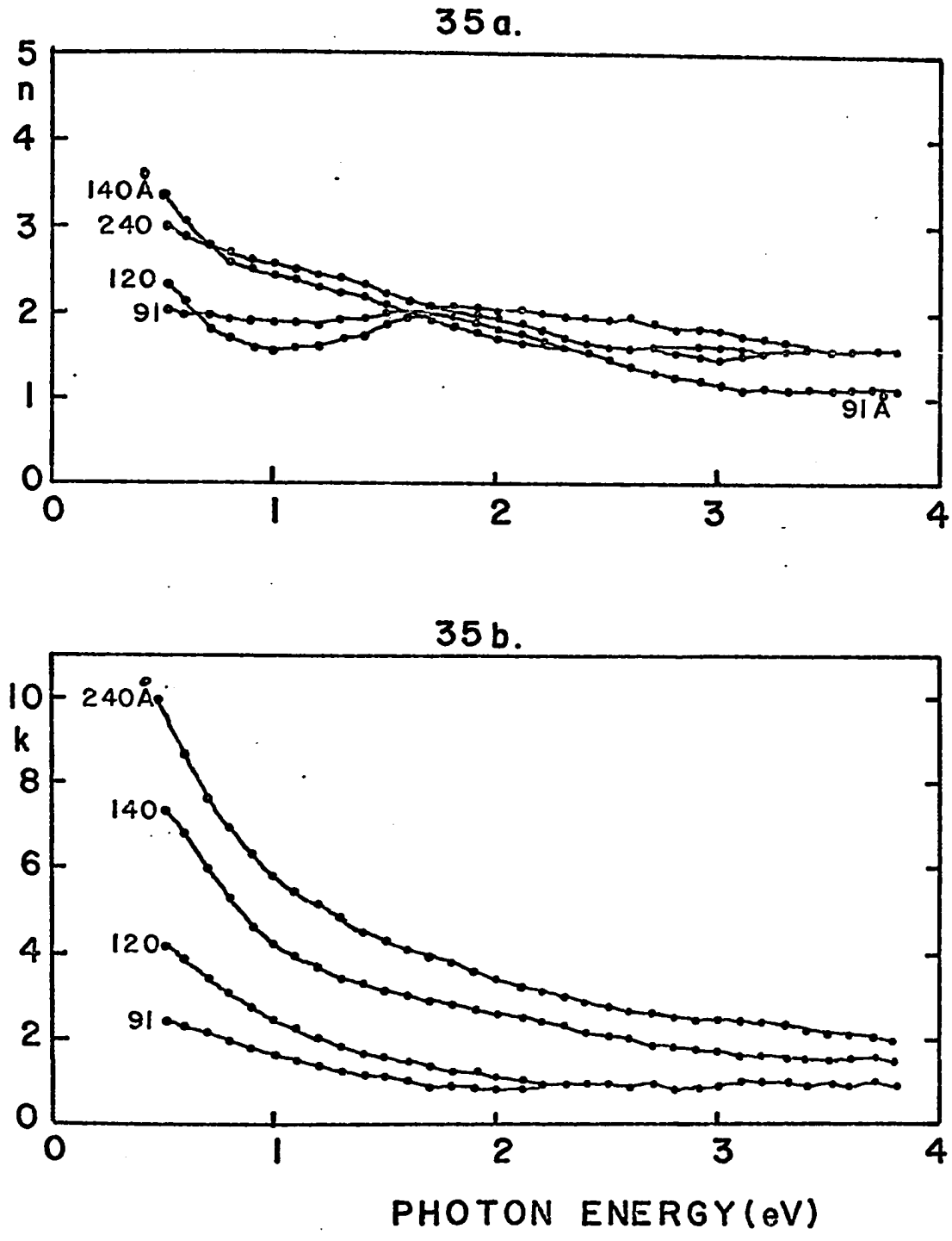

FIGURE 35: Spectral dependence of the optical constants n (Figure 35a) and k (Figure 35b) of vacuum heat treated Ni films. Heat treatment temperature was 200°C. The geometrical film thickness d_{opt} is indicated opposite each curve.

CHAPTER 4

INTERPRETATION OF THE RESULTS

A quantitative interpretation of the experimental data is attempted on the basis of available theories. In the first part, these theories are briefly reviewed and in the second part, the interpretation is made. The theories yield approximate values of some phenomenological constants of Ni-P films.

4.1 Theory of Electrical Conduction in Metal Films. The DC conductivity σ_o of idealized homogeneous and isotropic bulk metals is given (e.g. Kittel (40) by the expressions

$$\sigma_o = \frac{Ne^2}{m}\tau = \frac{Ne^2}{mv_F}\ell \qquad [8]$$

where N is the density of carriers

e is the electronic charge

m is the free electron mass

τ is the relaxation time of carriers

v_F is the carrier velocity at Fermi energy

ℓ is the mean free path of carriers.

For real monovalent metals [8] may be preserved if m is replaced by m^*, the effective mass of carriers. The value of m^* for isotropic metals

generally differs from the free electron value according to its definition (e.g. Kittel (40)) as

$$m^* = \left(\frac{\partial^2 E}{\partial K^2} \right)^{-1}$$

where E and K are electron energy and wave vector respectively.

For multivalent metals the electrical conduction is more complicated. There may be several carriers, each with different carrier density and effective mass in various bands, having their own relaxation times. In this case the conductivity may be given by the expression

$$\sigma_o = \frac{ne^2}{M} \theta \qquad [9]$$

where n, M and θ have the same dimensions as N, m and τ in [8], but they are no longer material constants.

The temperature dependence of σ_o is through the temperature dependent τ or ℓ, as N and m^* are independent of temperature at moderate temperatures. τ (or ℓ) has a T^{-1} dependence (41) in the approximate range of 50°K to 500°K. Thus the DC resistivity $\rho_o = \sigma_o^{-1}$ of bulk metals may be expressed as an increasing linear function of temperature in the restricted temperature range, and consequently the temperature coefficient of resistivity α is a positive constant.

Metals, that are homogeneous, isotropic, behave according to [8], and have a τ with a T^{-1} dependence, are said to be Drude type (40), (or free electron type) solids. In practice the definition is sometimes extended to cover metals that conduct according to [9], with the understanding that n, M and θ are phenomenological constants.

4.11 Continuous Films: Fuchs-Sondheimer Theory. Assume that an ideal Drude type metal with a mean free path ℓ is thinned from the bulk to a thickness comparable with ℓ. From [8] it is evident that such a restriction on ℓ will alter the conductivity σ_B. If the conductivity of the thinned (film) specimen with thickness d is denoted by σ_F, then the ratio of σ_F/σ_B is given by the Fuchs-Sondheimer (2) expression as

$$\frac{\sigma_F}{\sigma_B} = 1 - \frac{3(1-\epsilon)}{8\kappa} + \frac{3}{4\kappa}(1-\epsilon)^2 \sum_{\nu=1}^{\infty} \epsilon^{\nu-1}\left\{X(\kappa^2\nu^2)\left(\kappa^2\nu^2 - \frac{\kappa^4\nu^4}{12}\right) + \right.$$

$$\left. + \epsilon^{-\kappa\nu}\left(\frac{1}{2} - \frac{5}{6}\kappa\nu - \frac{\kappa^2\nu^2}{12} + \frac{\kappa^3\nu^3}{12}\right)\right\} \qquad [10]$$

where $X(x) = \int_x^{\infty} \frac{e^{-\zeta}}{\zeta}\, d\zeta$,

$\kappa = d/\ell$, and

$0 \leq \epsilon \leq 1$.

ϵ is the measure of smoothness of the film surface. For atomically smooth surfaces $\epsilon = 1$ and for rough surfaces $\epsilon = 0$. An outline of the derivation of [10] is given in Appendix D.

A family of curves of expression [10] is plotted in Figure 36. Note from the curves that the conductivity of films with rough surface ($\epsilon = 0$) and small thickness may be smaller than that of the corresponding bulk metal by a factor as large as 20.

Continuous films behave according to the theory if their resistivities vary with film thickness below the $\epsilon = 0$ curve in Figure 36. If the resistivity values fall above the $\epsilon = 0$ curve the films do not

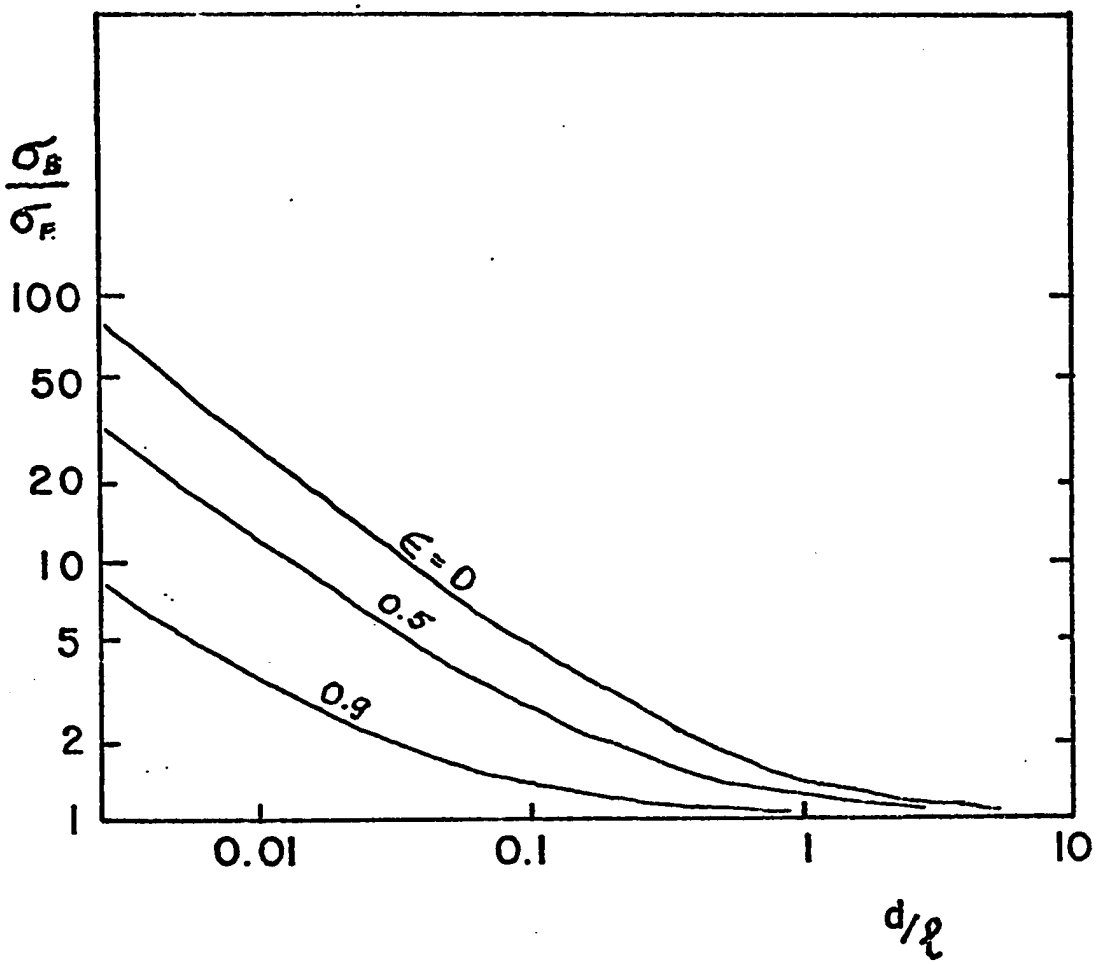

FIGURE 36: Fuchs-Sondheimer curves calculated from expression [10]. σ_B and σ_F are the conductivities of the bulk and film respectively, d is the geometrical film thickness, ℓ is the bulk mean free path of carriers, and ϵ is a parameter related to surface roughness of the film.

behave according to the theory. Such film behaviour may result from discontinuous films, and from films whose structure, purity etc. differ from those of the parent bulk metal. The latter condition applies to almost all but the most carefully prepared films of a few metals (8).

From the Fuchs–Sondheimer theory the mean free path ℓ of the bulk metal may be calculated by simple curve fitting of the experimental film data. The temperature dependence of ℓ is also directly measurable. This is a good example of the use of films in measuring bulk parameters that are not easily obtainable by other methods.

Another useful relation for the resistivity of films is the modified Matthiessen's rule (8). According to the rule, the resistivity of homogeneous, isotropic, plane parallel and Drude type films may be separated into parts

$$\rho_F = \rho_1 + \rho_2 + \rho_3 + \rho_4 \qquad [11]$$

where ρ_F is the film resistivity and ρ_1, ρ_2, ρ_3, ρ_4 are component resistivities due to structural imperfection, foreign atoms (impurities), phonon scattering (temperature dependent part) and boundary scattering (thin film part). Also according to the rule the resistivity of the same material in bulk form with the same structural imperfections and impurities may be written as

$$\rho_o = \rho_1 + \rho_2 + \rho_3 \,. \qquad [12]$$

In essence [11] and [12] express the possibility of separating the relaxation time into components due to the four scattering processes as $\frac{1}{\tau} = \frac{1}{\tau_1} + \frac{1}{\tau_2} + \frac{1}{\tau_3} + \frac{1}{\tau_4}$. Substitution of [8] into [11] and [12] and the combination of [11] and [12] give an expression similar to [10].

$$\frac{\rho_F}{\rho_o} = 1 + \frac{\tau_B}{\tau_4} \qquad [13]$$

where ρ_F and ρ_o are film and bulk resistivities, $\frac{1}{\tau_B} = \frac{1}{\tau_1} + \frac{1}{\tau_2} + \frac{1}{\tau_3}$ is the inverse bulk relaxation time made up of its components, and τ_4 is the relaxation time due to the film boundaries.

It is evident from the foregoing that continuous metal films that behave according to the Fuchs-Sondheimer theory are ohmic conductors with positive temperature coefficient.

4.12 Discontinuous Films. It was stated in a previous section that very thin films are discontinuous, consisting of islands, and that in some cases thin continuous films break up and aggregate during heat treatment. It was also seen that Ni-P films in their early growth stage consist of hemispherical islands. Such films were said to have high resistivity and negative temperature coefficient and their resistivity is not predicted by the Fuchs-Sondheimer theory. The outlines of one of the theories (3),(4) concerning discontinuous conduction is given below. For detailed considerations see Hartman's (4) paper.

According to this model the current conduction in the plane of the film is by electron tunnelling between neighbouring islands. For the treatment it is assumed that the metallic microparticles (islands) are homogeneous, isotropic and have a spherical Fermi surface. In the derivation of the conductivity formula the microparticles are taken to be cubes with sides "a" separated linearly by gaps "b" in the plane of the substrate.

Each island is represented by a potential box with discrete electronic levels. Tunnelling is considered between adjacent potential boxes at levels E_{n+1} with transition coefficient $P(E_{n+1})$. From lifetime considerations, the width of individual energy levels are calculated. It is shown that conduction between the highest filled levels E_n (Fermi level of the individual island) is not possible, as the width of these δE_n levels are approximately 10^{-7} eV, and very small applied electric fields would shift the relative positions of islands in energy sufficiently to uncross the levels of the adjacent islands.

It is concluded that tunnelling must take place at a level one higher (E_{n+1}) than the Fermi level, as this level is the first one wide enough for the neighbours to overlap even for large applied fields. The energy diagram of the potential boxes representing the microparticles under the influence of an externally applied potential is given in Figure 37.

For conduction, electrons are required to be excited (thermally) into the "conduction" level E_{n+1}, with activation energy ΔE_n. The conductivity of discontinuous films is finally given as

$$\sigma_F = \sigma \exp - \frac{\Delta E_n}{kT} \quad , \qquad [14]$$

where σ is a function of the transition coefficient $P(E_{n+1})$ and fundamental material constants, and ΔE_n is a function of the size of islands "a" and their separation "b".

$P(E_{n+1})$ is sensitive to applied electric fields. Thus discontinuous films are generally non-ohmic conductors. The temperature coefficient of resistivity can be seen from [14] to be negative, and

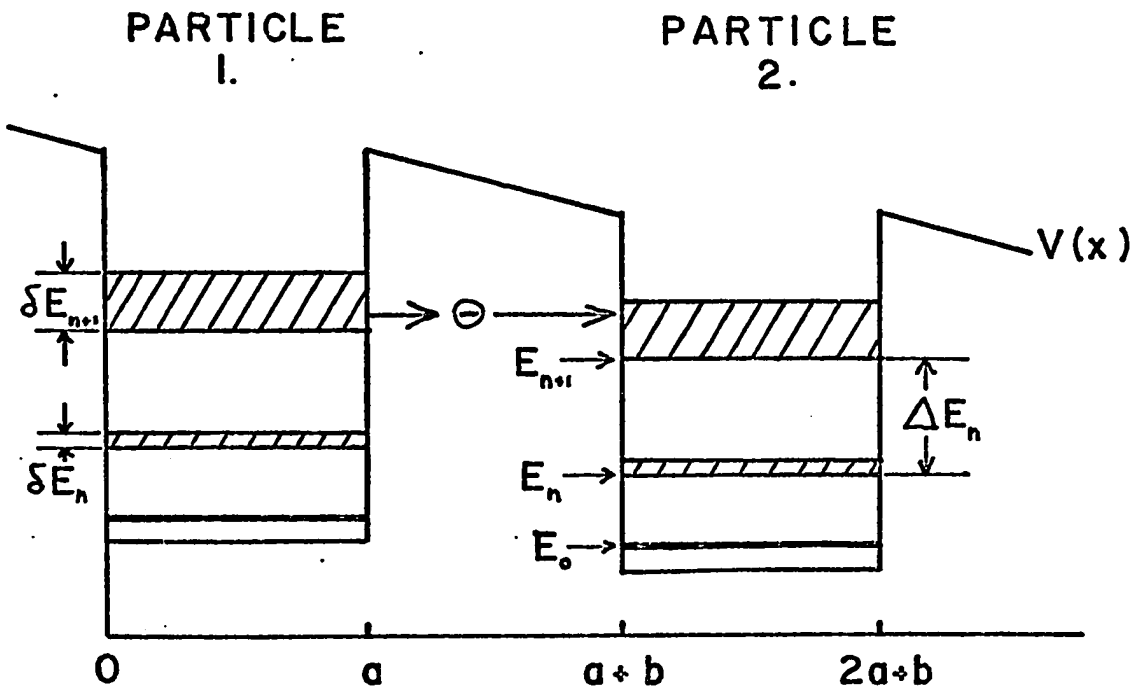

FIGURE 37: The energy diagram of the potential boxes representing microparticles of metals in a discontinuous film under the influence of an externally applied potential V. The particles of size "a" are separated by linear distances "b". Fermi energy is denoted by E_n, the conduction level by E_{n+1}. $E_{n+1} - E_n = \Delta E_n$ is the activation energy and δ denotes the width of bands. The conduction is between E_{n+1} levels by tunnelling.

variable with temperature. The room temperature resistivity range of typical discontinuous metal films is $10^{-3}\Omega$ cm to 10Ω cm. In contrast, the resistivity range of normal, well behaved continuous metal films is $10^{-5}\Omega$ cm to $10^{-3}\Omega$ cm.

4.2 Theory of Optical Constants of Metal Films. The macroscopic behaviour of a solid at photon energy E (or wavelength λ) is completely described by the optical constants n(E) and k(E), as is seen from Appendices A and B.

In this section n(E) and k(E) of metals in bulk and in film form will be described in terms of the microscopic material constants, according to current theories. In the following, E (photon energy = $h\nu$), ω (angular frequency) and λ (wavelength) will be used interchangeably.

4.21 General Considerations: Drude Theory. The connection between n and k and the microscopic constants are usually made through the complex dielectric constant $\tilde{\epsilon}$ or the complex conductivity $\tilde{\sigma}$ of the medium, where $\tilde{\epsilon} = -i\omega\tilde{\sigma}$ (see e.g. (32)). By definition (32) we have the following relations

$$\tilde{\epsilon} = \epsilon_1 + i\epsilon_2 = (\tilde{n})^2 = (n^2 - k^2) + i\,2nk = \epsilon + i\frac{\sigma}{\omega} \qquad [15]$$

where ϵ and σ are the real dielectric constant and conductivity respectively and ω is the angular frequency. Both ϵ and σ are functions of E (or λ, or ω). From [15] we see that

$$\epsilon(E) = n^2(E) - k^2(E) \qquad [16a]$$

$$\sigma(E) = 2\omega\, n(E)\, k(E)\ . \qquad [16b]$$

In the following (E) will be dropped for simplicity, e.g. we write $\sigma = 2\omega\, nk$ instead of [16b].

For a collection of semifree electrons (ideal Drude metal) ϵ and σ may be expressed in terms of N, m^*, τ, e and ω as

$$\epsilon = \epsilon_o - \frac{\sigma_o}{1 + \omega^2\tau^2}\,\tau = n^2 - k^2 \qquad [17a]$$

$$\sigma = \frac{\sigma_o}{1 + \omega^2\tau^2} = 2\omega\, nk \qquad [17b]$$

where $\sigma_o = \frac{Ne^2}{m^*}\,\tau$ is the DC conductivity. An outline of the derivation of [17] is given in Appendix E. For the derivation it is assumed that the idealized solid is homogeneous, isotropic, monovalent, single band Drude type metal, and that the conductivity at optical frequencies ω is due to electronic transport in the conduction band only. The dispersion curves of n and k of such an ideal solid is shown in Figure 38 and a set of conductivity curves are drawn in Figure 39. The curves were calculated from equation [17], using an arbitrary pair of values for τ and σ_o. Note the sharp decrease of σ for increasing values of photon energy.

The response of real metals to optical photons depends on the electronic structure of the metal and the photon energy. For low energies ($E \ll 1$ eV) the response of metals (especially alkalies) is in reasonable agreement with the predictions of the free electron theory i.e. [17]. At higher photon energies and especially for multivalent metals, other processes, e.g. band to band transitions of electrons, are predominent. Generally ϵ and σ for real metals may be

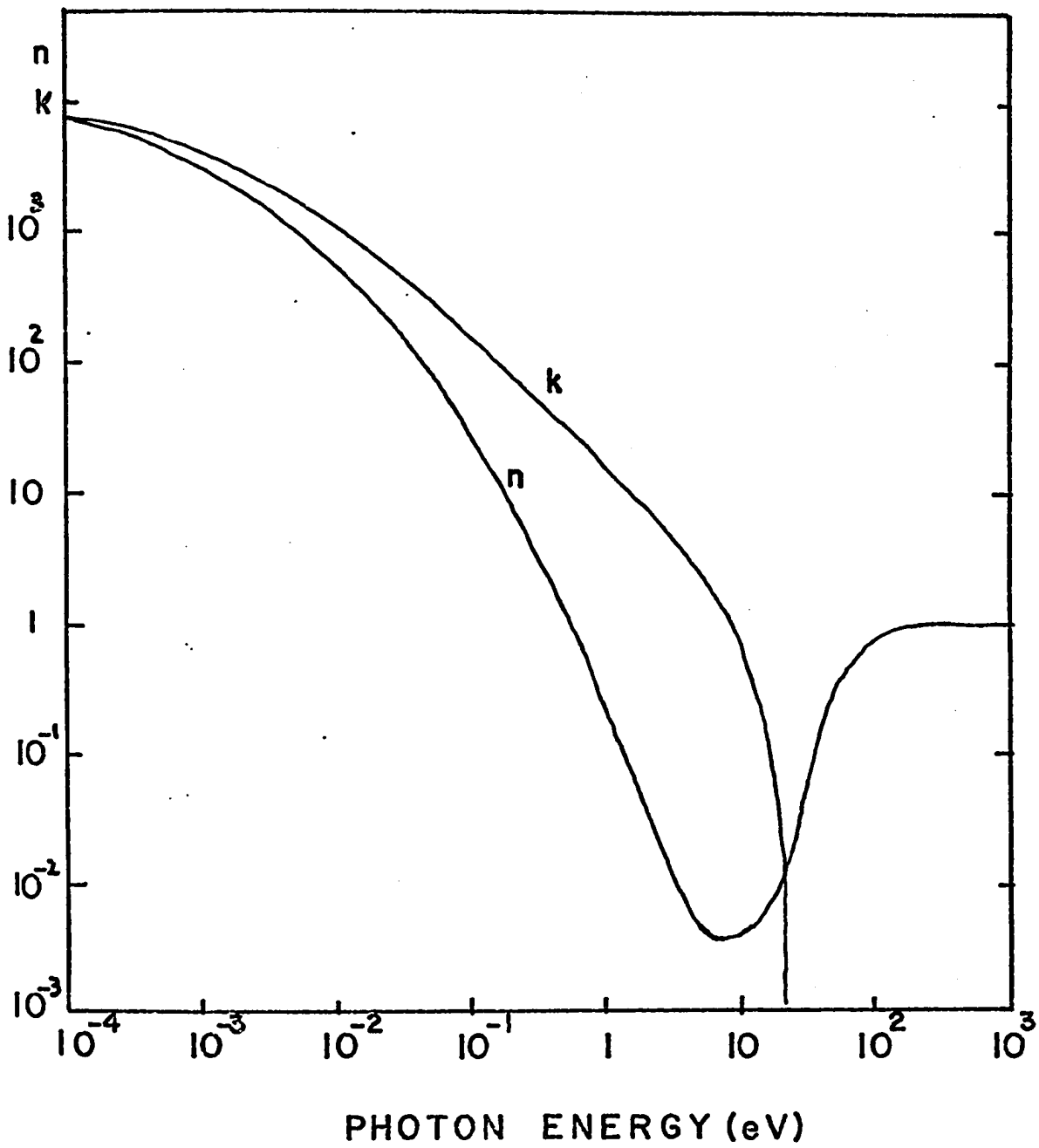

FIGURE 38: Dispersion curves of the optical constants n and k of an ideal Drude type metal calculated from expressions [17]. The values of σ_o and τ were taken arbitrarily.

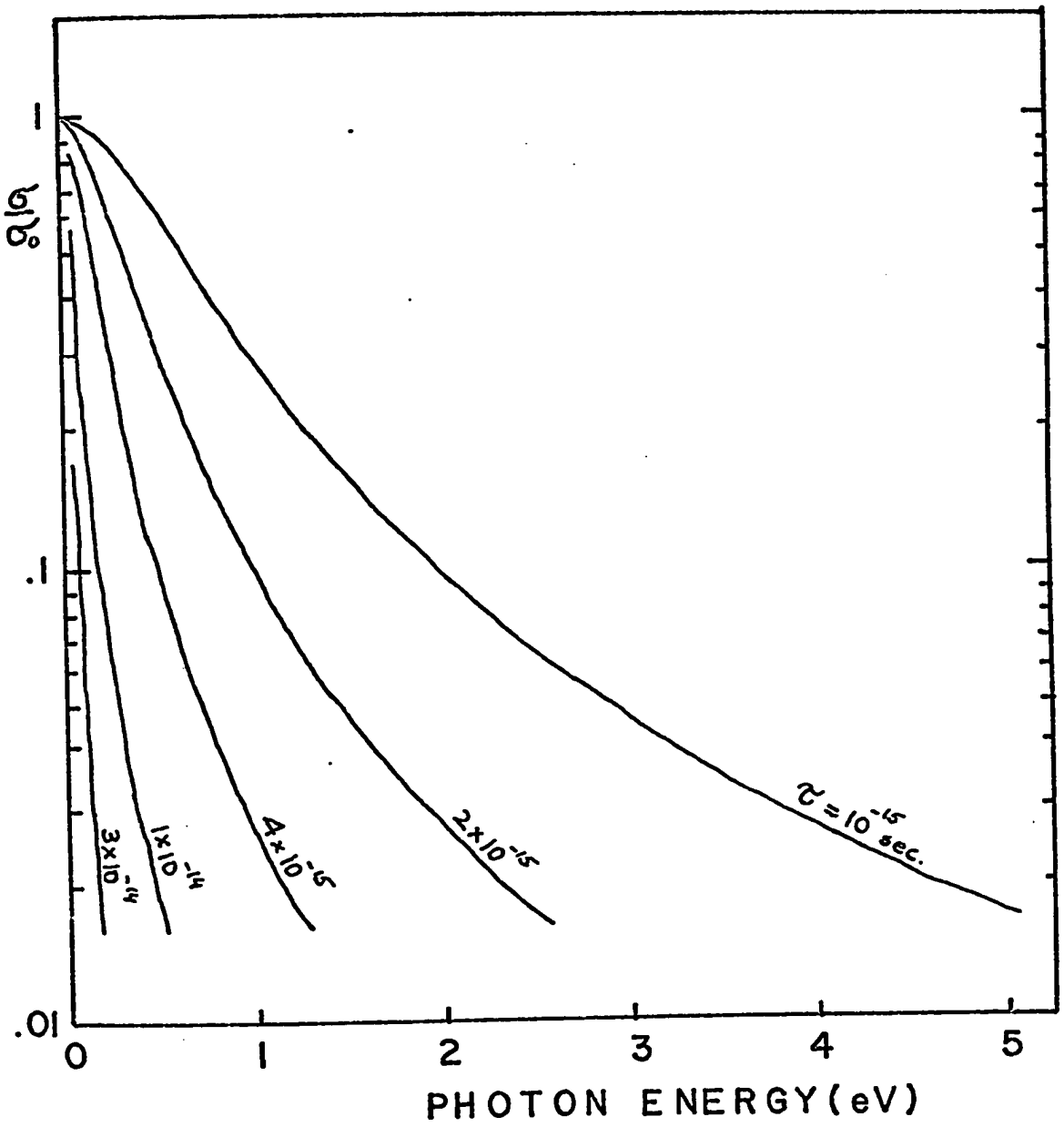

FIGURE 39: Optical conductivity curves of an ideal Drude type metal calculated from expression [17b]. The optical conductivity σ was normalized with the DC conductivity σ_o, and the relaxation time τ was used as a parameter. The conductivity is seen to be largest for E = 0 (DC), falling off sharply with increasing photon energy.

written as

$$\epsilon' = \epsilon_{Drude} + \epsilon_{others} \qquad [18a]$$

$$\sigma' = \sigma_{Drude} + \sigma_{others} \qquad [18b]$$

where subscripts "Drude" refer to the explicit parts given in [17]. If the separation of ϵ' or σ' into parts is possible for a range of photon energies then τ and N/m^* of the conduction electrons may be calculated from [17]. This is possible for some alkali metals for $E < 1.5$ eV as it was demonstrated by Mayer (9).

For multivalent metals, processes labelled "others" occur already at very low photon energies and ϵ' and σ' are not separable. In this case only estimates for τ and N/m^* may be obtained from the measured data.

4.22 Continuous Films. Due to the lack of a theory* predicting the values of n and k of continuous films, film constants are normally assumed to be the same as those for the bulk metal. Naturally, this does not mean that the macroscopic (observable) optical properties (e.g. spectral reflection, absorbtion etc.) of films are the same as those of the bulk parent metal. They are different by far for the same n and k values, as they are explicit functions also of film thickness and the wavelength, whereas those of the bulk metal are not (cf. Appendices A and B).

We suggest here a speculative refinement of the above statement

---

* Anomalous skin effect, cyclotron resonance and other phenomena involving applied magnetic fields are not considered here.

"$(n,k)_{film} = (n,k)_{bulk}$" for an ideal metal film. If the film is examined only in the Drude region of wavelengths and is not allowed to have "other" components, then equations [17] may be modified in the spirit of the Fuchs-Sondheimer theory. It is reasonable to expect that τ in equations [17] is less for films than for bulk due to boundary scattering, and that σ_o is smaller for films than for bulk by the Fuchs-Sondheimer ratio (Eq'n. [10]). If we accept that [17] is valid for films with the provisions stated above, then an equivalent to the Fuchs-Sondheimer relation may be written for the optical conductivity. From [17b] then

$$\frac{\sigma_o(\omega)}{\sigma_F(\omega)} = \frac{\sigma_o}{\sigma_F} \frac{1 + \omega^2 \frac{\sigma_F^2}{\sigma_o^2} \tau_B^2}{1 + \omega^2 \tau_B^2} \qquad [19]$$

where $\sigma_o(\omega)$ and $\sigma_F(\omega)$ are the optical conductivities of bulk and film respectively as given by [17b], σ_o and σ_F are DC resistivities of bulk and film respectively, τ_B is the relaxation time of electrons in bulk and ω is the angular frequency of light.

If $\sigma_o(\omega)$, $\sigma_F(\omega)$, σ_o, σ_F and film thickness d were measured (as they usually are in optical experiments) independently for the Drude range of wavelengths and for a number of films at different thicknesses, and if all the previous assumptions (homogenity, isotropy etc.) were met, then from this data all important fundamental constants of the bulk may be calculated as follows: from the Fuchs ratio σ_o/σ_F , ℓ may be found. From [19] τ_B may be obtained by curve fitting. Thus with τ_B and σ_o, N/m* may be calculated. Also ℓ and τ_B would give v_F which was assumed to be isotropic. From v_F and the normal Fermi-Dirac

distribution N may be obtained, and the known N/m* ratio would give the value for m*.

This scheme may work for a few alkali metals whose Drude region extends to 1 or 2 eV, and whose vacuum deposited films are well behaving i.e. they satisfy the Fuchs and Drude assumptions.

4.23 Discontinuous Films: Maxwell-Garnett Theory. It is known (5),(26) that the values of n and k of discontinuous metal films deviate widely from those of the parent bulk material. An example of this is the vivid colors of very thin films of metals (e.g. gold, silver). A theory due to Maxwell-Garnett (5), reviewed by Sennett and Scott (26) and Chopper (6) relate the measured film constants n' and k' to those of the parent bulk n and k with a geometric parameter of the film q.

It is assumed that the film consists of a random two-dimensional array of spherical or elliptical metal islands whose size is smaller than the wavelength used, and are separated from each other by gaps. No assumption is made regarding the electronic structure of the parent metal or of the metal islands. When light falls on this collection of micro particles, the individual spheres polarize with the periodic field of the light beam. From the net polarization of the whole film an effective complex dielectric constant $\tilde{n}'$ is defined with real and imaginary parts $n'^2 - k'^2$ and $2\,n'k'$ respectively. It is these quantities that may be derived from the measured values of R, T etc.

In terms of the bulk* constants n and k, the effective dielectric

---

* In the theory it is implicitly assumed that the constants n and k of the individual microparticles are identical with those of the bulk parent material. Evidence to the contrary will be given in Section 4.42.

constant is given by the theory as

$$n'k' = \frac{3\,qb}{(1 - qa)^2 + 4\,q^2b^2} \qquad [20]$$

$$k'^2 - n'^2 = 2 - \frac{3\,(1 - qa)}{(1 - qa)^2 + 4\,q^2b^2}$$

where

$$a = \frac{(k^2 - n^2 + 1)(k^2 - n^2 - 2) + 4\,n^2k^2}{(k^2 - n^2 - 2)^2 + 4\,n^2k^2}$$

$$b = \frac{3\,nd}{(k^2 - n^2 - 2)^2 + 4\,n^2k^2}$$

and $q = \frac{V_{metal}}{V_{total}}$ is the fractional volume occupied by the metal particles.

q is a measure of aggregation of a film, similarly to the (low) densities of discontinuous films, referred to in Section 3.2. If q = 0 (metal volume = 0) we get k' = 0 and n' = 1 from [20] as we should for an empty volume, and if q = 1 (metal volume = total volume) we get k' = k and n' = n as expected. The influence of q on the optical constants n' and k' in terms of n and k are shown in Figures 40a and 40b. The curves were calculated from [20]. Sennett and Scott (26) found [20] to give qualitative agreement with experimental results.

4.3 Interpretation of the Electrical Data. The mechanism of DC current conduction in Ni-P materials is not known. Pure Ni is known

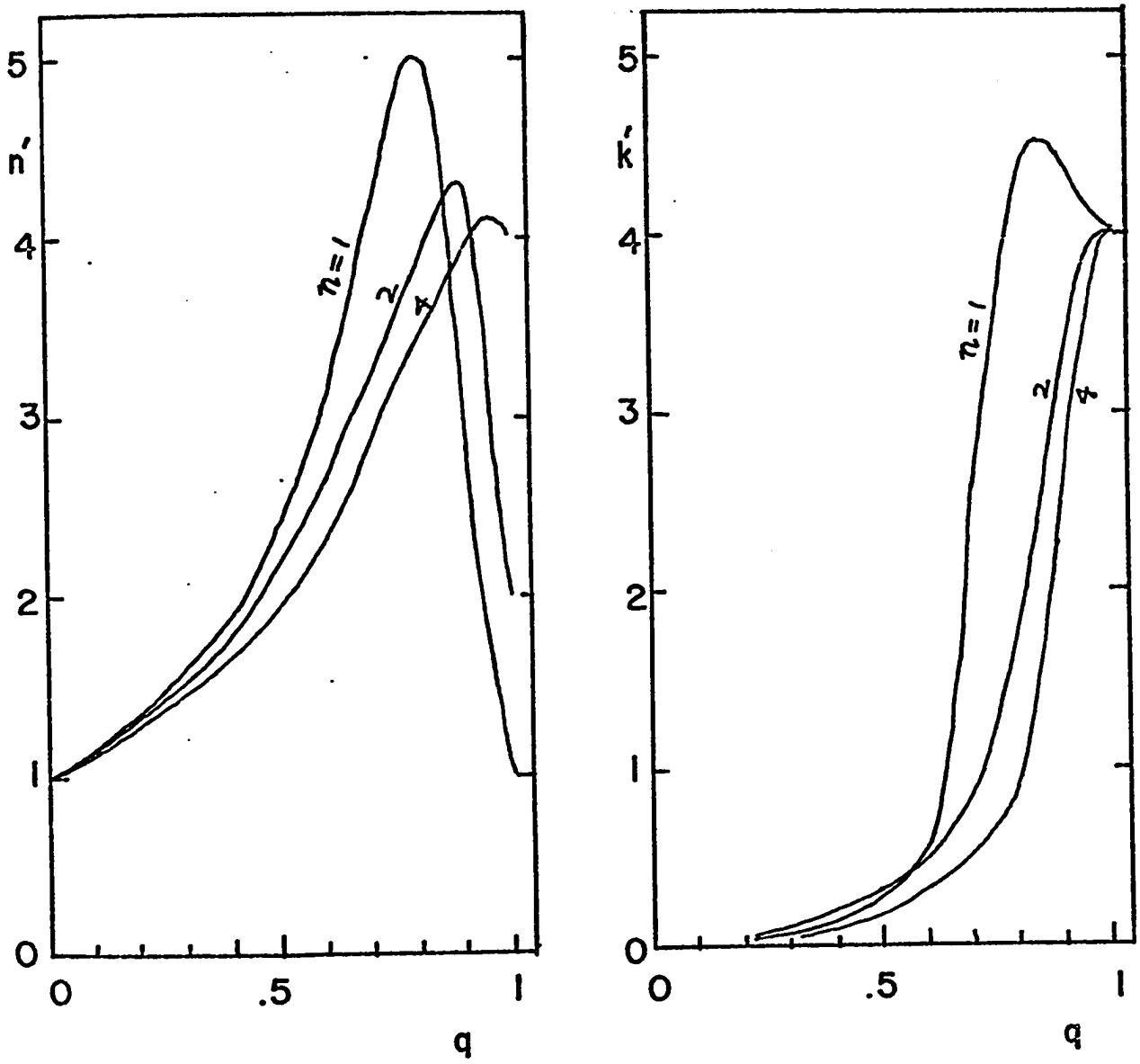

FIGURE 40: The influence of q on the optical constants n' and k' of discontinuous films with bulk constants n = 1, 2, 4 and k = 4. The curves were calculated from expressions [20]. q is the fractional volume occupied by the metal particles.

(44),(45) to have an incomplete 3d band and a partially filled 4s band in the solid state with approximately 0.6 "heavy" holes in the 3d band and approximately 0.6 electrons in the 4s band per atom, available for current conduction. The conductivity due to the holes is thought (45) to be negligible in comparison with that due to the electrons. Therefore Ni may be considered to be a monovalent Drude type conductor in the first approximation. However, the role of the heavy holes is said (45) to be important as scattering centres. They scatter the 4s conduction electrons through s-d transitions with high probability due to the high density of the (narrow) d band. The s-d scattering results in a short relaxation time τ (cf. expression [8]) and is proposed (45) as the reason for the high resistivity of nickel.

4.31 Bulk Ni-P Deposits. The room temperature resistivity of Ni-P deposits was seen to be higher than that of pure Ni. It was also seen to increase with increasing P content (cf. Figure 24). The variation of resistivity with temperature was found linear and the slope $d\rho/dT$ was shown to decrease with increasing P content (cf. Figure 25).

If we assume that the Ni-P system is an alloy and that Matthiessen's rule applies (cf. Ref. 44) then we may write the resistivity of Ni-P deposits in parts as

$$\rho_{Ni-P} = \rho_{Ni} + \rho(P) \qquad [21]$$

where $\rho(P)$ is a function of the P content and ρ_{Ni} is the resistivity of pure nickel. From Figure 24 we can determine $\rho(P)$ in the first approximation as $\rho(P) = 3.3$ P where P is the P content in the alloys by percent weight.

If we further assume that $\rho(P)$ is independent of temperature, and take the temperature coefficient of ρ_{Ni} to be $6.8 \cdot 10^{-3} C^{-1}$ (36), then $\rho_B(T)/\rho_B(25)$ in Figure 25 may be expressed as

$$\frac{\rho_B(T)}{\rho_B(25)} = \frac{\rho_{Ni}(25)\left[1+\Delta T \times 6.8 \times 10^{-3}\right]+ 3.3\ P}{\rho_{Ni}(25) + 3.3\ P} . \qquad [22]$$

With $\rho_{Ni}(25) = 6.84\ \mu\Omega$ cm, and for $\Delta T = 100$ (between 300 and 400 Kelvin) the calculated and measured ratios for P = 9.5, 13.0 and 16 w/o differ by only 2%, showing that the application of Matthiessen's rule is a reasonable first order approximation.

We thus view our Ni-P deposits as alloys where the P atoms contribute to the resistivity as additional scattering centres only. This is not contradictory to the interpretation of Albert et al. (20) of their results on Ni-P deposits. They interpret their results on the magnetization of Ni-P in terms of the Mott (46) model of nickel, according to which electrons from the 3p levels of phosphorus enter the available holes in the 3d band of nickel, and reduce its magnetic moment. In our case the filling of 3d holes by the 3p electrons of phosphorus would not change the carrier density appreciably as the conduction, due to the heavy holes, was said to be negligible. The presence of P ions in the Ni lattice would only introduce additional scattering and reduce the relaxation time.

The testing of the independence of carrier concentration on P content was not possible by Hall effect measurements due to reasons stated earlier. The carriers were established however to be electrons from the sign of the Hall voltage. In the following, the above model

will be used and it will be assumed that bulk Ni-P deposits are Drude type metals with P dependent relaxation time and constant carrier density.

4.32 Ni-P Films. According to the Fuchs-Sondheimer theory the comparison of film resistivities to that of the bulk parent metal may determine the mean free path of carriers (ℓ) if the metal is Drude type, and the films are continuous, isotropic, homogeneous and plane parallel. Attempts were made to measure ℓ of Ni-P deposits as it was thought that the conditions required by the theory can be satisfied. Ni-P was conjectured to be a Drude type metal (see above) and fresh films of Ni-P on suitably activated substrates were known from electron microscopy (see 3.1) to be continuous in the plane of the substrate for thicknesses greater than 150Å. They were also known to be homogeneous, isotropic (amorphous) and relatively plane parallel. The room temperature value for ℓ was expected to be a few hundred angstroms, typical of other metals at room temperature (see e.g. (45)).

The experimental results did not bear out the expectations. In fact the resistivity of fresh Ni-P films (Figure 26) were up to five orders of magnitude higher than that of the bulk Ni-P deposit. To fit such results to the Fuchs curves (Figure 36), the value of ℓ would have to be a few centimeters. This is clearly impossible. In contrast, results from fresh Ni films (Figure 26) could be fitted reasonably well to a Fuchs curve at $\ell \approx 500$Å and $\epsilon = 0$.

In spite of their very high resistivity, fresh Ni-P films showed metallic conduction. The temperature coefficient of resistivity was determined to be positive, and the sign of carriers to be negative.

One possible reason for the high resistivity of fresh Ni-P films was thought to be their liquid-like (amorphous) state (Figure 20). If this were the case, then a phase transformation to a crystalline state would be accompanied by a decrease of resistivity. This was indeed found when fresh films were heated in vacuum (Figures 21 and 27). The difficulty with this interpretation is that the resistivity decreases already at temperatures well below the crystallization temperature of films (Figure 27).

A more likely reason for the high resistivity of fresh Ni-P films was thought to be their low density (Figure 23b). Low density continuous films may be viewed as slabs with very high defect density and amorphous structure. On heating in the vacuum the density was shown to increase, along with the decrease of resistivity. In addition to structural causes, the possible presence of hydrogen in fresh Ni-P deposits may also contribute to the high resistivity. Nickel is known to absorb hydrogen (47) and Ni-P should be no different, especially since Ni-P films grow in an environment of H^+ ions (17). Absorbed hydrogen is known (48) to prevent proper crystallization of nickel and increase its resistivity. It is also known (47) that the absorption process is reversible at room temperature i.e. the hydrogen readily desorbs from thin films. It is thought that the initial decrease in resistivity of fresh films upon evacuation (Figure 27) is due to hydrogen desorption. Observed losses of mass of fresh Ni-P films during vacuum heat treatment may also be due to this process.

On the basis of the above reasoning then, Figure 27 may be interpreted as follows: first decrease (common to all films) may be

due to hydrogen desorption, while the last decrease (common to all films) may be due to crystallization. The decreases at intermediate temperatures may be due to increasing densities. For very thick films the latter decrease is small, but for thin films it may be as large as two orders of magnitude. At temperatures between 500°C and 750°C no further decrease in resistivity occurs.

Fully heat treated Ni-P films showed resistivity film thickness relation more closely following that predicted by the Fuchs-Sondheimer relation but still could not be fitted to a single curve with a constant value of ℓ and a constant value of bulk resistivity. The failure is likely due to the difference between film and bulk densities (Figure 23b) that still remains after heat treatment.

The conductivity of heat treated Ni-P films was determined to be metallic from the positive slopes of resistivity-temperature curves (Figure 28). The slopes are relatively constant, indicating that the relaxation times τ are film thickness dependent (cf. Matthiessen's rule), and that the ratio of carrier density N and effective mass m^* of electrons is constant in the first approximation. N was determined to be between 10^{22} and 3×10^{22} cm^{-3} from Hall effect measurements, and to be independent of film thickness within the accuracy of measurements.

It may be assumed then that N and m^* are constants for heat treated Ni-P films and that the variation of τ is responsible for the variation of resistivity with film thickness.

4.4 Interpretation of the Optical Data. The electronic structure of Ni-P materials is not known. Pure Ni has been investigated in the bulk form and its band structure is known with some certainty (38), (49). Free electron (Drude) behaviour has been observed for pure Ni for photon energies below 0.15 eV only due to the influence of low energy band to band transitions (50). The first pronounced low energy transition is observed at 0.3 eV and is interpreted by Ehrenreigh et al. (38) to be a d band to Fermi level transition.

In spite of the interband transitions, our low energy (0.5 eV) optical data of Ni and Ni-P will be analysed in terms of the free electron model (Drude theory) to obtain an approximate value for relaxation time and an approximate value for N/m^*. From the higher energy optical data some qualitative conclusions will be made.

4.41 Bulk Ni-P Deposits. The optical conductivity σ of bulk Ni and Ni-P deposits was calculated from the experimental values of n and k (see Figure 30) in practical units using the relation

$$\sigma\ [\mu\Omega\ \text{cm}]^{-1} = 2.68 \times 10^{-4}\ nkE \qquad [23]$$

where E is the photon energy in electron volts. This relation was derived from [16b]. σ values calculated from it are plotted against E in Figure 41.

From the optical conductivity σ at E = 0.5 eV and the DC conductivity σ_o of each sample, a quantity t, similar to the relaxation time τ, was calculated from the relation

$$t\ [\text{sec}] = \frac{6.56 \times 10^{-16}}{E} \sqrt{\frac{\sigma_o}{\sigma} - 1} \quad . \qquad [24]$$

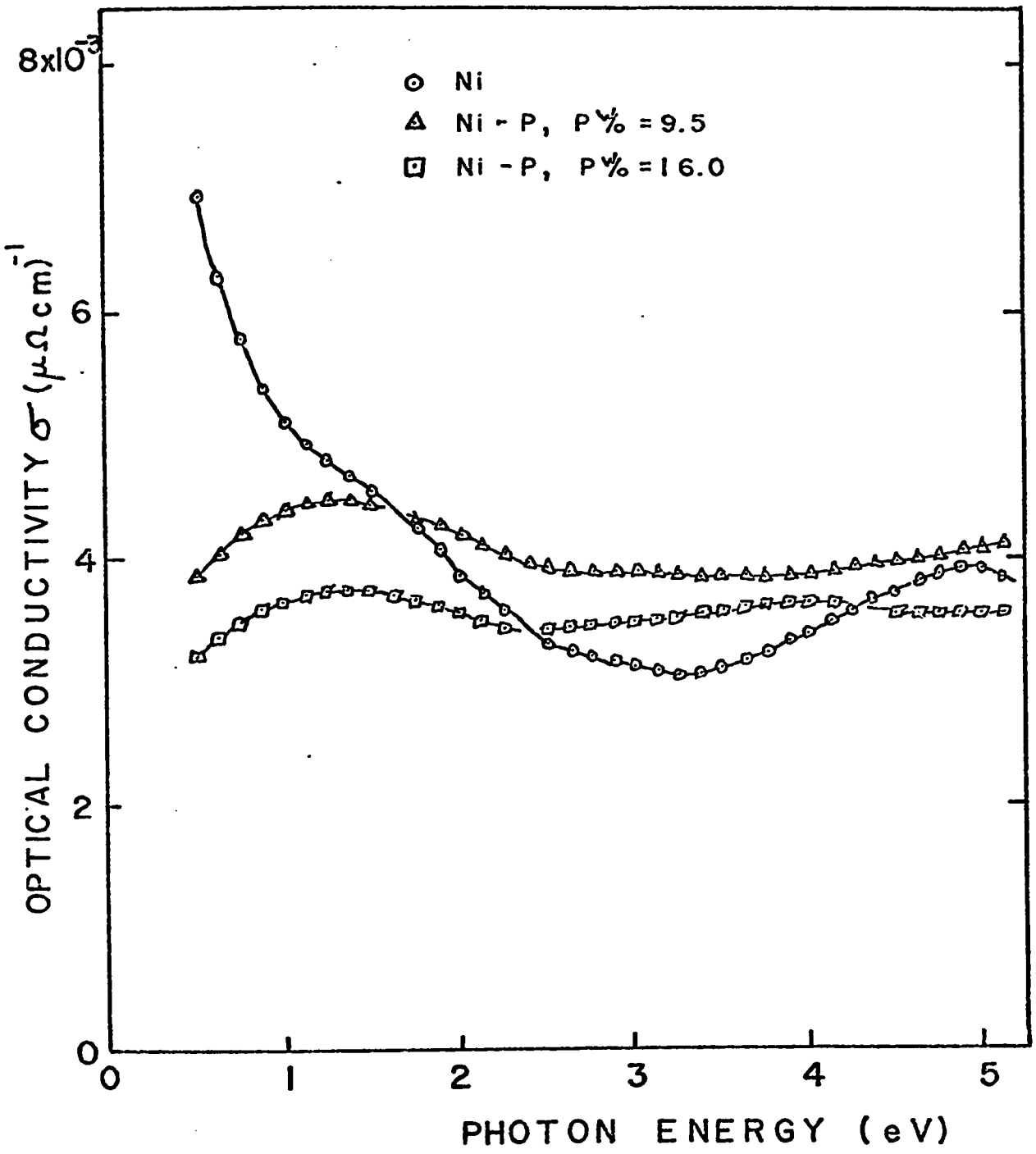

FIGURE 41: Spectral dependence of optical conductivity of Ni and Ni-P bulk specimens. The values were calculated from experimental n and k data.

Relation [24] was derived from [17b]. The quantity t in relation [24] is equal to τ in relation [17b] if $\sigma = \sigma_{Drude}$ (cf. equation 18b), otherwise $t < \tau$. The calculated values of t are listed in Table III.

Using these values of t and the DC conductivity, a ratio R similar to N/m^* was calculated from the relation

$$R = 5.91 \times 10^{-15} \frac{M\sigma_o}{\rho t} \qquad [25]$$

where M is atomic mass and ρ density in gr cm^{-3} . If $t = \tau$ then $R = N/m^*$, where N is number of carriers per (Ni) atom and m^* is effective mass of carriers in units of free electron mass. If $t < \tau$ then $R > N/m^*$. The calculated values of R are also listed in Table III.

TABLE III

Values of t and R of bulk Ni and Ni-P Samples
Calculated from Experimental Values of n and k.

w/o P Content	t (sec)	R
0	5.9×10^{-15}	0.97
9.5	3.2×10^{-15}	0.40
16.0	2.7×10^{-15}	0.33

The extent of deviation of t from τ and that of R from N/m^* cannot be determined, as the interband part of σ is not known. For this reason the above data is not sufficient to test the model of bulk Ni-P deposits proposed in 4.31. However the figures for t and R in

Table III may be used as order of magnitude values of τ and N/m^* respectively.

The optical conductivity of Ni-P materials in Figure 41 shows no sharp structure between one and six electron volts, whereas Ni has sharp peaks (not evident in Figure 41, but shown to exist by Ehrenreich et al. (38)) at 1.4 eV and 4.8 eV identified (38) as transitions between $d \rightarrow E_F$ and $E_F \rightarrow$ higher bands (E_F is Fermi energy) respectively. One possible explanation for the missing structure in the Ni-P curves is that the presence of P widens the energy bands of Ni (or narrows the gaps). This would shift the structure (absorption peaks) to lower energies, or eliminate them altogether.

4.42 Ni-P Films. The optical conductivity σ of fresh and heat treated Ni-P films deposited using solution with pH = 5.3 (P content 9.5 w/o) was calculated from the experimental values n and k (see Figure 33) using relation [23]. The spectral distribution of σ for a number of films is plotted in Figures 42a (fresh) and 42b (heat treated). The change of σ of a Ni-P film with the temperature of heat treatment is shown in Figure 43. This was calculated from data in Figure 34 using relation [5].

A calculation of t was attempted for the samples from their corresponding values of σ at E = 0.5 eV and DC resistivity σ_o^{-1} using relation [24]. For all fresh films and the thinnest of heat treated films, the quantity under the square root in [24] became negative, consequently no t value could be obtained. The values of t for thicker heat treated films are listed in Table IV. Values of R were also calculated for these films using relation [25]. In the calculation the measured film densities (see Figure 23b) were used. Values of R

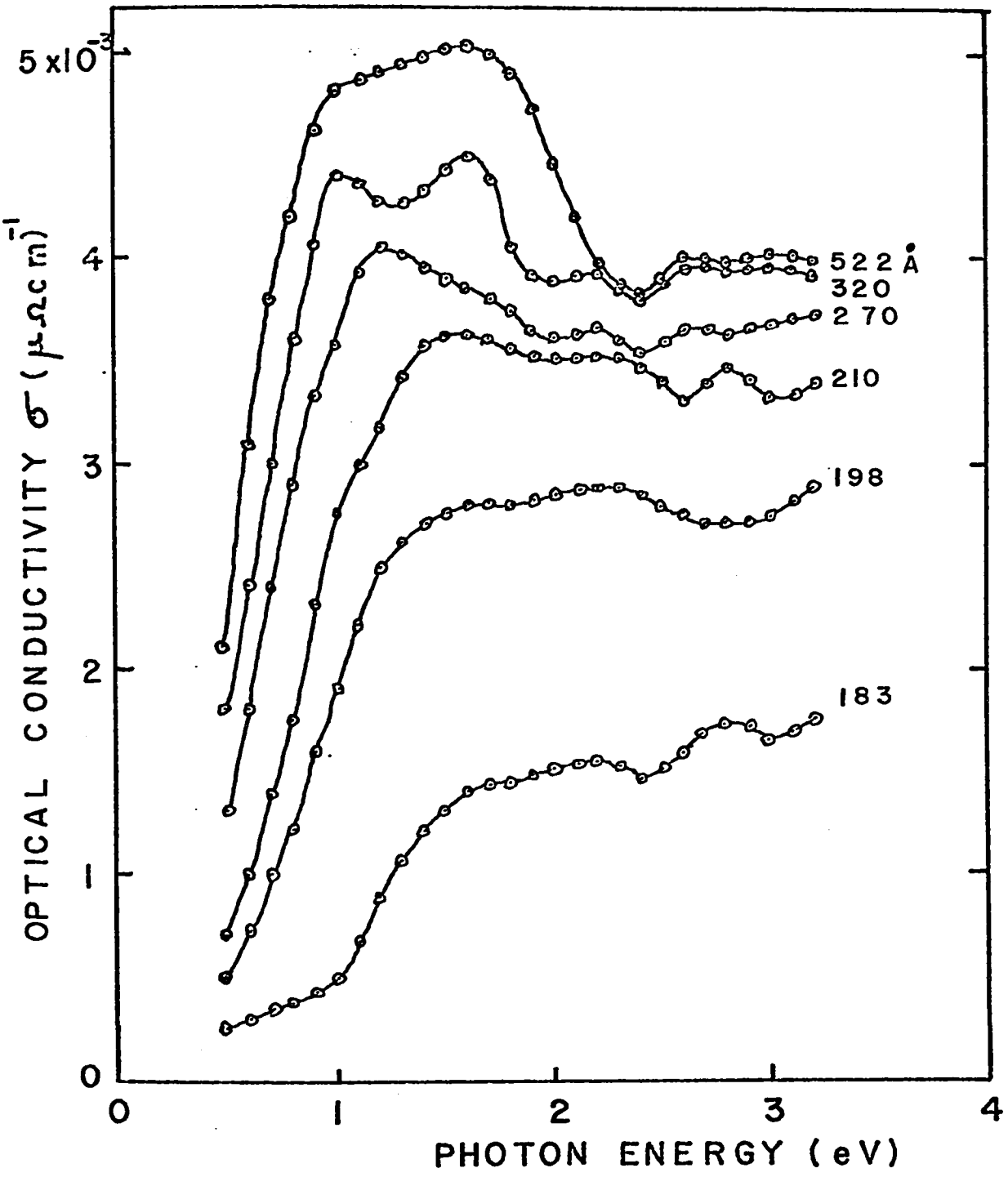

FIGURE 42a: Spectral dependence of optical conductivity of fresh Ni-P films. The values were calculated from experimental n and k data. The geometrical film thickness d_{opt} is indicated at each curve.

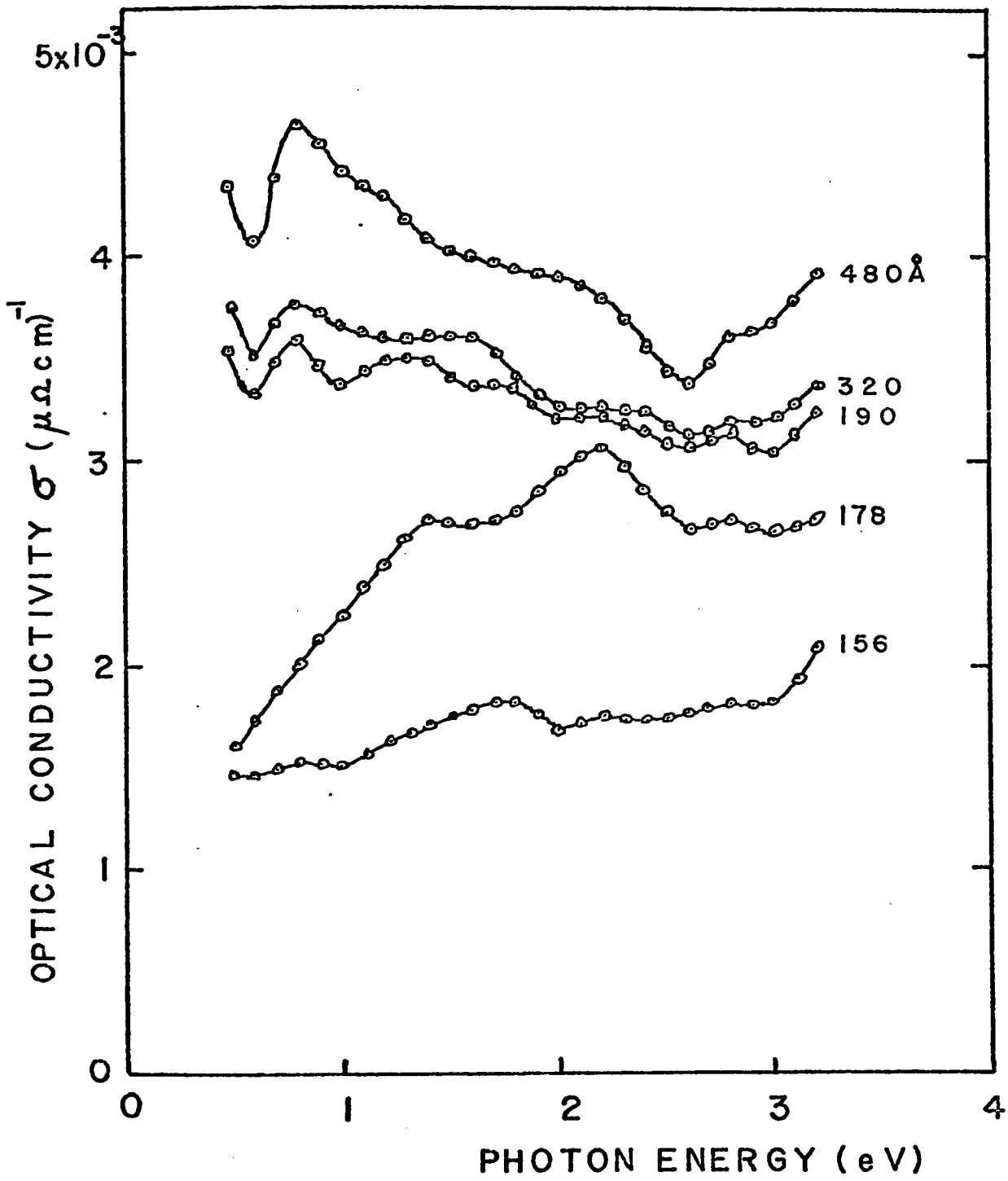

FIGURE 42b: Spectral dependence of optical conductivity of vacuum heat treated Ni-P films. The values were calculated from experimental n and k data. The geometrical film thickness d_{opt} is indicated at each curve.

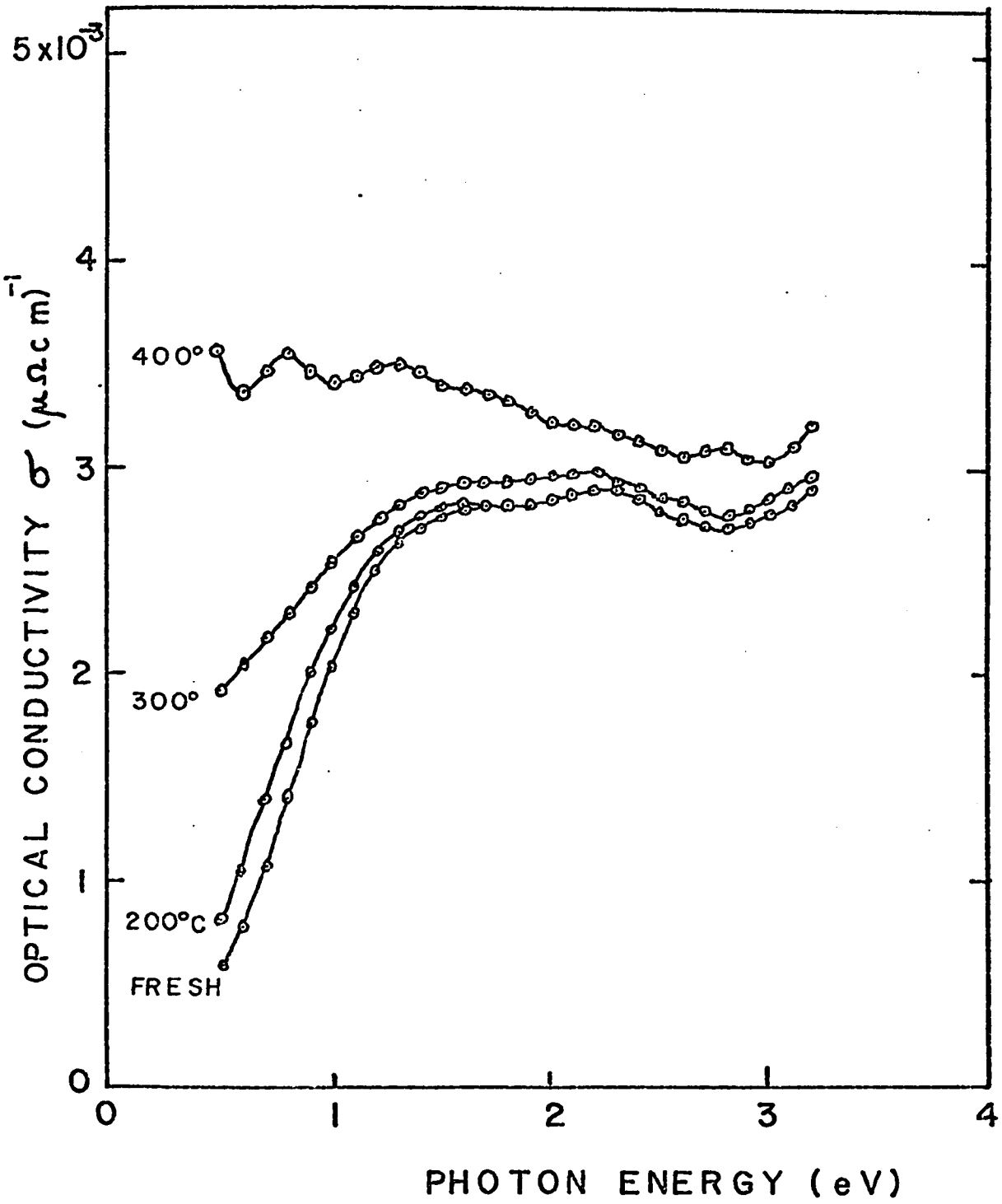

FIGURE 43: The change of optical conductivity of a Ni-P film with temperature of vacuum heat treatment. The values of σ were calculated from data in Figure 34. Temperature of heat treatment is marked opposite each curve.

are also listed in Table IV. For reference, the bulk values are included from Table III.

TABLE IV

Values of t and R of heat treated Ni-P Films
Calculated from Experimental Values of n, k and σ_o^{-1}

w/o P Content	d_{opt} (Å)	σ_o^{-1} μΩ cm	t (sec)	R
9.5	Bulk	35.0	3.2×10^{-15}	0.40
9.5	494	73.5	1.8×10^{-15}	0.37
9.5	320	132.0	1.14×10^{-15}	0.38
9.5	218	230.0	0.86×10^{-15}	0.36

From Table IV, R is seen to be relatively independent of film thickness and t is seen to be thickness dependent. The same was found earlier (cf. end of Section 4.32) for N/m^* and τ from temperature coefficient measurements (see Figure 28). The comparison of the two sets of numerical data (using Matthiessen's rule) shows that R and t in Table IV may be considered to be reasonable values (± 20%) for N/m^* and τ respectively. The approximate value of m^* calculated from R and our previous Hall data turns out to be $m^* = 0.7 \pm 0.3$ in units of free electron mass.

Turning now to fresh films (Figure 42a) for which no real t could be obtained, we note that the low energy conductivity is much smaller than that for heat treated films. We also note that the shapes of σ curves in the figure are reminiscent of those for dielectrics or

semiconductors (see e.g. (51)) with an apparent absorption edge in the region of 1 eV. This cannot be so as Ni-P is known to be a metal from DC conductivity and Hall effect measurements. The only way for a metal to exhibit such optical behaviour is for it to be in a finely aggregated form. In this case the affairs would be described by the Maxwell-Garnett theory.

On the basis of the nucleation and growth study of Ni-P films it did not appear likely that the subject films are aggregated in the plane of the substrate, especially as all films were grown on substrates with maximum activation density. (Maximum activation density allows films to be discontinuous - see Section 3.1 - only for thicknesses less than 100Å, and the films considered here were all thicker than this). On the other hand, it was thought possible that fresh films were aggregated in three dimension due to the evolving hydrogen bubbles during growth. The arrangement of the material particles in such a film may be similar to that of the pebbles in a layer of gravel. This is not contradictory to any experimental evidence discussed so far. In fact, reflection photographs of specially made Ni-P films suggests such a "pebbly" geometry. An exaggerated example of this is shown in Figure 44.

It was assumed then that fresh films were three dimensionally aggregated, and that the <u>film</u> results could be interpreted in terms of the <u>bulk</u> constants, using the Maxwell-Garnett theory.

For the interpretation of the film results, we denote film constants by primed symbols i.e. n', k', σ', bulk constants by unprimed symbols i.e. n, k, σ etc., and calculate σ' from the bulk constants n

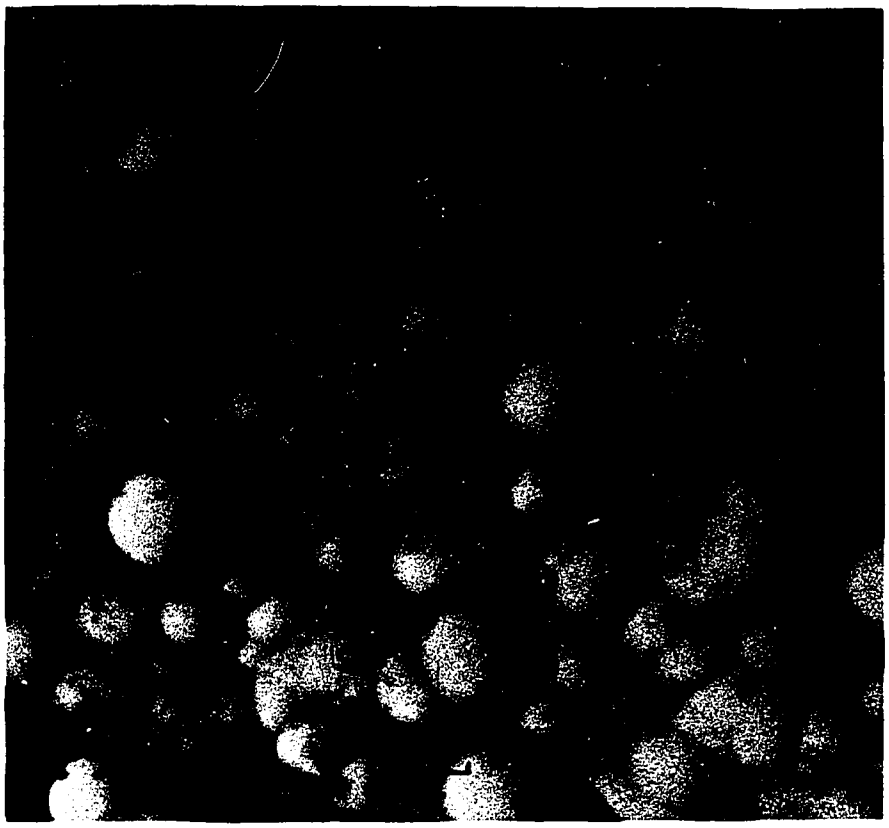

FIGURE 44: A reflection microscope photograph showing the "pebbly" geometry of a Ni-P film. The film was grown specially to develop such large component pebbles.

and k using the Maxwell-Garnett theory (expressions [20] and [23]). The results are shown in Figure 45. The curve marked q = 1 is the conductivity σ of bulk Ni-P (see Figure 41) and those of q < 1 are conductivity curves σ' of films with various degrees of aggregation. A comparison of the experimental conductivity curves of Ni-P films in Figure 42a and the calculated ones in Figure 45 shows similarities but no fit can be obtained for any single value of q. Assuming still that our fresh films are aggregated, that the Maxwell-Garnett theory applies and that the measurements were correct, it must be concluded that the optical properties of microparticles in the films are <u>unlike</u> those of the parent bulk materials. (This conclusion was also made speculatively for thin films of metals by Heavens(29)).

For our new approach then, we continue with the original assumptions, and we let the constants of the microparticles be n'', k'' and the conductivity be σ'', and calculate σ'' from the experimental values of n', k' (Figures 33) and q (Figure 23b) using the inverse to the Garnett relation [20] and relation [23]. Figure 46 shows σ'' along with σ of the bulk. The σ'' curves calculated for many samples ranging in thickness from 160Å to 600Å and in q value from 0.70 to 0.92, were nearly identical and fell within the error bars in the figure. This result shows that our assumption regarding three dimensional discontinuity in fresh Ni-P films was correct, and that the optical properties of microparticles constituting the fresh films are indeed <u>different</u> from those of the corresponding bulk material.

σ'' has similar characteristics to the conductivity curves of heat treated Ni-P films in Figure 42b. Its low energy portion

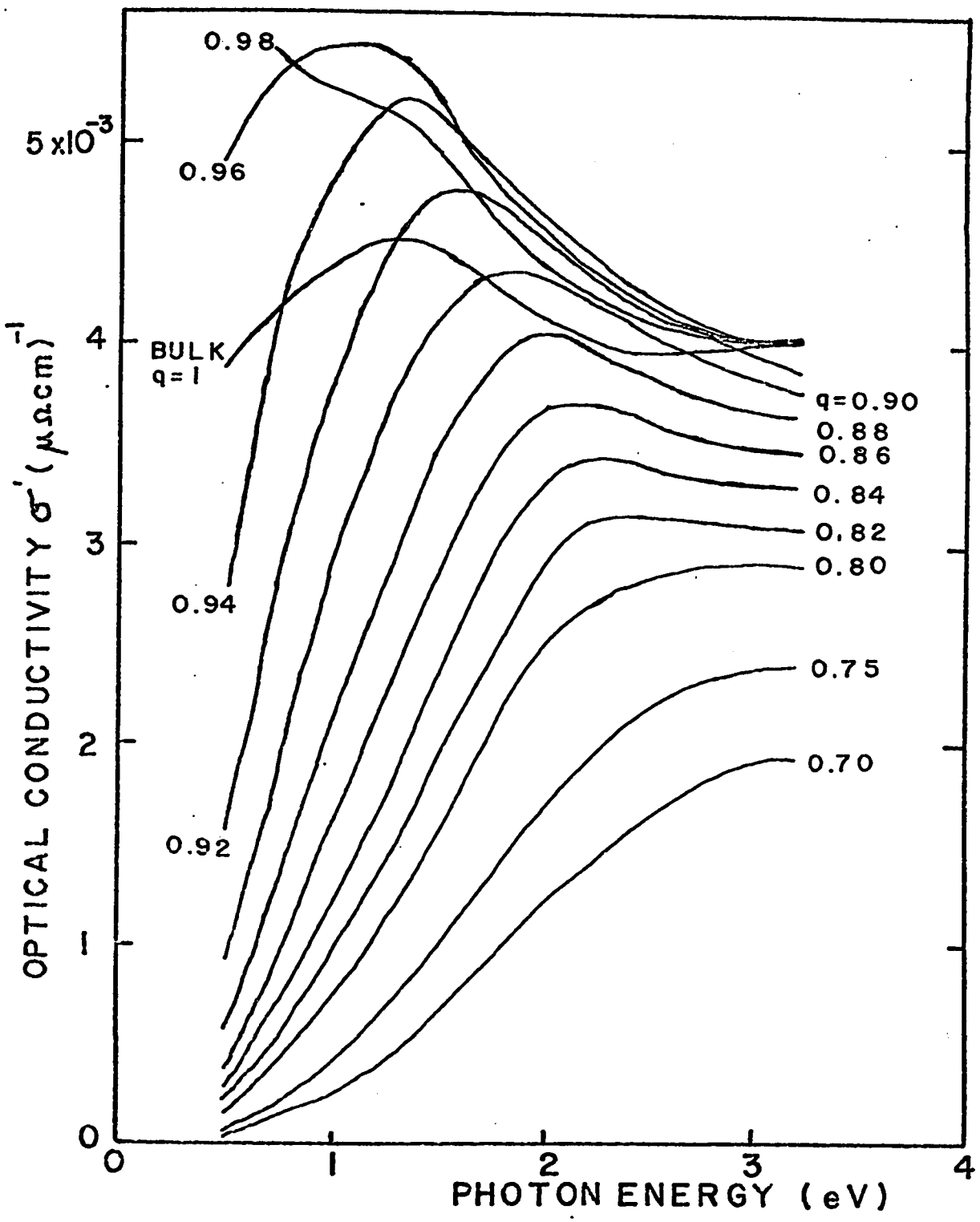

FIGURE 45: Maxwell-Garnett curves of optical conductivity calculated from experimental values of bulk Ni-P constants n and k. The values of parameter q are marked opposite each curve. The curve q = 1 is the conductivity σ of the bulk.

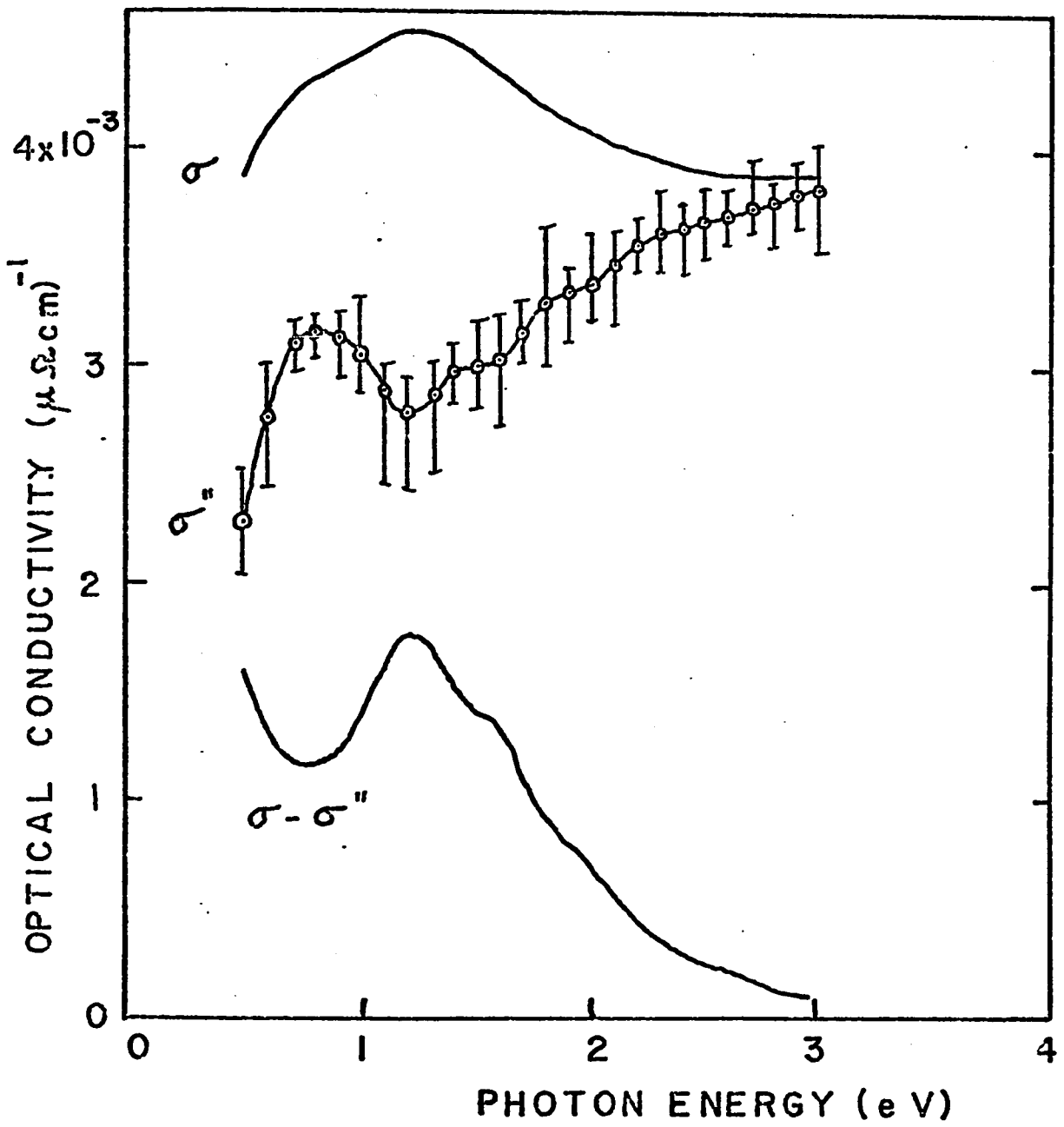

FIGURE 46: Spectral dependence of optical conductivity σ'' of microparticles composing the fresh Ni-P films. The values of σ'' were calculated from the experimental n' and k' data of a number of films with different thicknesses using the Maxwell-Garnett theory. Parameter q was calculated from the measured density of each film. σ of the bulk, and σ - σ'' are also included for reference.

(0.5 - 2 eV) could be fitted between curves marked 190Å and 178Å. This may be an indication of size of the microparticles composing the fresh films. Another feature of the curves is the peak at 0.8 eV. This may be the 1.4 eV d → E_F transition of Ni shifted down by the presence of P, as it was already suggested for bulk Ni-P in part 4.41 above.

Finally, an estimate of the DC resistivity σ_o^{-1} of microparticles is made using our previous assumption of N/m^* being constant. Taking $R = N/m^* = 0.38$ (see Table IV) and $\sigma'' = 2.25 \times 10^{-3}$ $(\mu\Omega\ cm)^{-1}$ at E = 0.5 eV (see Figure 46), we get from [24] and [25] the values $\sigma_o^{-1} \approx 410\ \mu\Omega$ cm and $\tau \approx 0.37 \times 10^{-15}$ sec. A comparison of this resistivity value with those of Ni-P films in Figure 26 and Table IV shows the resistivity of microparticles (410 μΩ cm) to be comparable with those of bulk Ni-P (35 μΩ cm) and heat treated Ni-P films, whereas the resistivities of fresh films composed of 410 μΩ cm microparticles are from two to four orders of magnitude higher than this.

CHAPTER 5

DISCUSSION

Based on the experimental results interpreted in the previous section, a working model for Ni-P films is developed in the first part. In the second part some features of Ni-P films are compared to those of vacuum evaporated Ni films and the major differences are discussed. It is suggested that our model for Ni-P films is applicable to "dirty" vacuum deposited metal films. Finally, the theoretical consequences of the model are discussed and suggestions are made to improve the current theoretical situation.

5.1 A Model for Ni-P Films. A working model for Ni-P films based on experimental results is given below. It is developed from structural, electrical and optical features of films. The model is valid for films grown on substrates catalysed with maximum activation density (10^4 sites per square micron) and grown thick enough ($\approx$ 100Å) to be geometrically continuous in the plane of the substrate. Both the fresh and the vacuum heat treated states of films are described.

5.11 Structural Features. In the electroless solution Ni and P atoms collect on catalytic sites on the substrate in a ratio determined

by the composition of the solution. The by-product of the reaction is hydrogen. The growth of Ni-P on catalytic sites is isotropic, resulting in a spherical Ni-P island geometry. A continuous film in the plane of the substrate is formed when the islands grow large enough to merge. The maximum population of catalytic sites on a substrate surface is approximately one site in an area 100Å x 100Å. Film continuity at such activation density in the plane of the substrate is reached at an average film thickness of 100Å. At this point of film growth the "building blocks" of the film are roughly spherical Ni-P microparticles, each measuring about 150Å in diameter, forming a continuous layer on the substrate. The structure of individual particles is not known; they may be amorphous or crystalline with crystallite sizes of a few tens of angstroms (showing a liquid-like electron diffraction pattern).

The growing Ni-P microparticles are in an environment of hydrogen, and absorb up to 0.6H for each Ni atom. The excess hydrogen collects in the crevices of the uneven, single layer film surface and forms bubbles of microscopic size. The bubbles mask the surface from the solution and deposition stops in that region. When enough H_2 is collected by the bubble from neighbouring regions to grow large enough and break away from the film, deposition is resumed. This stop-and-go process produces an aggregated film, full of faults, crevices and microscopic voids, resembling a layer of gravel as was suggested earlier.

The building blocks of the three-dimensional (seemingly continuous) film are microscopic Ni-P-H pebbles each with bulk density (8.1 gr cm^{-3} for P = 9.5 w/o) causing the film density to be as low as 70% of the bulk density.

The order of the size of the pebbles is that of the original islands ($\approx$ 150Å) and their structure is still liquid-like (or very fine polycrystalline).

Upon evacuation, the Ni-P-H material looses its H content, and upon heating in the vacuum the density of films (now composed of Ni-P microparticles) increases to a value that approaches the bulk density with increasing film thickness. The increase in density is due to the partial annealing of crevices, defects and faults, and the process eventually (at a temperature between 300°C and 500°C) leads to crystallization. Films of Ni-P do not break up into islands on the substrate during heating (as, for example, pure Ni does at as low a temperature as 250°C) indicating that the presence of P in the nickel increases its free energy, thus decreasing the relative free energy of the substrate-film interface. The defect density in fully heat treated and crystallized films remains higher than that of the bulk, and approaches that of the bulk with increasing film thickness. Therefore such a film (or for that matter any type of Ni-P film considered here) having a thickness less than a few thousand angstroms may not be considered to be physically the same as a slice of equally thick slab cut out of the bulk.

5.12 Electrical Features. The value of DC conductivity of Ni-P materials is P dependent. The P content does not modulate the N/m^* ratio of the majority carriers (electrons) in Ni in the first approximation. The conductivity is influenced through τ, as P acts as additional scatterer in the lattice. The electronic configuration

of Ni-P materials is thought to be that of Ni, modified by the 3p electrons of P entering into the available 3d holes of Ni. The P content of the Ni-P material used for film work was 9.5 w/o with $N/m^* \approx 0.40$, $\tau \approx 3.2 \times 10^{-5}$ sec $\sigma_o^{-1} = 35$ $\mu\Omega$ cm, and density of 8.13 gr cm^{-3}.

The extremely high resistivity of continuous fresh films is the result of the three dimensionally aggregated structure of films, the lack of crystallinity and the presence of hydrogen in the films. The Ni-P-H microparticles that form the film (three dimensional "pebble" structure) are only in slight contact with their neighbours, and the boundaries are saturated with hydrogen, forming an electronic barrier between the conductive particles. Some microparticles establish more direct contact with neighbouring ones during film growth, forming occasional chains for metallic conduction. These chains criss-cross the film and are responsible for the metallic conduction of films. The chains are few in number however (and very meager in cross section). Thus the very high net resistivity of fresh films. Any slight environmental disturbance will reduce the resistivity of fresh films (e.g. the resistivity of fresh films has been observed in the present work to decrease permanently by one or two orders of magnitude by the application of a slight mechanical pressure on the surface of films).

Upon evacuation the fresh film loses its H content, the microparticles become Ni-P in composition and establish better contact between neighbours, free of high potential barriers. The conductivity consequently increases. Upon heating in the vacuum the particle boundaries become larger due to the increased mobility of atoms (the free energy of the film decreases and the configuration becomes more

stable) resulting in further increase in conductivity. Eventually at a high enough temperature, the most ordered state of a given film is reached through crystallization, and the highest conductivity is achieved for that film. The degree of ordering and the value of conductivity in this condition is film thickness dependent, with thinner films more disordered than thicker ones. The film thickness dependence of conductivity is not that predicted by the Fuchs-Sondheimer theory (limitation of electronic free paths by the thickness of films) due to the remaining structural deviations of films from that of bulk.

5.13 Optical Features. The optical constants of Ni-P materials are P dependent. It may be argued that the P widens the energy bands (or narrows the gaps) of Ni. (The 4.8 eV $E_F \rightarrow$ higher bands transition of Ni is missing for Ni-P with P $\geq$ 9.5 w/o, and the 1.4 eV d $\rightarrow E_F$ transition may have shifted to 0.8 eV at P = 9.5 w/o, see Figures 42b and 46).

The optical properties of fresh films are controlled by the properties of the Ni-P microparticles composing the films. The fit of experimental results with the Maxwell-Garnett theory shows the majority of microparticles to be isolated from their neighbours and to be electrically polarizable (thus the dielectric-like optical response of fresh films in Figure 42a). This is in agreement with the structural and electrical behavior. Also from the agreement of experiment and theory, the composition, density, structure and average size of microparticles appear to be independent of film thickness.

We assume now that the composition, density and structure of

microparticles are identical with those of the corresponding bulk Ni-P material and assert that the difference in properties between them and the bulk is due only to the limitation of electronic mean free paths in the microparticle. Another way of expressing this idea is to say that a Fuchs-like relation exists for microparticles (but not for films, fresh or heat treated), where the DC conductivity, the Drude part of optical conductivity and the interband part of optical conductivity are all some functions of the particle size and bulk parameters only.

Such functions have not yet been formulated (for further discussion on this see Section 5.3) but some qualitative support for the idea is evident. An inspection of Figure 46 shows the conductivity of microparticles σ'' to be lower than that of the bulk σ. The conductivity σ'' approaches σ with increasing E, and at photon energy $E \approx 3.2$ eV, $\sigma'' = \sigma$. This indicates that electronic processes (e.g. intra- and interband transitions) with relaxation times shorter than $\tau \approx 10^{-15}$ sec ($E \approx 3.2$ eV corresponds to $t \approx 10^{-15}$ sec) have mean free paths shorter than the size of the microparticles and the processes are not influenced by the boundaries. As the relaxation times increase however, the mean free paths become constrained by the particle boundaries and are reduced to $\approx 150\text{Å}$. Consequently, we get $\sigma'' < \sigma$.

Additional evidence in support of the Fuchs-like idea is provided by the calculated DC value of relaxation time for the microparticles. The calculated value of $\tau = 0.37 \times 10^{-15}$ sec. is approximately a tenth of the bulk value, indicating* a bulk electronic mean free path two to

---

* cf. Section 5.3

three times that of the size of the microparticle. An approximate value for ℓ of 300Å - 450Å is certainly reasonable.

Upon vacuum heat treatment the microparticles lose their isolated configuration in the film, and with that they lose their identity. The macroscopic optical properties of films change with the temperature of heat treatment (see e.g. Figure 43) and can no longer be interpreted by the Maxwell-Garnett theory. In the fully heat treated condition, the material part of films (i.e. the merged collection of microparticles) may have optical properties identical to those of the bulk. However this cannot be detected by observing the optical response of films, as they are composed of the material part and voids, and exhibit film thickness dependent (i.e. density dependent) properties (see e.g. Figure 42b).

From low energy optical data N/m^* was determined for fully heat treated films to be independent of film thickness in the first approximation and the approximate value of m^* was estimated to be 0.7 ± 0.3 free electron mass.

Finally, allowing a few lines for speculation, it is suggested that the shape of the $\sigma - \sigma''$ curve in Figure 46 may be due to the above mentioned size effect, influencing not one but two types of carriers (either 4s electrons and 3d holes, or electrons with two different effective masses etc.). The first part (0.5 eV - 0.8 eV) of the curve may be a Drude-like response of carriers with a large value of τ and the second part (1.2 eV - 3 eV) may be that of carriers with a small value of τ. This is conceivable as the size restriction would influence the large ℓ of the slow carriers (τ large) more than

the small ℓ of the fast carriers (τ small).

5.14 The Model of Ni-P Films. Massive electroless nickel in a stable (vacuum heat treated) state is composed of Ni and P with $0 \text{ w/o} \leq P \leq 16 \text{ w/o}$, and its structure is crystalline. The 3p electrons of P appear to enter the 3d holes of Ni, and P acts as additional scatterer for the carriers. In the single carrier approximation the presence of P influences τ only and has no appreciable effect on N/m^* of the conduction electrons. The resistivity of Ni-P is approximately ten times that of pure Ni. The presence of P also appears to widen the bands of Ni, eliminating or shifting the optical absorption peaks.

Films of Ni-P grown on activated substrates differ from the corresponding bulk in many ways. Film properties are structure and composition dependent, and both the structure and the composition of fresh films are unlike those of the bulk. The structure of fresh films is inhomogeneous (consisting of three dimensional Ni-P "pebbles" or microparticles and voids) and liquid-like (amorphous or very fine polycrystalline). The composition of fresh films is Ni-P-H. The H appears to be adsorbed on the Ni-P microparticles, forming potential barriers between neighbouring islands. The resulting DC resistivity of films is several orders of magnitude higher than that of the corresponding bulk, and the optical properties resemble those of a dielectric or semiconductive film. However, the individual Ni-P microparticles have optical properties corresponding to those of bulk Ni-P as predicted by theory. The DC conductivity of the individual microparticles is not known but is proposed to be that of the bulk,

modified by a Fuchs-like (three dimensional) boundary scattering of the carriers.

Upon heating fresh Ni-P films in the vacuum, the films lose their H content, the component microparticles merge, and eventually crystallization takes place. The properties of films become similar to those of the bulk but remain thickness dependent as the structure of only the thickest films approach the structure of the bulk.

5.2 A Comparison of Ni-P Films with those of Ni. Most physical properties of Ni-P films differ from those of Ni films, as the respective nucleation, growth, structure, composition and film geometry of the films differ from one another. It is not these differences that deserve attention. Rather, we will look briefly at the difference between Ni-P films and Ni films, as their properties deviate from bulk Ni-P and bulk Ni respectively.

The structural, electrical and optical properties of continuous vacuum evaporated Ni films were seen not to deviate excessively from those of bulk Ni. The geometry of fresh Ni films is relatively plane parallel for thicknesses over 100Å and the films are polycrystalline. The density of fresh films is approaching that of bulk Ni for thicknesses greater than 200Å, and the conductivity of Ni films have a reasonable fit with the Fuchs-Sondheimer theory. Upon vacuum heat treatment, fresh Ni films aggregate into irregularly shaped islands on the substrate and become discontinuous. The extent of aggregation is temperature and film thickness dependent. At 200°C there is the first hint of aggregation for thin Ni films for thicknesses below 200Å,

resulting in a decrease of density, an increase in DC resistivity and a film thickness dependent deviation of optical conductivity from that of bulk Ni. The deviation of optical conductivities of some heat treated Ni films from that of bulk Ni is shown in Figure 47. Such behavior, as described above for Ni films, is typical for vacuum evaporated metals deposited on dielectric substrates, provided that the deposition is "clean" (i.e. vacuum better than 10^{-6}torr, pure vapor source, little or no hydrocarbons in the vacuum, etc.).

In contrast, electroless films, electrodeposited films, "dirty" vacuum deposited films and sputtered films have highly anomalous properties, quite different from those of which vacuum evaporated Ni was said to be typical. Electroless Ni-P films are suggested to be typical of the "dirty" class of films, as their properties in the fresh state differ drastically from those of the corresponding bulk material, and their properties in the vacuum heat treated state approach those of the corresponding bulk material. Thus the difference between Ni and Ni-P films is the difference between clean well behaving films and dirty, anomalous films in the fresh state. However, the role changes on heating the films in vacuum i.e. Ni films become anomalous at high temperatures and Ni-P films become less anomalous.

5.3 Comments on the Film Theories. Some suggestions are made below as consequences of the present work and of the resulting model for Ni-P films. They are aimed, as a possible rectification, at the present theoretical situation.

It is suggested that the optical properties of continuous plane

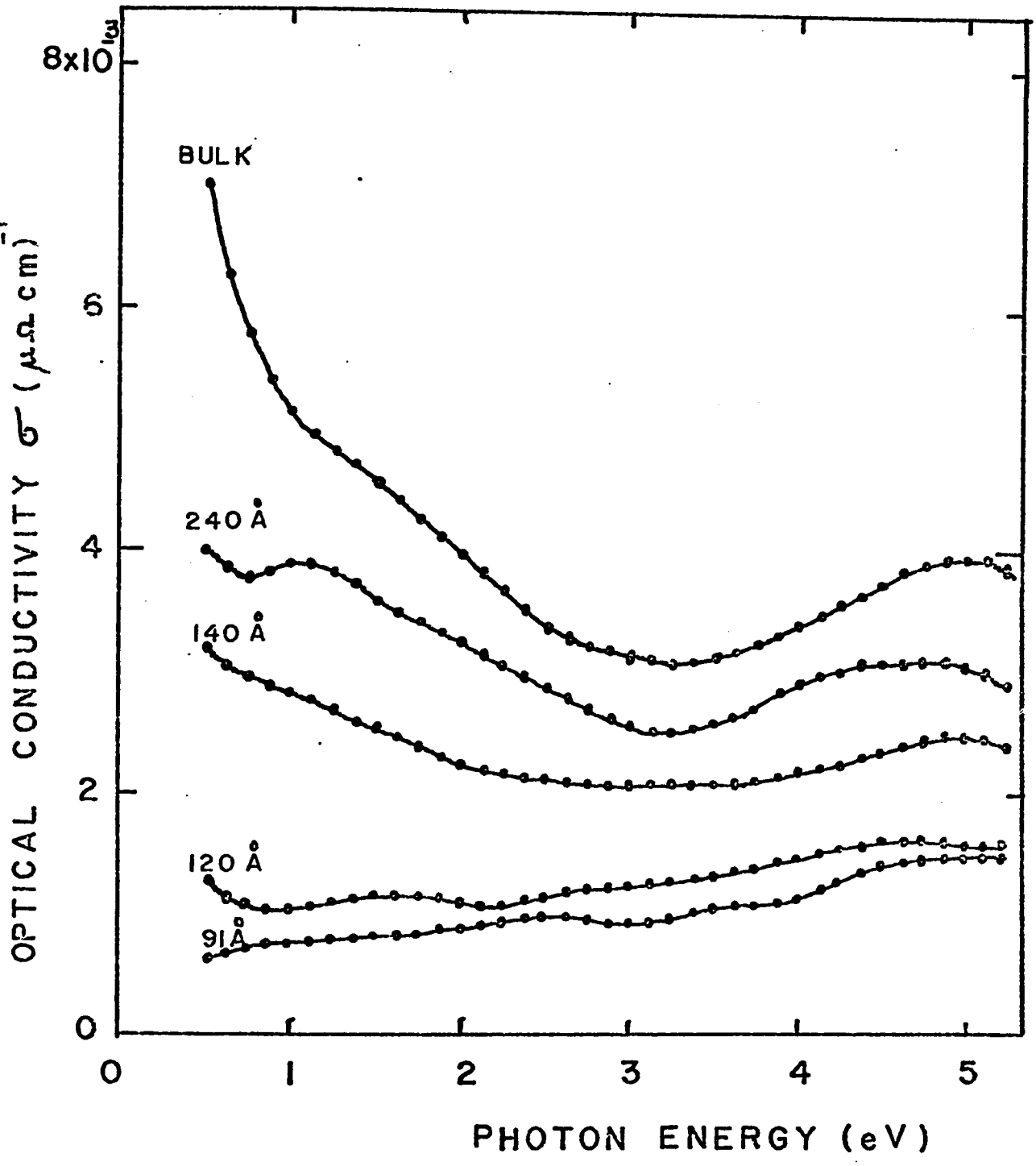

FIGURE 47: Spectral dependence of optical conductivity of evaporated Ni films. The films were vacuum heat treated at 200°C. The geometrical film thickness d_{opt} is indicated at each curve. The bulk curve from Figure 41 is included for reference.

parallel homogeneous isotropic films of monovalent metals are governed by the thickness limited electronic mean free path, similar to the film thickness dependence of the DC electrical conduction of such films as described by the Fuchs-Sondheimer theory. A naive quantitative suggestion was made in this direction in Section 4.22 concerning the Drude part of the optical conductivity.

An optical theory such as this one would be of no great value however, for the same reason as the one dimensional Fuchs theory ("one dimensional" refers to one out of three spatial dimensions of the metal to be compatible with the mean free path) is of use only in special cases, since films are usually not identical to slices of the bulk.

Instead, and this is the second suggestion, a three dimensional Fuchs-type theory may be developed (the two dimensional Fuchs-type law i.e. the DC conductivity of thin wires is due to Dingle (52)) and applied to aggregates of metals that usually form "anomalous" films, either as islands in the plane of the substrate e.g. Ni (26), or islands arranged in three dimensions, e.g. the "pebbles" in Ni-P films.

A qualitative picture of this idea is shown in Figure 48. In the figure the three curves correspond to the 1D Fuchs curve (see Figure 36), the 2D Dingle curve (reference 52) and the present 3D proposal. All curves were drawn for $\epsilon = 0$. The symbol ⊗ refers to the measured value for Ni-P microparticles as discussed in 5.13 above.

With a 3D Fuchs-type theory the rest of the theoretical development would be relatively straightforward. A refinement of the Maxwell-Garnett theory could be made by assuming that the optical

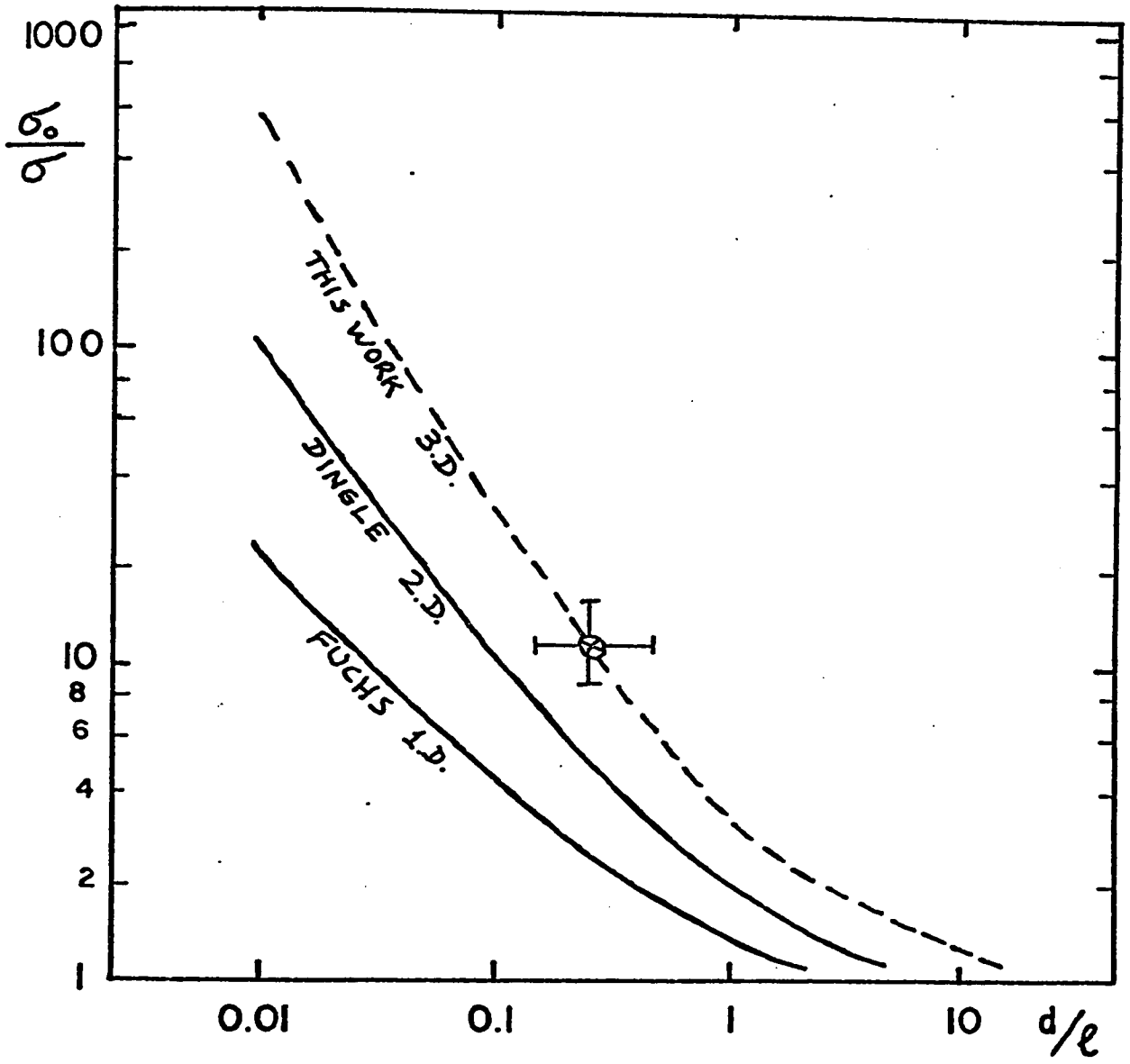

FIGURE 48: The D.C. conductivity σ of metals with one, two and three dimensions comparable to the electronic mean free path ℓ. σ_o is the conductivity of the corresponding bulk metal and d is the film thickness (1D), the wire diameter (2D), and the diameter of sphere (3D) of the samples. ⊗ is the measured value for Ni-P microparticles. The curves are drawn for $s = 0$.

constants of the constituent microparticles are not the same as those of the bulk parent metal, but that they are size dependent in the 3D Fuchs sense. (Naturally the direct influence of a 3D Fuchs effect would be only on the Drude part of the optical constants, but the scheme may also be extended to intraband parts). This could be checked experimentally by measuring n and k of films (either Ni-P or others) with variable island size, substituting the results into the inverse of the Garnett theory (as it was done for Ni-P films in Section 4.42 above), and obtaining the size dependent constants of the microparticles.

Among other features of such a treatment it may be shown from the results that metals in aggregated film form reveal their low energy interband peaks much more readily than in bulk form. Examples of this may be seen for Ni (E = 1.2 eV) in Figure 47 and for Ni-P (E = 0.8 eV) in Figure 42b. The reason, based on the present speculation, is that there is a higher suppression for the Drude component in microparticles than for components due to other processes. As another feature, the Drude suppression by microparticles holds the possibility of the separation of the otherwise inseparable intra- and interband components of multivalent metals.

Finally, it is suggested that the theory describing the DC conduction of island type metal films in the plane of the substrate could be unified with this new 3D electrical-optical Fuchs-type theory. With such unified theory, the bands (or the lack of them) of metals in microscopic form may be studied (by the use of only a spectrophotometer and an ohmmeter) ranging in size from practically a few tens of

atoms (no bands, only discreet electronic levels), through particles of 10^6 atoms (normal Ni-P type islands) to the massive bulk metal. From such studies one may learn more about the electronic structure of metals. Work on possible modifications and extensions of theories, as described above, has begun and is planned to continue.

CHAPTER 6

CONCLUSIONS

6.1 Summary. The structural, electrical and optical properties of electrolessly deposited Ni-P films were studied. This included the study of Ni-P bulk materials (film with large thickness) as no references on its properties were available. Ni-P bulk material was seen to be an electronic conductor with DC resistivity 5 - 10 times that of pure Ni, depending on the P content. The P ions in the Ni host (9.5 w/o $\leq$ P $\leq$ 16 w/o) appeared to act as additional scatterers for conduction electrons, having little influence on the number of carriers. The P ions appeared also to widen the energy bands, and/or to narrow the gaps close to the Fermi surface.

The nucleation of Ni-P films on activated substrates was shown to be selective, the growth to be homogeneous, and the structure to be liquid-like. The film geometry was shown to be that of spherical islands growing into a seemingly continuous film. Indirect evidence suggested the continuous films to be "pebbly" with Ni-P-H microparticles being the constituent building blocks, reducing to Ni-P upon evacuation. On vacuum heating, the initially low density was seen to increase and the constituent microparticles to merge. At a critical temperature (300°C - 500°C) the Ni-P material in the film

changed from liquid-like to crystalline.

The electrical and optical properties of Ni-P films (and bulk Ni-P materials) were shown to depend on material composition, film geometry and structure, and film properties were seen to be anomalous. The anomalies (e.g. the very low conductivity) were more pronounced in the fresh state of films, as the film composition and structure deviated more from that of a slice of the bulk in this condition, than after heat treatment.

The properties of fresh and vacuum heated Ni-P films were anlaysed in terms of current film theories. In order to obtain some quantitative estimates of the electronic constants τ and N/m^*, certain modifying assumptions had to be made regarding the theories. From the analysis of the experimental data, and its comparison with film theories, a model for Ni-P films was evolved.

The model depicts fresh films as a collection of isolated Ni-P microparticles (or Ni-P-H before evacuation) where the electrical properties of the microparticles are bulk-like, being modified by the size-dependent electronic mean free path. The properties of the collection of these particles (i.e. the film) depend on their mutual configuration. In the fresh (aggregated) condition, the metallic behaviour is weak and in the heat treated (merged, crystallized etc.) condition, the films show a strong metallic character.

It was suggested that Ni-P films are representative of the "dirty" class metal films, and a method to remove the anomalies was described. Based on the Ni-P film model and additional experimental results, suggestions were made for an extension and refinement of the film

theories. The development of a three dimensional Fuchs-like theory was proposed.

6.2 Future Work. The benefits and consequences of a 3D Fuchs-like scheme were briefly outlined. This also serves the purpose to help suggest topics for future work.

Topic number one for future work may be the development of a three dimensional conduction theory to describe the electrical and optical properties of thin films, with two or three dimensional discontinuities.

As a direct consequence of this development, an experimental test of the theory could be made. This may be topic number two. Spherical islands, ideally suited for such a test, may be grown of Ni-P materials to a well defined size. This may be accomplished by growing the islands on a substrate, with a certain predetermined value of surface activation density, in the beam of the spectrophotometer, monitoring the size by the transmitted light, and stopping the growth at the desired island size. An illustration of this is given in Figure 49. Samples, ranging in island size from a few tens to many thousand angstroms, would serve as the test specimens.

Other topics for future work on Ni-P films (or other films) may include variations on the above suggestions. Perhaps the most important of this would be the development of a "thin film method" or "microparticle method" to separate the net optical response of multivalent metals into their (Drude, interband, etc.) components.

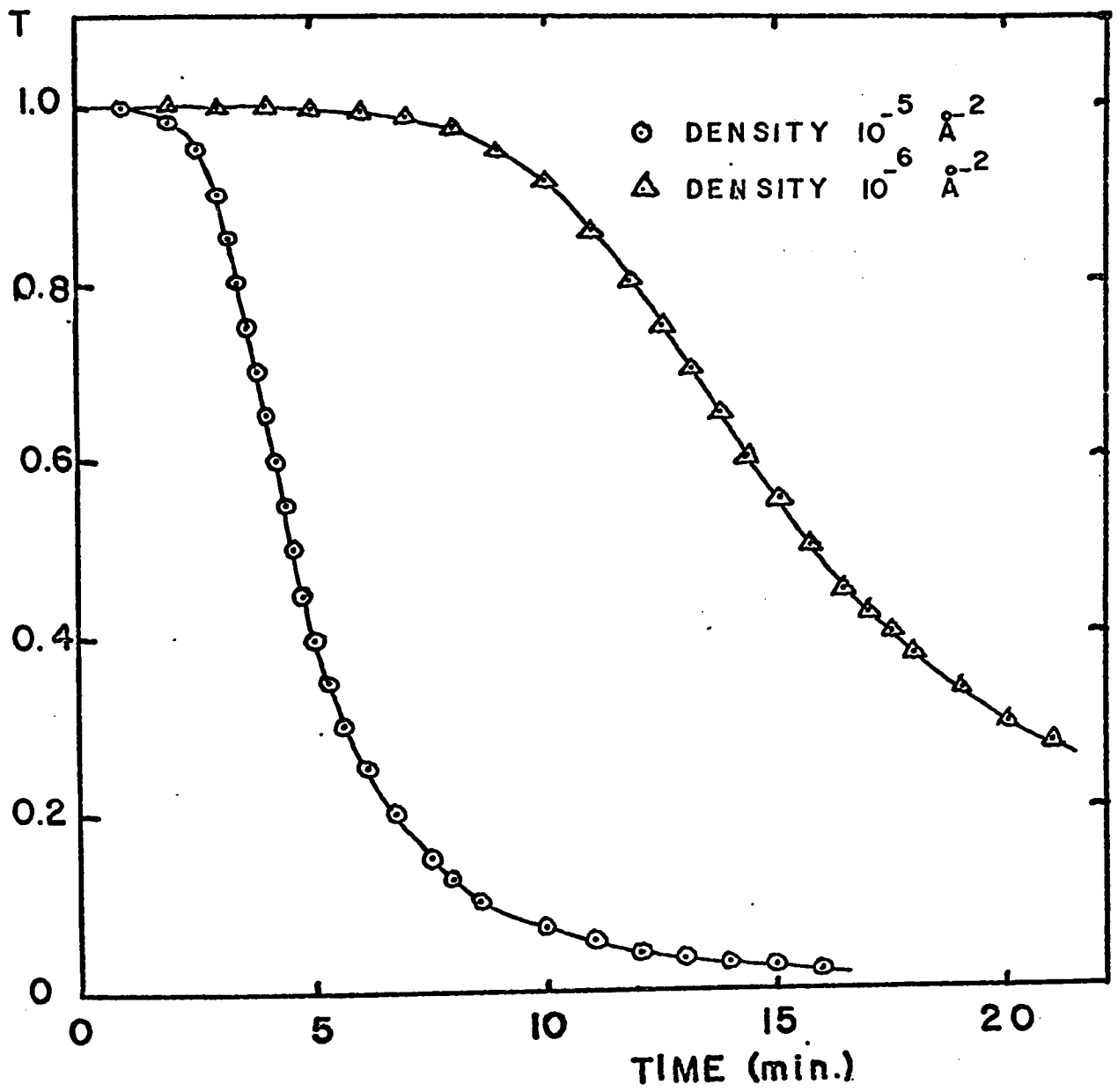

FIGURE 49: The transmittance T of growing Ni-P films, as grown in the spectrophotometer on substrates activated at two different activation densities. The value of T gives a direct measure of comparative island size. T was measured at λ = 5000Å.

REFERENCES

1. K. Fuchs, Proc. Cambr. Phyl. Soc., 34, 100 (1938).

2. E.H. Sondheimer, Advances in Phys., 1, 1 (1952).

3. C.A. Neugebauer and M.B. Webb, J. Appl. Phys., 23, 74 (1962).

4. T.E. Hartman, J. Appl. Phys., 34, 943 (1963).

5. J.C.M. Garnett, Phil. Trans., 203, 385 (1904).

6. H. Schopper, Z. Phys., 130, 565 (1951).

7. J.P. Marton, U.W.O. Review Paper "Electrical and Optical Properties of Thin Metal Films", (1965) Unpublished.

8. H. Mayer, in "Structure and Properties of Thin Films". Proceedings of an International Conference, 1959. John Wiley and Sons 1959.

9. H. Mayer and B. Hietel in "Optical Properties and Electronic Structure of Metals and Alloys". Proceedings of the Paris Colloquium 1965. North Holland Publishing Company 1966.

10. J.P. Marton, Welwyn Canada Ltd. Internal Research Report "Ultrahigh Resistivity of Ni-P Films", (1964) Unpublished.

11. A. Brenner and G.E. Riddell, J. Research Natl. Bur. Standards, 37, 31 (1946), 39, 385 (1947).

12. G. Gutzeit, W.J. Crehan and A. Krieg, U.K. Pat. 761, 556.

13. A. Brenner, Metal Finishing, 52, 68 (1954).

14. A.S.T.M. Special Technical Publication No. 265 (1959).

15. P. Baeyens (Philips Electrical Industries), U.K. Pat. 749, 824.

16. E.A. Bergstrom, U.S. Pat. 2,702,253.

17. A.W. Goldenstein, W. Rostaker, F. Schossberger and G. Gutzeit, J. Electrochem Soc., 104, 104 (1957).

18. A.H. Graham, R.W. Lindsay and H.J. Read, J. Electrochem Soc., 112, 401 (1965).

19. J.P. Marton and M. Schlesinger, J. Electrochem Soc., 115, 16 (1968).

20. P.A. Albert, Z. Kovac, H.R. Lilienthal, T.R. McGuire and Y. Nakamura, J. Appl. Phys., 38, 1258 (1967).

21. M. Schlesinger and J.P. Marton, J. Phys. Chem. Solids, 29, 188 (1968).

22. J.P. Marton and M. Schlesinger, Bull. Am. Phys. Soc., 12, 394 (1967).

23. Lord Rayleigh, Scientific Papers, Vol. VI (1911 - 1919), pp. 26 and 127.

24. J.P. Randin and H.E. Hintermann, J. Electrochem. Soc., 115, 480 (1968).

25. L. Holland, "Vacuum Deposition of Thin Films", Chapman & Hall Ltd., 1963.

26. R.S. Sennett and G.D. Scott, J.O.S.A., 40, 203 (1950).

27. S. Tolansky, "Multiple-Beam Interferrometry", Claredon Press, Oxford, 1948.

28. Van der Pauw, Philips Res. Reports, 13, 1 (1958).

29. O.S. Heavens, "Optical Properties of Thin Solid Films", Dover Publications Inc., 1965.

30. J.S. Toll, Phys. Rev., 104, 1760 (1956).

31. L. Ward and A. Nag, Brit. J. Appl. Phys., 18, 277 (1967).

32. F. Stern, "Elementary Theory of Optical Properties of Solids", in 'Solid State Physics', Vol. 15, Academic Press (1963).

33. J.S. Judge, J.R. Morrison, D.E. Speliotis and G. Bate, J. Electrochem. Soc., 112, 681 (1965).

34. A.F. Schmeckenbecher ibid., 113, 778 (1966).

35. A.S. Frieze and R. Weil, Sixth International Conference for Electron Microscopy, Kyoto (1966), p.533.

36. Handbook of Chemistry and Physics, The Chemical Rubber Company Publishers (1966).

37. A. Brenner, D.F. Couch and E.K. Williams, J. Res. Nat. Bur. Standards, 44, 109 (1950); also Plating, 37, 36 (1950).

38. H. Ehrenreich, H.R. Philipp and D.J. Olechna, Phys. Rev., 131, 2469 (1963).

39. F. Goos, Zeits. Fur Physik, 100, 95 (1936).

40. C. Kittel, "Introduction to Solid State Physics", John Wiley & Sons, 1956.

41. J.M. Ziman, "Electrons and Phonons", Oxford University Press, 1960.

42. J.P. Marton, Welwyn Canada Ltd., Internal Research Report, "The R, R', T Method for Thin Films", 1968, Unpublished.

43. L.N. Hadley, "Transmittance and Reflectance vs. Thickness/ Wavelength for Thin Films", Report available from Colorado State University, Fort Collins, Colorado.

44. N.F. Mott and H. Jones, "The Theory and Properties of Metals and Alloys", Dover Publications Inc., 1958.

45. A.H. Wilson, "The Theory of Metals", Second Edition Cambridge University Press, 1965.

46. N.F. Mott, Advances in Phys., 13, 325 (1964).

47. B. Baranowski and M. Smialowski, J. Phys. Chem. Solids, 12, 206, (1959).

48. C.L. Lewis, W.L. Ott and N.M. Sine, "The Analysis of Nickel", Pergamon Press (1966).

49. W.E. Spicer, in "Optical Properties and Electronic Structure of Metals and Alloys", Proceedings of the Paris Colloquium, 1965. North Holland Publishing Company, 1966.

50. A.P. Lenham, J.O.S.A., 57, 473 (1967).

51. J.C. Phillips, "The Fundamental Optical Spectra of Solids", in Solid State Physics, Vol. 18, Academic Press (1966).

52. R.B. Dingle, Proc. Royal Soc., A201, 545 (1950).

APPENDIX A

EXPERIMENTAL DETERMINATION OF n AND k FOR BULK METALS

Of the large number of intensity methods for the experimental determination of n and k (29), the most suitable one appears to be the Kramers-Kronig method (30). In essence the method consists of measuring the spectral reflectance $R(\lambda)$ at normal incidence for as wide a range of λ as possible, then from this data the spectral dependence of the reflected phase angle $\beta(\lambda)$ is calculated. From the intensity of the reflected radiation $R(\lambda)$ and its phase $\beta(\lambda)$, $n(\lambda)$ and $k(\lambda)$ are readily calculated by means of the Fresnel equations (29). For the calculation of $\beta(\lambda)$ the knowledge of $\beta(\lambda_o)$ is required where λ_o is a wavelength in the range of wavelengths considered. This calls for an independent measurement of β at λ_o. In practice the so-called R_p/R_s method may be used at λ_o to determine $\beta(\lambda_o)$. The value of λ_o is dictated by polarization considerations i.e. ordinary poloroid polarizers work well at $\lambda = 0.75\mu$ without absorption. Before giving details of the Kramers-Kronig considerations, some standard relations will be reviewed and the R_p/R_s method discussed.

1. Theoretical Considerations. A plane wave of E.M. radiation falling on the plane surface of a homogeneous and isotropic metal will

be partly reflected and partly transmitted. The transmitted part will be absorbed in the metal. The situation can be fully described by the Maxwell equations. The application of the proper boundary conditions representing the surface of the metal) to the Maxwell equations give another set of equations known as the Fresnel equations (see e.g. Ref. 32). These equations give the (complex) ratios of reflected and incident amplitudes $\tilde{r}_S$ and $\tilde{r}_P$, and those of transmitted and incident amplitudes $\tilde{t}_S$ and $\tilde{t}_P$ as

$$\left.\begin{aligned}
\tilde{r}_S &= \frac{\cos\theta - (\tilde{n}^2 - \sin^2\theta)^{1/2}}{\cos\theta + (\tilde{n}^2 - \sin^2\theta)^{1/2}} \\
\tilde{r}_P &= \frac{\tilde{n}^2\cos\theta - (\tilde{n}^2 - \sin^2\theta)^{1/2}}{\tilde{n}^2\cos\theta + (\tilde{n}^2 - \sin^2\theta)^{1/2}} \\
\tilde{t}_S &= \frac{2\cos\theta}{\cos\theta + (\tilde{n}^2 - \sin^2\theta)^{1/2}} \\
\tilde{t}_P &= \frac{2\tilde{n}^2\cos\theta}{\tilde{n}^2\cos\theta + (\tilde{n}^2 - \sin^2\theta)^{1/2}}
\end{aligned}\right\} \quad [A1]$$

where subscripts P and S refer to polarizations of the electric vector in the plane, and normal to the plane of incidence respectively. $\tilde{n} = n + ik$ is the complex index of refraction and θ is the angle of incidence.

The intensity reflectance R and transmittance T then are

$$\left.\begin{aligned}
R_P &= \tilde{r}_P\,\tilde{r}_P^* \quad , \quad R_S = \tilde{r}_S\,\tilde{r}_S^* \\
T_P &= \tilde{t}_P\,\tilde{t}_P^* \quad , \quad T_S = \tilde{t}_S\,\tilde{t}_S^* \quad .
\end{aligned}\right\} \quad [A2]$$

For normal incidence ($\theta = 0$), $R_P = R_S$, and we get the well known reflectance formula of metals from [A1] as

$$R = \frac{(n-1)^2 + k^2}{(n+1)^2 + k^2} \quad . \qquad [A3]$$

For an angle of incidence of 45° we see from [A1] that

$$R_P = R_S^2 \qquad [A4]$$

this serves to check the homogenity and isotropy of samples.

2. The R_P/R_S Method. This is an easy method involving the measurements of reflected intensities R_P and R_S at two different angles. For the measurements a polarizer is required, as the output of most spectrophotometers is not polarized. The wavelength at which these measurements may be made is dependent on available polarizers.

The sample is first inclined at 45° to the incident beam, and R_P and R_S are measured. If relation [A4] is satisfied, measurements of R_P and R_S are made at $\theta = 45°$ and $\theta = 80°$. From this data n and k are determined graphically. To do this, the values of R_P/R_S at 45° and at 80°, as functions of n and k, have to be calculated from the relations

$$\left.\begin{aligned} R_S &= \frac{(a - \cos\theta)^2 + b^2}{(a + \cos\theta)^2 + b^2} \\ R_P &= \frac{(a - \sin\theta\tan\theta)^2 + b^2}{(a + \sin\theta\tan\theta)^2 + b^2} R_S \end{aligned}\right\} \qquad [A5]$$

where

$$a^2 = \frac{1}{2}\left\{\left[(n^2 - k^2 - \sin^2\theta)^2 + 4n^2k^2\right]^{1/2} + (n^2 - k^2 - \sin^2\theta)\right\}$$

$$b^2 = \frac{1}{2}\left\{\left[(n^2 - k^2 - \sin^2\theta)^2 + 4n^2k^2\right]^{1/2} - (n^2 - k^2 - \sin^2\theta)\right\} .$$

An example of working curves plotted on the n - k plane is shown in Figure A1.

3. The Kramers-Kronig Analysis. Consider the reflection of radiation from the surface of metal at normal incidence, and write the electric vector of the reflected wave in terms of its amplitude $\tilde{r}$ and phase β. If the incident wave has unit amplitude and zero phase, then the amplitude of reflected wave is

$$\tilde{r} = |\tilde{r}| \exp i\beta .$$

On the other hand, the amplitude of the reflected wave at normal incidence in terms of n and k from [A1] is

$$\tilde{r} = \frac{n + ik - 1}{n + ik + 1} .$$

Setting the real and imaginary parts of the two expressions equal we have

$$\left.\begin{aligned} n &= \frac{1 - R}{1 + R - 2\sqrt{R}\cos\beta} \\ k &= \frac{2\sqrt{R}\sin\beta}{1 + R - 2\sqrt{R}\cos\beta} \end{aligned}\right\} \quad [A6]$$

where $\sqrt{R} = |\tilde{r}|$.

Thus n and k may be calculated from measured values of R and β at normal incidence. An example of working curves computed from relations

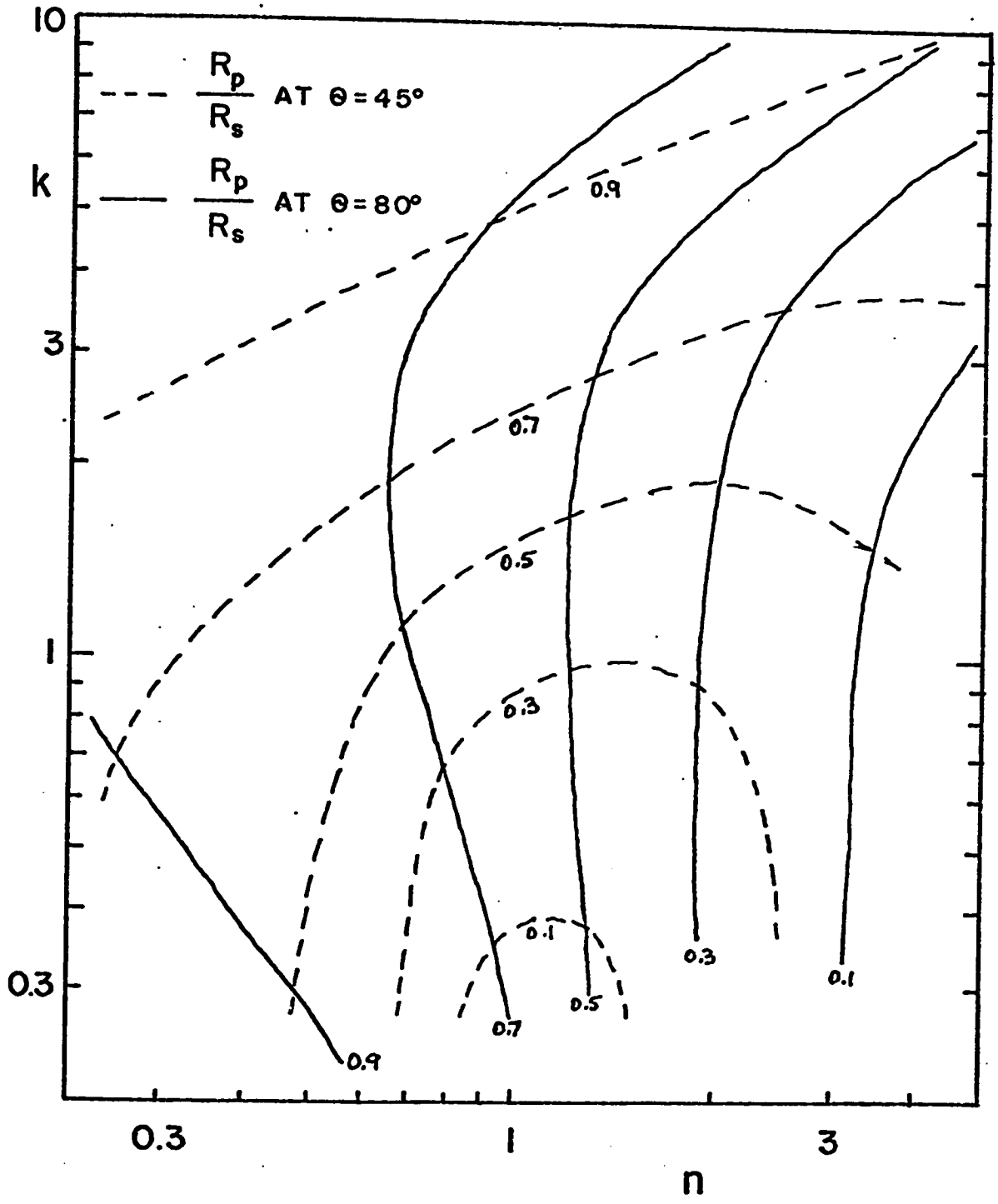

FIGURE A1: Working curves of R_p/R_s at 45° and 80° plotted in the n-k plane. The curves were calculated from relation [A5] .

[A6] in the n - k plane are shown in Figure A2.

The Kramers-Kronig analysis is concerned with obtaining the necessary β values for the (n, k) determination from sets of measured R(λ) data. The relation between β at one wavelength and R(λ) is given (32) as

$$\beta(\omega_o) = \frac{2\,\omega_o}{\pi} \int_o^\infty \frac{\ell n\, r(\omega)}{\omega_o^2 - \omega^2}\, d\,\omega$$

where ω is the angular frequency of radiation.

The expression in terms of photon energy and R then becomes

$$\beta(E_o) = \frac{E_o}{\pi} \int_o^\infty \frac{\ell n\, R(E) - \ell n\, R(E_o)}{E_o^2 - E^2}\, dE \,. \qquad [A7]$$

In practice R(E) may be measured for $0.5\ eV \leq E \leq 5\ eV$, and as the integral has to be evaluated from 0 eV to ∞, extrapolation of the measured R(E) data is necessary. For metals R(E) may be extrapolated between 0 and 0.5 eV smoothly so that R(0) = 1 and above 6 eV linearly on a log-log plot with good results. An example of such an extrapolation is given in Figure A3.

It was indicated above that an independent β value is necessary for the determination of β(λ). It can be pointed out that such an independent value at a wavelength λ_o determines the slope of the upper wing in the R(E) extrapolation. (In Figure A3 this is signified by choices A, B, and C of the upper wing).

To carry out the calculation for β(E), it has to be evaluated at points E_o where $0.5\ eV \leq E_o \leq 5\ eV$ individually from [A7] using the measured R(E) curve. The actual calculation of one β value at a

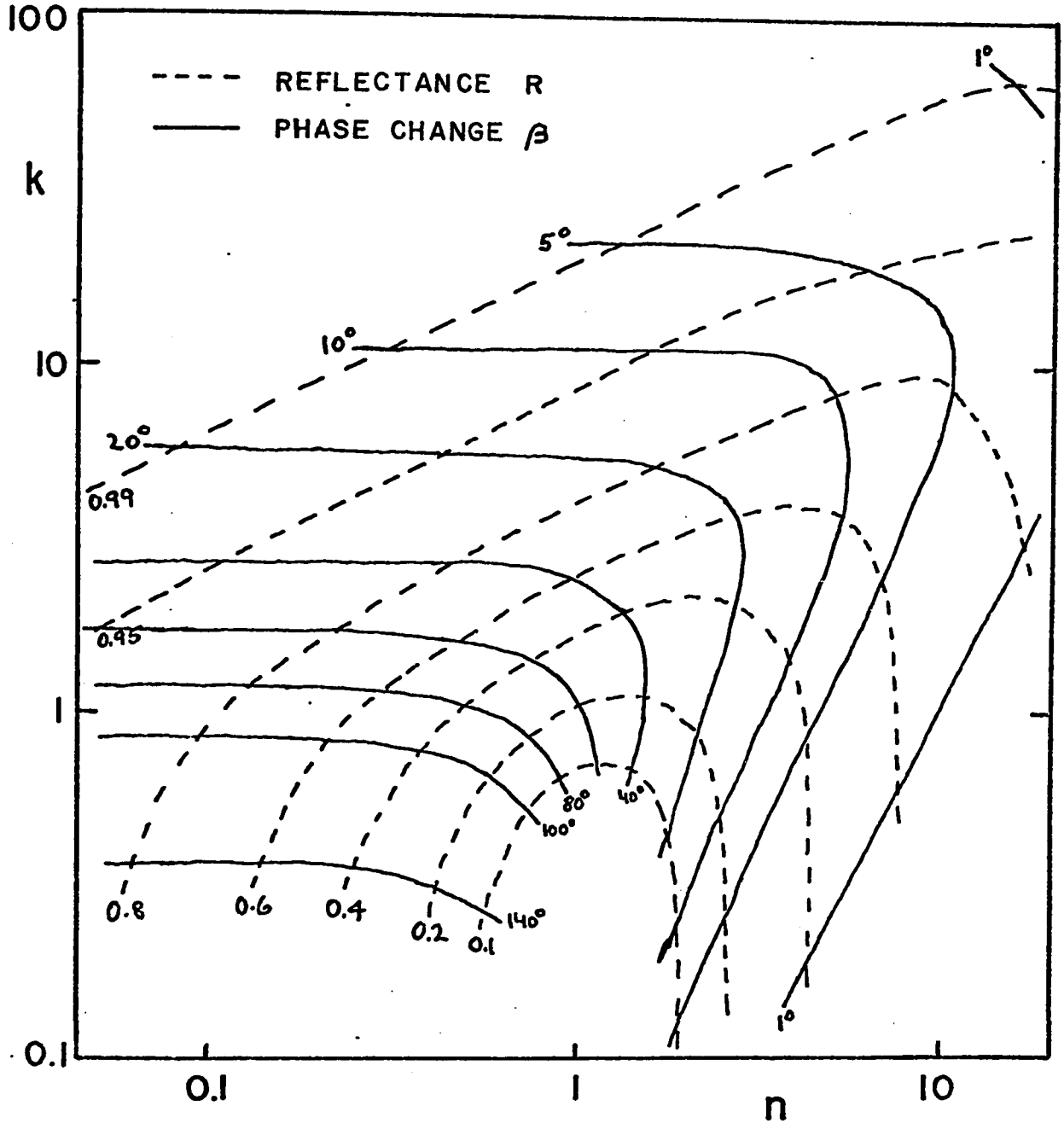

FIGURE A2: Working curves R (Reflectivity) and β (phase change on reflection) plotted in the n-k plane. The curves were calculated from relation [A6] .

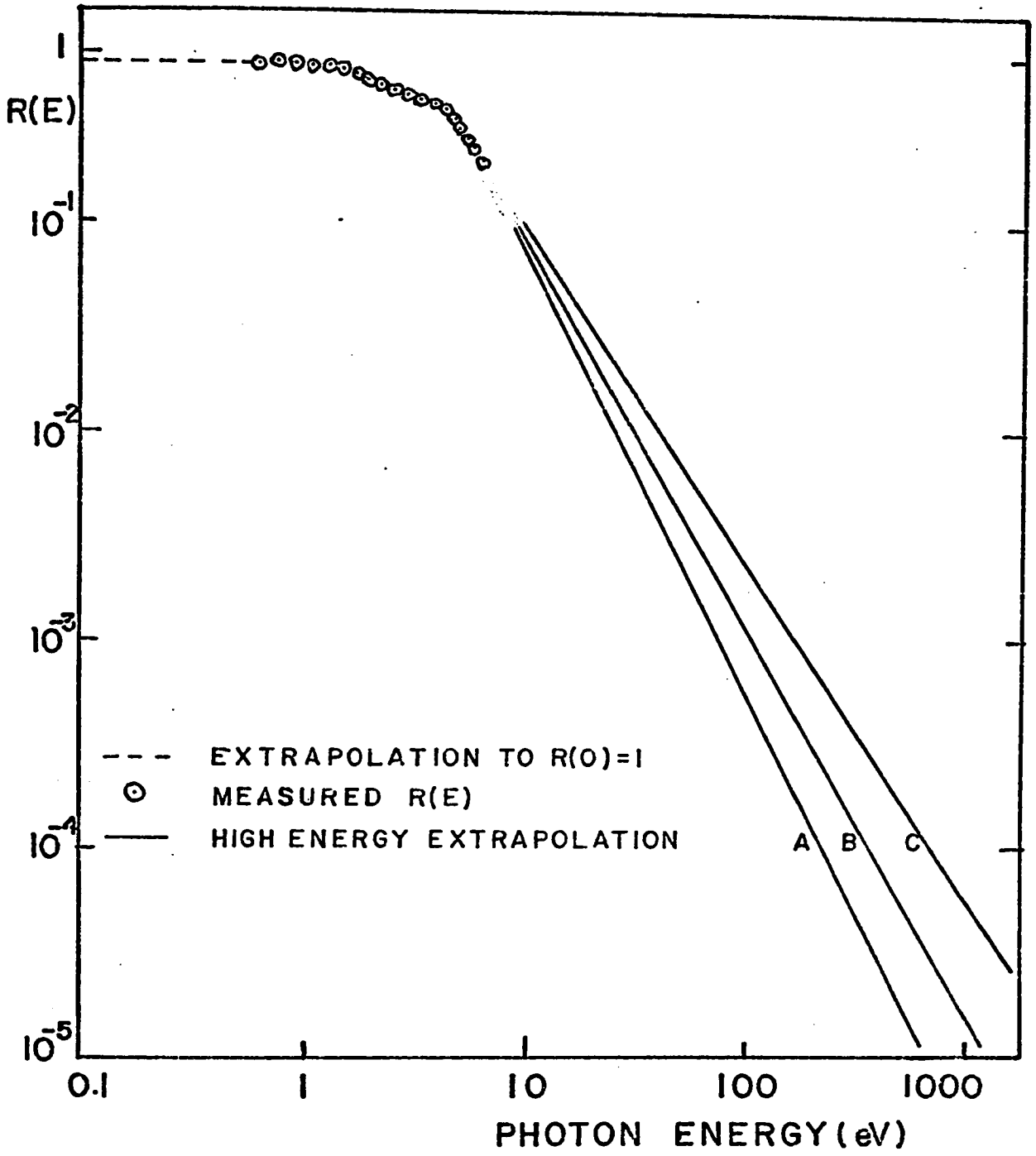

FIGURE A3: An example of extrapolation of the R(E) curve for the Kramers-Kronig analysis. The slope (A, B and C) is determined from independent measurements.

point E_o may be done by the approximate equivalent of [A7]

$$\beta(E_o) = \beta_1(E_o) + \beta_2(E_o) + \beta_3(E_o) + \beta_4(E_o) + \cdots\cdots$$

where

$$\beta_1(E_o) = 18.24\, E_o \sum_{E=0}^{6} \frac{\ell n\, R(E) - \ell n\, R(E_o)}{E_o^2 - E^2}\, \Delta E$$

$$\beta_2(E_o) = 18.24\, E_o \sum_{E=6}^{10} \frac{\ell n\, R(E) - \ell n\, R(E_o)}{E_o^2 - E^2}\, \Delta E$$

$$\beta_3(E_o) = 18.24\, E_o \sum_{E=10}^{100} \frac{\ell n\, R(E) - \ell n\, R(E_o)}{E_o^2 - E^2}\, \Delta E$$

$$\beta_4(E_o) = 18.24\, E_o \sum_{E=100}^{1000} \frac{\ell n\, R(E) - \ell n\, R(E_o)}{E_o^2 - E^2}\, \Delta E$$

.
.
.
.
.
.

The factor 18.24 is to convert β from radians to degrees. Normally the contribution of β_6 and higher terms are negligible and they are omitted in the calculations.

Having gone through the above steps a large number of times to obtain a β(E) curve, that curve together with the measured R(E) curve gives n(E) and k(E) from [A6], or from working curves such as in Figure A2, in the wavelength range considered. In the present work, these calculations were made by a digital computer.

APPENDIX B

EXPERIMENTAL DETERMINATION OF n AND k FOR METAL FILMS

Similar to the situation in determining $n(\lambda)$ and $k(\lambda)$ for bulk metals, many methods are available for n and k measurements for metal films. Of the intensity methods the most attractive one appears to be the (R, R', T) method (31) for films of reasonable transmittance. The method is attractive, as the measurements involve only simple spectrophotometry, and the data provides values of $n(\lambda)$, $k(\lambda)$ and d_{opt}. The difficulty lies in the heavy algebra connecting the triplets (R, R', T) and (n, k, d_{opt}). Moreover, only the former set can be expressed in terms of the latter analytically; n, k and d_{opt} cannot be directly calculated from the measured quantities. The determination has to be done by machine iteration or graphically.

1. Theoretical Considerations. The Fresnel equations* for a homogeneous isotropic and plane parallel film of index $\tilde{n} = n + ik$ and geometrical thickness d supported by a non-absorbing substrate of index n_s in air with index 1 for normal incidence at wavelength λ are

---

* See Appendix A

$$\tilde{r} = \frac{\dfrac{n-1-ik}{n+1-ik} + \dfrac{n_s-n+ik}{n_s+n-ik}\exp\left[-2i\left(\dfrac{2\pi d}{\lambda}(n-ik)\right)\right]}{1+\dfrac{n-1-ik}{n+1-ik}\cdot\dfrac{n_s-n+ik}{n_s+n-ik}\exp\left[-2i\left(\dfrac{2\pi d}{\lambda}(n-ik)\right)\right]}$$

$$\tilde{t} = \frac{\dfrac{2}{n+1-ik}\cdot\dfrac{2(n-ik)}{n_s+n-ik}\exp\left[-i\left(\dfrac{2\pi d}{\lambda}(n-ik)\right)\right]}{1+\dfrac{n-1-ik}{n+1-ik}\cdot\dfrac{n_s-n+ik}{n_s+n-ik}\exp\left[-2i\left(\dfrac{2\pi d}{\lambda}(n-ik)\right)\right]}\, n_s^{1/2} \qquad [B1]$$

The calculation of R, R' and T from [B1] is straightforward but very lengthy (42) therefore only the end results are given here. The expressions for R and T are similar to those given by Hadley (43). The schematic representation of the situation is given below.

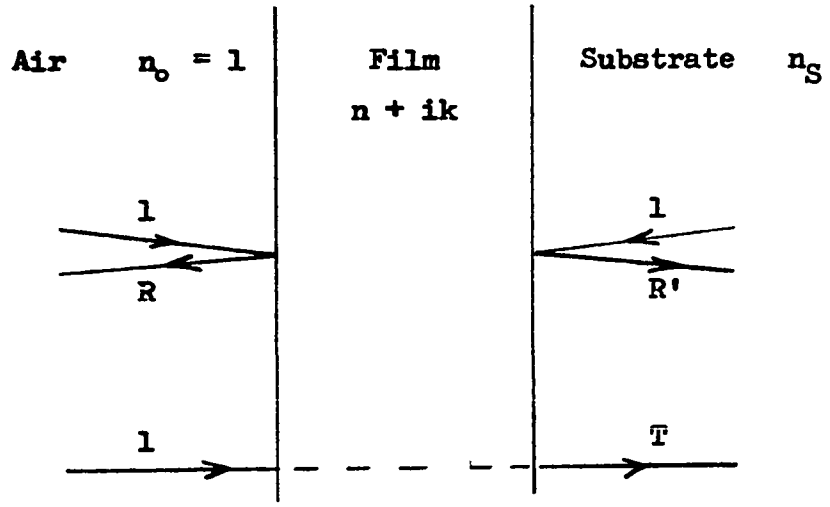

Where the reflectances and the transmittance are

$$R = \frac{A^2 + B^2 + 2e^{-\alpha}\left\{(\cos\beta)(AC + BD) + (\sin\beta)(BC - AD)\right\} + e^{-2\alpha}(C^2 + D^2)}{E^2 + F^2 + 2e^{-\alpha}\left\{(\cos\beta)(EG + FH) + (\sin\beta)(FG - EH)\right\} + e^{-2\alpha}(G^2 + H^2)}$$

$$R' = \frac{C^2 + D^2 + 2e^{-\alpha}\left\{(\cos\beta)(AC + BD) - (\sin\beta)(BC - AD)\right\} + e^{-2\alpha}(A^2 + B^2)}{E^2 + F^2 + 2e^{-\alpha}\left\{(\cos\beta)(EG + FH) + (\sin\beta)(FG - EH)\right\} + e^{-2\alpha}(G^2 + H^2)}$$

$$T = \frac{16\, n_S\, e^{-\alpha}(n^2 + k^2)}{E^2 + F^2 + 2e^{-\alpha}\left\{(\cos\beta)(EG + FH) + (\sin\beta)(FG - EH)\right\} + e^{-2\alpha}(G^2 + H^2)}$$

[B2]

where $\alpha = 4\pi\, k\, \frac{d}{\lambda}$

$\beta = 4\pi\, n\, \frac{d}{\lambda}$

and

$A = n(n_S + n - 1) - n_S - k^2$

$B = k(2n + n_S - 1)$

$C = n(n_S - n - 1) + n_S + k^2$

$D = k(-2n + n_S - 1)$

$E = n(n_S + n + 1) + n_S - k^2$

$F = k(2n + n_S + 1)$

$G = n(n_S - n + 1) - n_S + k^2$

$H = k(-2n + n_S + 1)$.

This formulation however does not describe the precise experimental situation as it ignores the substrate-air surface on the R' side. In order to make the description exact, a correction is necessary. The experimental situation is shown below, together with the new quantities R_M, R'_M and T_M . The M stands for "measured".

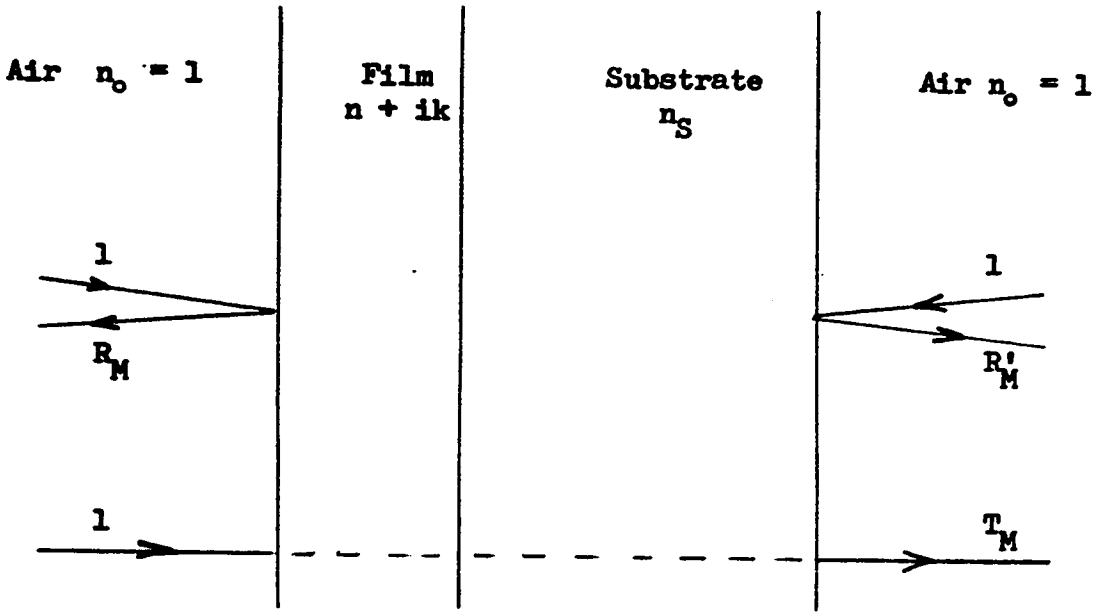

The new (real) reflectances and transmittance in terms of R, R' and T are (42)

$$R_M = R + \frac{T^2 R_S}{1 - R' R_S}$$

$$R'_M = R_S + R' \frac{(1 - R_S)^2}{1 - R' R_S} \qquad [B3]$$

$$T_M = T\left(1 - R_S \frac{1 - R'}{1 - R' R_S}\right)$$

where

$R_S = \frac{(1 - n_S)^2}{(1 + n_S)^2}$ is the reflectance of the substrate-air surface.

2. n and k Determination. The measured quantities of a film in the spectrophotometer, are $R_M(\lambda)$, $R'_M(\lambda)$ and $T_M(\lambda)$. From this triplet, $n(\lambda)$, $k(\lambda)$ and d_{opt} may be derived through [B3] and [B2]. This, in principle, is possible, but in practice it is a difficult task. First, $n(\lambda)$, $k(\lambda)$ and d_{opt} are not explicit functions of R_M, R'_M, T_M and λ, therefore iterations or graphical methods must be used. Second, the functions connecting the two sets of triplets are not single valued. This is illustrated in Figure B1.

To overcome these difficulties, the approximate values of n, k and d_{opt} are desirable as starting values in an iterating program. A good high speed machine can then determine n and k for a sample in the wavelength range of interest in a few hours.

In a real situation the approximate values of n and k are known, at least in a limited range of wavelengths from previous measurements, and d_{opt} can be measured by the Tolansky method (27) independently. These were the steps that were taken during the present set of experiments on Ni and Ni-P films. First, n and k were determined graphically by using an independent thickness, then these values, along with the measured triplet (R_M, R'_M, T_M), were put in a computer to calculate a refined set of (n, k, d_{opt}) values. The process was repeated at small intervals of wavelengths and for each sample.

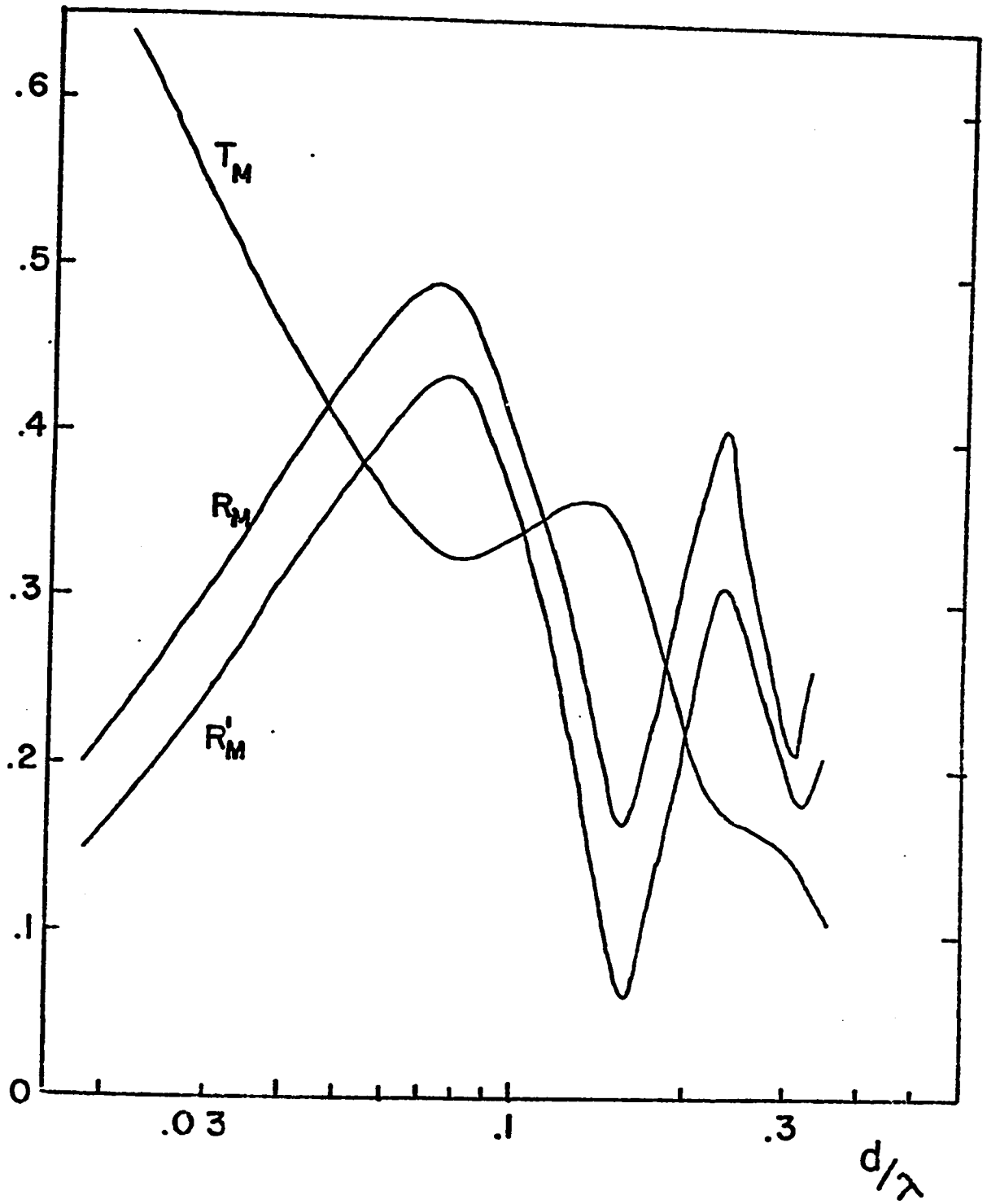

FIGURE B1: Reflectance R_m and R'_m, and transmittance T_m plotted against d/λ from relations [B2] and [B3] at $n = 3.2$ and $k = 0.4$. Note that the functions are multivalued.

APPENDIX C

RATE OF GROWTH FORMULI FOR Ni-P FILMS

Assume that the small catalytic sites are half spheres with radius r_o, situated "base-down" on the substrate. Let σ be the number of active half spheres per unit substrate area. Assume that the Ni-P deposition parameters (solution concentration and temperature) are constant in time, and that the density of Ni-P deposit ρ is constant. Let m be the mass of the deposit on each active island, and r be the radius of the growing half sphere. Then $m = (2/3)\pi(r^3 - r_o^3)\rho$, and the time rate of change of m is

$$\frac{dm}{dt} = \frac{dm}{dr}\frac{dr}{dt} = 2\pi\rho r^2 \frac{dr}{dt} .$$

Since $dr/dt = c$, (cf. Fig. 15 in Text) and $r = r_o + ct$ we get

$$dm = 2\pi \rho c (r_o + ct)^2 dt .$$

After integration

$$m = 2\pi \rho ct [r_o^2 + r_o ct + (1/3) c^2 t^2] .$$

Assuming an average value of σ on the substrate, the total mass M on the substrate with surface area A is

$$M = A\sigma 2\pi \rho ct [r_o ct + (1/3) c^2 t^2] .$$

With the definition of the mass thickness $d = M/A\rho$ we get

$$d(t) = 2\pi\sigma\, ct\,[r_o^2 + r_o ct + (1/3)\, c^2t^2] \qquad [C1]$$

Further assume the islands to form a close packed surface distribution on the substrate. In this configuration each island may occupy a maximum surface area of σ^{-1}. As the islands grow in time the base of each island spreads in the available surface area of σ^{-1}. After a time t_o the islands touch and begin to form a continuous film whose surface retains the hemispherical features of the islands. At time, t_o, the area of the base of each hemisphere, $\pi r^2 \approx \sigma^{-1}$ for large values of σ. Since $r = r_o + ct$, $t_o \approx (c\sqrt{\sigma\pi})^{-1}$ for small values of r_o. Relation [C1] is therefore valid for times $0 \le t \le (c\sqrt{\sigma\pi})^{-1}$. For times longer than t_o the now-continuous film is visualized to grow at a constant macroscopic rate. This growth may be described by

$$d(t) = d(t_o) + c(t - t_o) = 2r_o(1 + r_o\sqrt{\sigma\pi}) - \frac{1}{3\sqrt{\sigma\pi}} + ct \qquad [C2]$$

$d(t_o)$ having been evaluated by setting $t = t_o = (c\sqrt{\sigma\pi})^{-1}$ in equation [C1]. Combining [C1] and [C2] the final expression is

$$d(t) = \left\{ \begin{array}{ll} 2\pi\sigma\, ct[r_o^2 + r_o ct + (1/3)\, c^2t^2]\ ; & 0 \le t < (c\sqrt{\sigma\pi})^{-1} \\ 2r_o(1 + r_o\sqrt{\sigma\pi}) - \dfrac{1}{3\sqrt{\sigma\pi}} + ct\ ; & t > (c\sqrt{\sigma\pi})^{-1} \end{array} \right\}. \qquad [C3]$$

APPENDIX D

THE FUCHS-SONDHEIMER THEORY

The treatment of film conductivity given below is due to Fuchs (1) and Sondheimer (2). Only an outline of the derivation is given here. Assume free electron model of metals (Drude type) and assume the collisions of electrons to be elastic, homogeneous and isotropic, and that a unique relaxation time τ exists. The mean free path ℓ of electrons is then $\ell = v\tau$ where v is the Fermi velocity. In this case the bulk conductivity is written (see e.g. (40)) as

$$\sigma_o = \frac{Ne^2}{m^*}\tau = \frac{Ne^2\ell}{m^*v} \quad . \qquad [D1]$$

Now consider a homogeneous isotropic film, its plane in the x - y plane and its thickness d in the positive z direction. Let $f(\underline{v},z)$ $d\underline{r}\ d\underline{v}$ be the number of electrons in $d\underline{r}$ at z and in $d\underline{v}$ at $\underline{v}$. Let the electric field be in the x direction and write f as $f(\underline{v},z) = f_o(\underline{v},z) + f_1(\underline{v},z)$, where f_o is the equilibrium distribution function with E = 0. Assume that $f_o(\underline{v},z) = f_o(\underline{v}) = f_o$(of bulk) = normal Fermi distribution function i.e. $(\exp(E - E_F/kT) + 1)^{-1}$.

With the above assumption regarding collisions, the change of f in time due to collision can be written as

$\left(\frac{\partial f}{\partial t}\right)_{coll} = -\frac{f - f_o}{\tau}$ and from $f = f_o + f_1$ it equals $-\frac{f_1(\underline{v},z)}{\tau}$.

The Boltzmann equation

$$-\frac{e\underline{E}}{m} \cdot \text{grad}_{\underline{v}} f + \underline{v} \cdot \text{grad}_{\underline{r}} f = \left(\frac{\partial f}{\partial t}\right)_{coll.}$$

then reduces to

$$\frac{\partial f_1(\underline{v},z)}{\partial z} + \frac{f_1(\underline{v},z)}{\tau v_z} = \frac{eE}{mv_z}\frac{\partial f_o(\underline{v})}{\partial v_x} \quad ,$$

where the non-ohmic term Ef_1 was dropped. The general solution is

$$f_1(\underline{v},z) = \frac{e\tau E}{m}\frac{\partial f_o(\underline{v})}{\partial v_x}\left[1 + F(\underline{v})\exp\left(-\frac{z}{\tau v_z}\right)\right] \qquad [D2]$$

$F(\underline{v})$ is an arbitrary function and will be determined from the boundary conditions.

1. Diffuse Surface Scattering. This is the simplest case. Free paths are terminated at surfaces $z = 0$ and $z = d$. The distribution function $f(\underline{v},z) = f_o(\underline{v}) + f_1(\underline{v},z)$ of electrons leaving the surface is independent of direction of $\underline{v}$. Since $f_o(\underline{v})$ depends on the magnitude of $\underline{v}$ only, $f(\underline{v}, 0) = f_o(\underline{v})$ and $f(\underline{v}, d) = f_o(\underline{v})$ at $z = 0$ and $z = d$ for the electrons leaving the surfaces. Then from the above

at $z = 0$, $(v_z > 0)$, $f_1(\underline{v}, 0) = 0$ so $F(\underline{v}) = -1$ and

at $z = d$, $(v_z > 0)$, $f_1(\underline{v}, d) = 0$ so $F(\underline{v}) = -\exp\left(\frac{d}{\tau v_z}\right)$

so from [D2]

$$f_1(\underline{v}, z) = \begin{cases} \frac{e\tau E}{m} \frac{\partial f_o(\underline{v})}{\partial v_x} \left[1 - \exp\left(-\frac{z}{\tau v_z}\right)\right], & (v_z > 0) \\ \frac{e\tau E}{m} \frac{\partial f_o(\underline{v})}{\partial v_x} \left[1 - \exp\left(\frac{d - z}{\tau v_z}\right)\right], & (v_z < 0) \, . \end{cases}$$

The current density j in the x direction is

$$j = e \int v_x f_1(\underline{v}, z) \, dv_x \, dv_y \, dv_z \qquad \text{and}$$

the effective current density in the whole film is

$$\dot{J} = \frac{1}{d} \int_o^d j \, dz \, .$$

Introduce polar coordinates $v_z = v \cos\theta$ and get

$$\dot{J} = \frac{\pi e^2 E \tau}{m} \int_o^\infty \frac{\partial f_o}{\partial v} v^2 dv \left[\int_o^\pi \sin^3\theta \, d\theta - \int_o^{\pi/2} \sin^3\theta \, d\theta \, \frac{1}{d} \int_o^d \exp U dz - \right.$$

$$\left. - \int_{\pi/2}^\pi \sin^3\theta \, d\theta \, \frac{1}{d} \int_o^d \exp W dz \right]$$

where $U = -\frac{z}{\ell \cos\theta}$ and $W = \frac{d - z}{\ell \cos\theta}$, $\ell = \tau \bar{v}$; $\bar{v} = v_F$.

Now set $d = \infty$, carry out integration of first term in bracket and get for the bulk

$$\dot{J}_o = \frac{4\pi}{3} \frac{e^2 E \tau}{m} \int_o^\infty \frac{\partial f_o}{\partial v} v^3 dv \, .$$

Take $\frac{\dot{J}}{\dot{J}_o} = \frac{\sigma_F}{\sigma_o}$ = ratio of film and bulk conductivity, and carry out

integration in Z, then

$$\frac{\sigma_F}{\sigma_o} = 1 - \frac{3}{4}\int_0^{\pi} \sin^3\theta\,|\cos\theta|\,\frac{\ell}{a}\left[1 - \exp\left(-\frac{d}{\ell\,|\cos\theta|}\right)\right] d\theta\,.$$

Change $\frac{d}{\ell} = \kappa$ and by repeated integration by parts get the final result

$$\frac{\sigma_F}{\sigma_o} = 1 + \frac{3}{4}\left(\kappa - \frac{\kappa^3}{12}\right)B(\kappa) - \frac{3}{8\kappa}\left(1 - e^{-\kappa}\right) - \left(\frac{5}{8} + \frac{\kappa}{16} - \frac{\kappa^2}{16}\right)e^{-\kappa}\,, \qquad [D3]$$

where $B(\kappa) = \int_{\kappa}^{\infty} \frac{e^{-\xi}}{\xi}\,d\xi$ is a tabulated integral.

2. Partially Diffuse Surface Scattering. This is the general case. An ideally smooth surface would be expected to reflect the electrons with no change in v_x and reverse the sign of v_z. In this case the conductivity would be the same as bulk.

Here we take the case where the proportion of the electrons scattered specularly is ϵ (in the previous section ϵ was zero). Starting again at the boundary conditions, we have from the symmetry of the film that $f_1(v_x, v_y, v_z, z) = f_1(v_x, v_y, -v_z, d - z)$. From [D2] then the general solution for $f_1(\underline{v}, z)$ becomes

$$f_1(\underline{v}, z) = \begin{cases} \dfrac{eE\tau}{m}\dfrac{\partial f_o}{\partial v_x}\left[1 + F(\underline{v})\exp\left(-\dfrac{z}{\tau v_z}\right)\right] = f_1'(\underline{v}, z), & v_z > 0 \\[2ex] \dfrac{eE\tau}{m}\dfrac{\partial f_o}{\partial v_x}\left[1 + F(\underline{v}')\exp\left(\dfrac{d - z}{\tau v_z}\right)\right] = f_1''(\underline{v}, z), & v_z < 0\,, \end{cases}$$

where $\underline{v}' = (v_x , v_y , - v_z)$. $f(\underline{v}, 0) = f_o(\underline{v}) + f_1''(\underline{v}, 0)$ is the distribution function of electrons arriving at $z = 0$ surface. ϵ proportion of these will scatter specularly $\epsilon\left(f_o(\underline{v}) + f_1''(\underline{v}', 0)\right)$, giving a contribution to the distribution function leaving the surface. The other part of the electrons leaving the surface (diffusely scattered) is g.

Now the distribution functions of electrons leaving the $z = 0$ surface altogether is

$$f(\underline{v}, 0) = f_o(\underline{v}) + f_1'(\underline{v}, 0) = \epsilon[f_o(\underline{v}) + f_1''(\underline{v}', 0)] + g .$$

Substituting for f_1' and f_1'' we get

$$g = f_o(\underline{v})(1 - \epsilon) + \frac{eE\tau}{m} \frac{\partial f_o}{\partial v_x} \left\{(1 - \epsilon) + F(\underline{v}) \left[1 - \epsilon \exp\left(- \frac{d}{\tau v_z}\right)\right]\right\} .$$

Note that $(\underline{v}')' = \underline{v}$.

g is independent of the direction of $\underline{v}$, and since $f_o(\underline{v}) = f_o(|\underline{v}|)$, the large bracket must vanish. From this we find $F(\underline{v})$ and $F(\underline{v}')$ as

$$F(\underline{v}) = - \frac{1 - \epsilon}{1 - \epsilon \exp(- d/\tau v_z)} , \quad F(\underline{v}') = - \frac{1 - \epsilon}{1 - \epsilon \exp(d/\tau v_z)} .$$

Substitution of $F(\underline{v})$ and $F(\underline{v}')$ back into $f_1'(\underline{v}, z)$ and $f_1''(\underline{v}, z)$ above yields

$$f_1(\underline{v}, z) = \begin{cases} \dfrac{eE\tau}{m} \dfrac{\partial f_o}{\partial v_x} \left[1 - \dfrac{1 - \epsilon}{1 - \epsilon \exp(-d/\tau v_z)} \exp\left(- \dfrac{z}{\tau v_z}\right)\right] , & v_z > 0 \\ \dfrac{eE\tau}{m} \dfrac{\partial f_o}{\partial v_x} \left[1 - \dfrac{1 - \epsilon}{1 - \epsilon \exp(d/\tau v_z)} \exp\left(\dfrac{d - z}{\tau v_z}\right)\right] , & v_z < 0 \end{cases}$$

Similar to the previous treatment, we calculate the current density, change to polar coordinates, find the bulk current density, carry out the integration from 0 to d and get

$$\frac{\sigma_F}{\sigma_o} = 1 - \frac{3}{8\kappa}(1-\epsilon) + \frac{3}{4\kappa}\int_0^{\pi} \sin^3\theta \,|\cos\theta| \frac{(1-\epsilon)^2 \exp(-\kappa/|\cos\theta|)}{1-\epsilon\exp(-\kappa/|\cos\theta|)}\, d\theta ,$$

here again $\kappa = \frac{d}{\ell}$, $\ell = \tau\bar{v}$ and $\bar{v} = v_F$. The final general expression is

$$\frac{\sigma_F}{\sigma_o} = 1 - \frac{3(1-\epsilon)}{8\kappa} + \frac{3}{4\kappa}(1-\epsilon)^2 \sum_{\nu=1}^{\infty} \epsilon^{\nu-1} \left\{ B(\kappa\nu)\left(\kappa^2\nu^2 - \frac{\kappa^4\nu^4}{12}\right) + \right.$$

$$\left. + e^{-\kappa\nu}\left(\frac{1}{2} - \frac{5}{6}\kappa\nu - \frac{\kappa^2\nu^2}{12} + \frac{\kappa^3\nu^3}{12}\right)\right\} \qquad [D4]$$

[D3] is a special case ($\epsilon = 0$) of [D4] . Approximate forms of [D4] are

$$\left.\begin{aligned} &\frac{\sigma_o}{\sigma_F} \approx 1 + \frac{3}{8\kappa}(1-\epsilon) \qquad \text{for } \kappa \gg 1 \\ &\frac{\sigma_o}{\sigma_F} \approx \frac{4}{3}\frac{1-\epsilon}{1+\epsilon}\,\frac{1}{\kappa \log \kappa^{-1}} \qquad \text{for } \kappa \ll 1 . \end{aligned}\right\} \text{[D5]}$$

The first of these is identical in form to expression [10] derived from Matthiessen's rule for thin films.

APPENDIX E

THE OPTICAL CONSTANTS OF PURE DRUDE METALS

Assume the solid to be Drude type, to be homogeneous and isotropic with one type of carrier (- e) only, and that a unique relaxation time τ exists. Assume also that only conduction band processes take place (i.e. no interband transitions etc.).

Let the perturbing electric field of the incident radiation be

$$E = E_o \exp - i\,(\underline{K} \cdot \underline{r} - \omega t) \qquad [E1]$$

and write Boltzmann's equation for the conduction electrons by including the explicit time dependence of the distribution function

$$f(\underline{v}, \underline{r}, t) = f_o(\underline{v}, \underline{r}, t) + f_1\,(\underline{v}, \underline{r}, t)$$

as

$$\frac{\partial f}{\partial t} - \frac{eE}{m^*}\frac{\partial f}{\partial \underline{v}} + \underline{v} \cdot \frac{\partial f}{\partial \underline{r}} = \left(\frac{\partial f}{\partial t}\right)_{coll} = - \frac{f - f_o}{\tau} = - \frac{f_1}{\tau} \qquad [E2]$$

where $\underline{v}$, $\underline{r}$ and m^* are the Fermi velocity, position and effective mass of electrons, if we take f_o to be the Fermi distribution function. As f_o is only a function $\underline{v}$ according to the Drude theory, [E2] reduces to

$$\frac{\partial f_1}{\partial t} - \frac{eE}{m^*}\frac{\partial f_o}{\partial |\underline{v}|} + \underline{v} \cdot \frac{\partial f_1}{\partial \underline{r}} = - \frac{f_1}{\tau} \quad . \qquad [E3]$$

Assume that the perturbation f_1 is propogated the same way as E in [E1] (linear solid), then the form of the general solution of [E3] is

$$f_1 = F(\underline{v}) \frac{\partial f_o}{\partial |\underline{v}|} \exp - i\,(\underline{K} \cdot \underline{r} - \omega t) \,. \qquad [E4]$$

To find $F(\underline{v})$, put [E4] back in [E3], and with

$$\frac{\partial f_1}{\partial t} = i\,\omega\, f_1 \quad \text{and} \quad \frac{\partial f_1}{\partial \underline{r}} = i\,\underline{K}\, f_1 \quad \text{get}$$

$$i\,\omega\, f_1 - \frac{eE}{m^*} \frac{\partial f_o}{\partial |\underline{v}|} - i\underline{v} \cdot \underline{K}\, f_1 = - \frac{f_1}{\tau}$$

or

$$- i\,\omega\, F(\underline{v}) + \frac{eE_o}{m^*} + i\,\underline{v} \cdot \underline{K}\, F(\underline{v}) = \frac{F(\underline{v})}{\tau} \,.$$

From this

$$F(\underline{v}) = \frac{eE_o}{m^*} \frac{\tau}{1 + i(\omega - \underline{v} \cdot \underline{K})\,\tau} \,,$$

so

$$f_1 = \frac{eE_o}{m^*} \left(\frac{\tau}{1 + i(\omega - \underline{v} \cdot \underline{K})\,\tau} \right) \frac{\partial f_o}{\partial |\underline{v}|} \exp - i(\underline{K} \cdot \underline{r} - \omega t) \,.$$

As the phase velocity ω/K of E is much greater than the Fermi velocity $|\underline{v}|$ of the electrons, the term $\underline{v} \cdot \underline{K}$ may be dropped. We get

$$f_1 = \frac{eE_o}{m^*} \frac{\tau}{1 + i\,\omega t} \frac{\partial f_o}{\partial |\underline{v}|} \exp - i(\underline{K} \cdot \underline{r} - \omega t) \,.$$

The conductivity is now written as

$$\tilde{\sigma} = \frac{J}{E} = \left(E_o \exp - i(\underline{K} \cdot \underline{r} - \omega t) \right)^{-1} \frac{eE_o}{m^*} \exp - i(\underline{K} \cdot \underline{r} - \omega t) \frac{\tau}{1 + i\omega t}\, e \int \frac{\partial f_o}{\partial |\underline{v}|}\, d\underline{v}$$

and as the integral equals the carrier density N, we get

$$\tilde{\sigma} = \frac{Ne^2}{m^*} \frac{\tau}{1 + i\,\omega\,\tau} \quad . \qquad [E5]$$

In terms of the D.C. conductivity σ_o, [E5] is

$$\tilde{\sigma}(\omega) = \frac{\sigma_o}{1 + i\,\omega\,\tau} \quad . \qquad [E6]$$

The real and imaginary parts of $\tilde{\sigma}(\omega)$ are

$$\sigma(\omega) = \frac{\sigma_o}{1 + \omega^2\tau^2} \qquad [E7a]$$

$$\tilde{\sigma}_{Im}(\omega) = - \frac{\sigma_o}{1 + \omega^2\tau^2}\,\omega\tau \qquad [E7b]$$

Also, if we take the lattice contribution to the real part of dielectric constant to be ϵ_o , then the real and imaginary parts of $\tilde{\epsilon}(\omega)$ are

$$\epsilon(\omega) = \epsilon_o - \frac{\sigma_o}{1 + \omega^2\tau^2}\,\tau \qquad [E8a]$$

$$\tilde{\epsilon}_{Im}(\omega) = \frac{\sigma_o}{1 + \omega^2\tau^2} \frac{1}{\omega} \quad . \qquad [E8b]$$

We have thus established relationships between optical constants n and k and material constants N, e, m* and τ at frequencies ω for Drude type metals through expressions [E7] and [E8] . A more familiar form of [E7a] and [E8a] is written in Gaussian units (replacing ϵ_o with $(4\,\pi)^{-1}$) as

$$\sigma = 2\,nk\,\omega = \frac{4\,\pi\,\sigma_o}{1 + \omega^2\tau^2} \qquad [E9a]$$

$$\epsilon = n^2 - k^2 = 1 - \frac{4\,\pi\,\sigma_o}{1 + \omega^2\tau^2} \quad . \qquad [E9b]$$

The combination of these two equations may be used to determine τ as

$$\tau = \frac{1 - n^2 + k^2}{2 \omega nk} , \qquad [E10]$$

[E10] serves to check the range of ω in which the metal behaves according to the theory, by requiring (through the initial assumptions) τ to be independent of ω .